PROGRESS REPORT

FOR

NASA GRANT NAG-1-541

Vibrations and Structureborne Noise in Space Station

For the period

July 1, 85 - Dec. 31, 85

Prepared by:

Rimas Vaicaitis
Principal Investigator
Department of Civil Engineering
and Engineering Mechanics
Columbia University
New York, N.Y. 10027

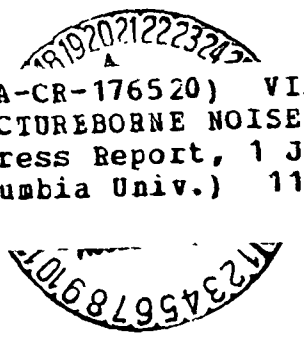

(NASA-CR-176520) VIBRATIONS AND STRUCTUREBORNE NOISE IN SPACE STATION Progress Report, 1 Jul. - 31 Dec. 1985 (Columbia Univ.) 119 p HC A06/MF A01
CSCL 22B G3/18

N86-20485

Unclas
16833

1. Summary of Major Activities

During the reporting period, the following major activities relating to the proposed work have been accomplished.

1.1 Papers published

1. Vaicaitis, R., "Noise Transmission into Propeller Aircraft," The Shock and Vibration Digest, Vol. 17, No. 8, Aug. 1985.

1.2 Papers prepared for publication

1. Bofilios, D.A. and Vaicaitis, R., "Response of Double Wall Composite Shells to Random Point Loads," submitted for publication, Journal of Aircraft, AIAA.

1.3 Conference papers (presented)

1. Vaicaitis, R., and Bofilios, D.A., "Noise Transmission of Double Wall Composite Shells," ASME 10th Biennnial Conference on Mechanical Vibration and Noise, Paper, No. H-334, Cincinnati, Ohio, Sept. 1985.

2. Vaicaitis, R., "Structureborne Noise in Space Station," 5th Science and Engineering Symposium, Chicago, Illinois, Nov. 1985.

1.4 Conference papers (accepted for presentation)

1. Vaicaitis, R., "Noise Transmission into Enclosures," Fourth International Modal Analysis Conference, Los Angeles, California, Feb. 1986.

2. Vaicaitis, R. and Bofilios, D.A., "Response Suppression in Composite Sandwich Shells," Vibration Damping Workshop II, Las Vegas, Nevada, March 1986.

1.5 Conference papers submitted for presentation

1. Vaicaitis, R. and Bofilios, D.A., "Vibro-Acoustics for Space Station Applications," AIAA 10th Aeroacoustics Conference, Seattle, Washington, July 1986.

2. Vaicaitis, R., "Nonlinear Response - A Time Domain Approach," AIAA 10th Aeroacoustics Conference, Seattle, Washington, July 1986.

2.0 Technical Highlights

The technical background and highlights of structureborne noise generation and transmission have been described in Refs. 1 and 2. In what follows, a brief review of new accomplishments and progress of new work is given.

2.1 Response and Noise Transmission of Double Wall Circular Plates and Laminated Composite Cylindrical Shells

Analytical models were developed in the Doctoral thesis by Dr. D.A. Bofilios for application to structureborne noise related problems. A copy of the thesis is enclosed with the present progress report. The main objectives of this work were to develop theoretical models capable of predicting structural response and noise transmission to random point mechanical loads. Fiber reinforced composite and aluminum materials were considered. Cylindrical shells and circular plates were taken as typical representatives of structural components for space station habitability modules. Analytical formulations include double wall and single wall constructions. Pressurized and unpressurized models were considered. Parametric studies were conducted to determine the effect on structural response and noise transmission due to fiber orientation, point load location, damping in the core and the main load carrying structure, pressurization, interior acoustic absorption, etc. These analytical models could serve as preliminary tools for assessing noise related problems, for space station applications.

2.2 Propagation and Transfer of Vibrational Energy for Structureborne Noise Applications

Structureborne noise arises as a result of mechanical vibrations which might start as flexural, torsional, dilatational or traveling waves. For space station operations, vibrations could be induced directly to the habitability modules by mechanical impacts, power generating systems, life support systems, proposed manufacturing devices, or it could arrive through interconnecting structures due to thruster action, payload deliveries, etc. In order to assess the significance of these vibrations on the vibroacoustic environmental inside the habitability modules, detailed understanding of structural response, wave propagation, transfer and attenuation of vibrational energy is needed. For this purpose, a structural model shown in Fig. 1 has been selected. The acoustic enclosure is subdivided (partitioned) into a number of individual or interconnecting compartments. Noise is generated in these compartments by the vibration of a stiffened wall or the partitions. The vibrational energy arrives via the stiffened structure and it is transferred into the stiffened wall at the points of load transfer. The number and locations of applied random loads are taken to be arbitrary. Such a model would allow for a more basic understanding of structureborne noise generation and transmission and still provide a tractable mathematical formulation. In this part of the study, we will be mainly concerned with modes of dynamic (mechanical) load generation, vibrational energy propagation and transfer into interconnected structures, and noise generation in partitioned

interiors. To construct the required analytical model, modal methods, wave propagation, and transfer matrix techniques will be used. We expect to present the mathematical formulations of the structural response problem in the next progress report.

2.3 Structureborne Noise Generation and Transmission into Habitability Modules

The analytical models described in Sec. 2.1 were developed for monocoque (single or double) cylindrical shells and idealized cylindrical acoustic enclosures. However, the final configuration of the habitability modules expected to be discretely stiffened cylindrical shells with truncated cone type end caps and partitioned interiors. The structural details of a typical (proposed) habitabilaity module is shown in Fig. 2. For the structural response analysis of the pressurized habitability module, the following analytical formulations are being considered.

1) Orthotropic Shell Model

In the orthotropic shell model, the effect of stiffeners (rings and stringers, Fig. 3) is smeared into an equivalent skin [3]. Such a model provides a relatively simple analytical tool for response estimation to point loads. However, this model is limited to a frequency range where the modal wavelengths are significantly larger than the spacing between stiffeners. The natural frequencies of an orthotropic shell (smeared) are shown in Figs. 4 and 5 for several cases of different structural parameters. The structural parameters chosen for these examples

are typical of the proposed habitability modules. We expect to incorporate the orthotropic formulation in the analytical model for structural response and noise transmission calculations described in Sec. 2.1.

2) Discretely Stiffened Shell Model

A transfer matrix technique is being used to devlop an analytical model for response estimation of ring stiffened shells to point loads acting on the stiffening rings or the shell skin. For this purpose, the general theory of transfer matrices presented in Ref. 4-6 is being utilized. Such a structural model allows for proper dynamic interaction of stiffening elements, shell skin and paplied load.

3) End Caps

The end caps of the habitability module shown in Fig. 2 are taken as truncated cones. We expect to develop analytical procedures for estimating response and noise transmission of these structures. Due to a very complex geometry of such a configuration, numerical techniques based on the finite element methods will be utilized.

4) Acoustic Model

The acoustic enclosure is a cylindrical cavity with a number of partitions as shown in Fig. 2. Noise inside various compartments can be generated by vibrations of the main shell structure, the end caps or the partitions. Analytical models for interior

noise are being developed for cylindrical, rectangular and irregular enclosures. For irregular enclosures, the acoustic modes are not readily available and numerical techniques will be utilized to calculate these modes.

References

1. Vaicaitis, R. and Mixson, J.S., "Review of Research on Structureborne Noise," 26th AIAA/ASME/ASCE/AHS SDM Conference, Paper No. 85-0786-CP, Orlando, Fl., April 1985.

2. Vaicaitis, R., "Vibrations and Structureborne Noise in Space Station," Progress Report for NASA Grant NAG-1-541, for the period Jan 1, 85 - June 30, 85.

3. Cockburn, J.A. and Jolly, A.C., "Structural acoustic response, noise transmission losses, and interior noise levels of an aircraft fuselage excited by random pressure fields," AFFDC-TR-68-2, Air Force Flight Dynamics Laboratory.

4. Pestel, E.C. and Leckie, F.A., "Matrix Methods in Elastomechanics," McGraw-Hill, 1963.

5. Lin, Y.K. and Donaldson, B.K., "A brief survey of transfer matrix techniques with special reference to the analysis of aircraft panels," Journal of Sound and Vibr., Vol. 10, pp. 103-143, 1969.

6. Chang, M.T. and Vaicaitis, R., "Noise Transmission into Semicylindrical Enclosures through Discretely Stiffened Curved Panels," Journal of Sound and Vibration, Vol. 85, No. 1, pp. 71-83, 1982.

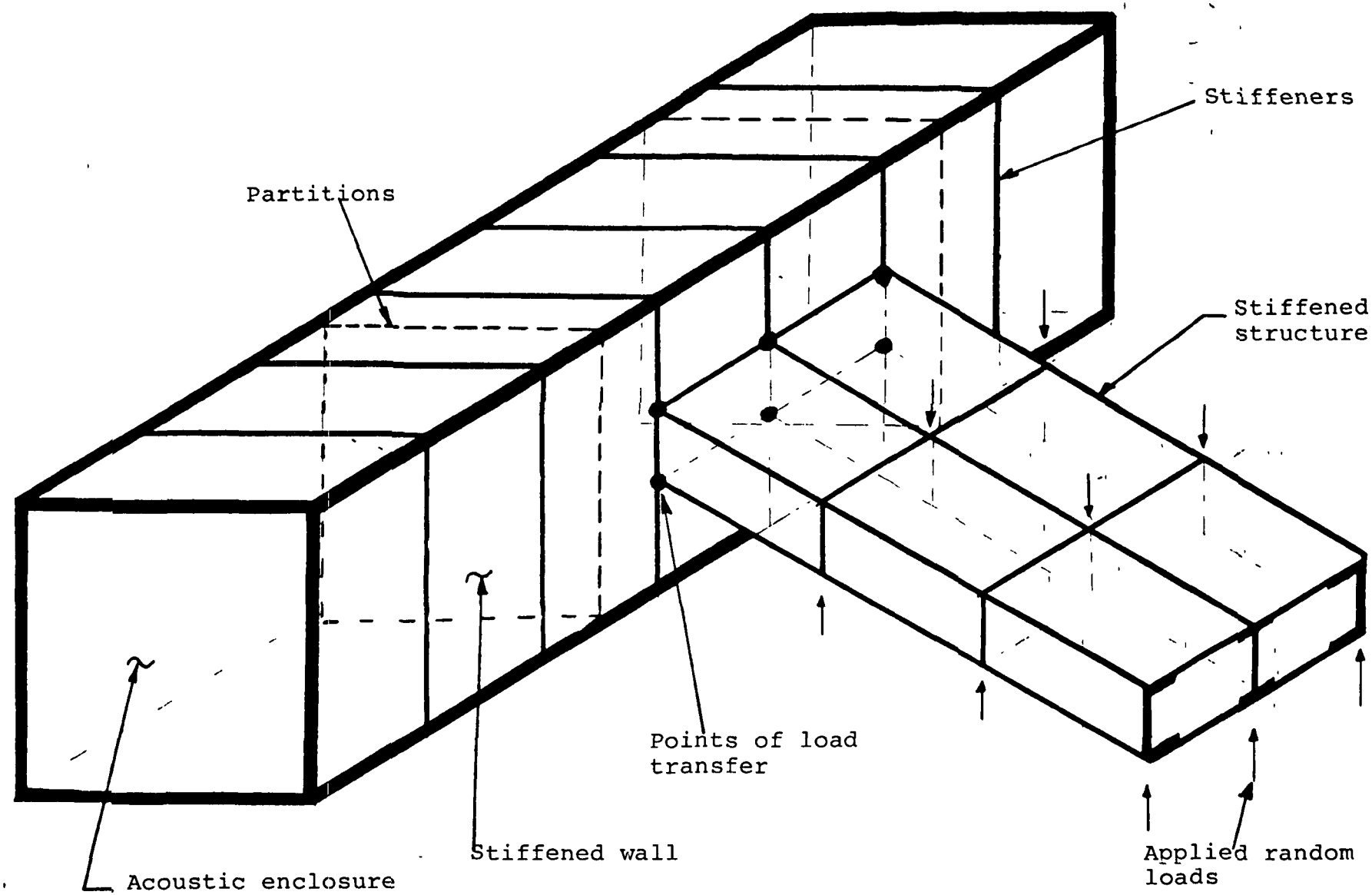

Fig.1 Partitioned acoustic enclosure and structured details of a structureborne noise transmission model

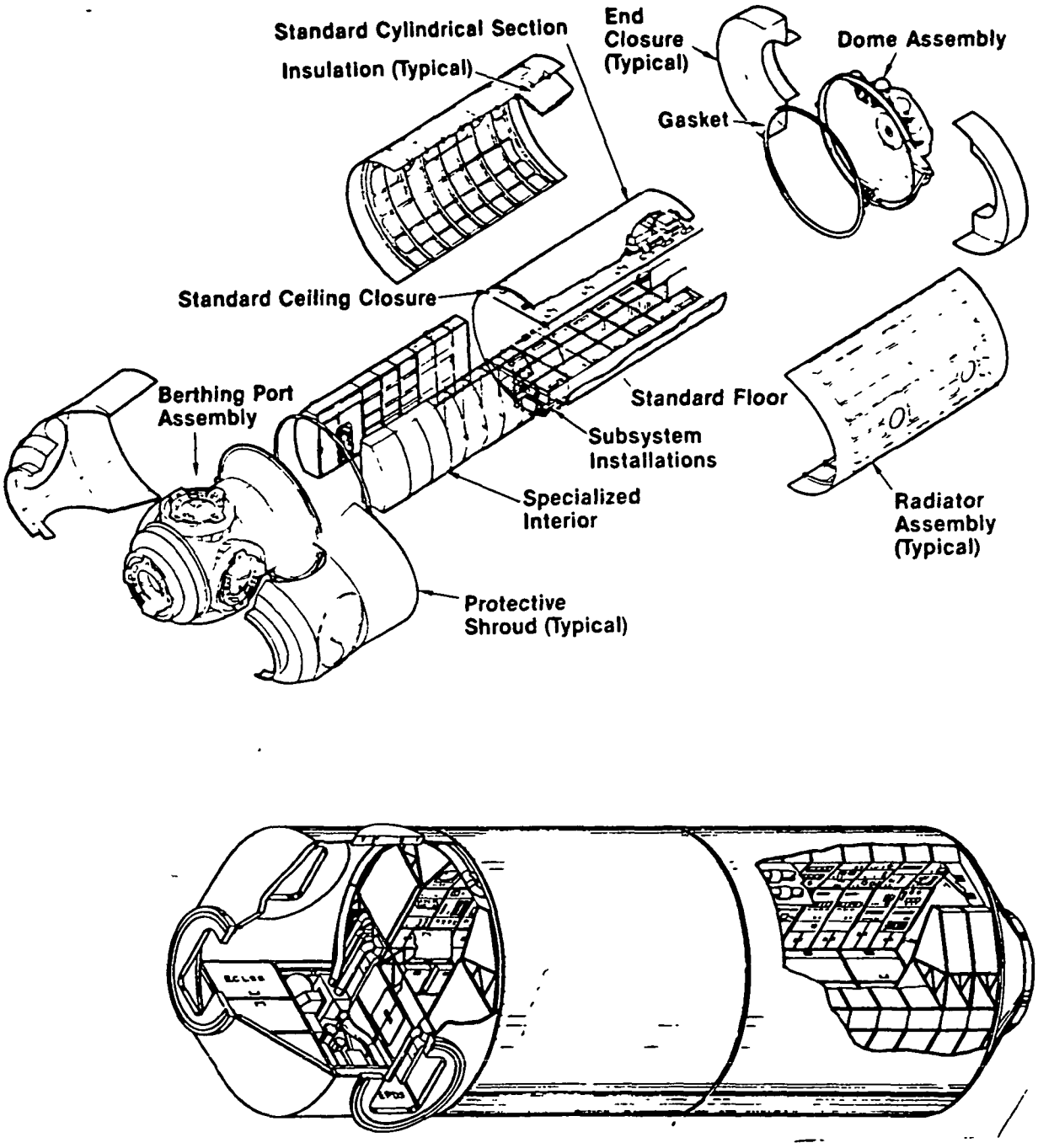

Fig.2 Proposed geometry of habitability modules

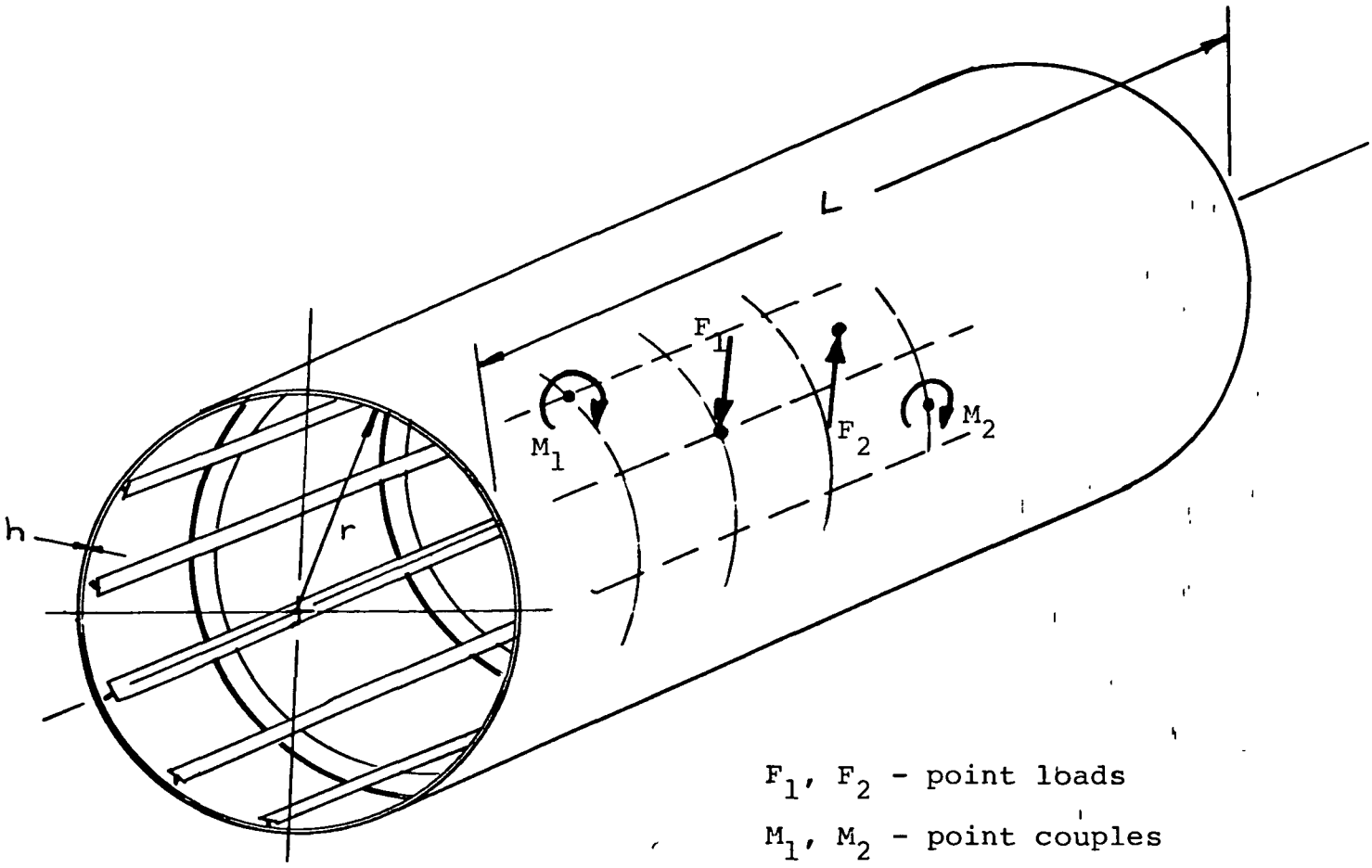

Fig.3 Geometry of a stiffened cylindrical shell

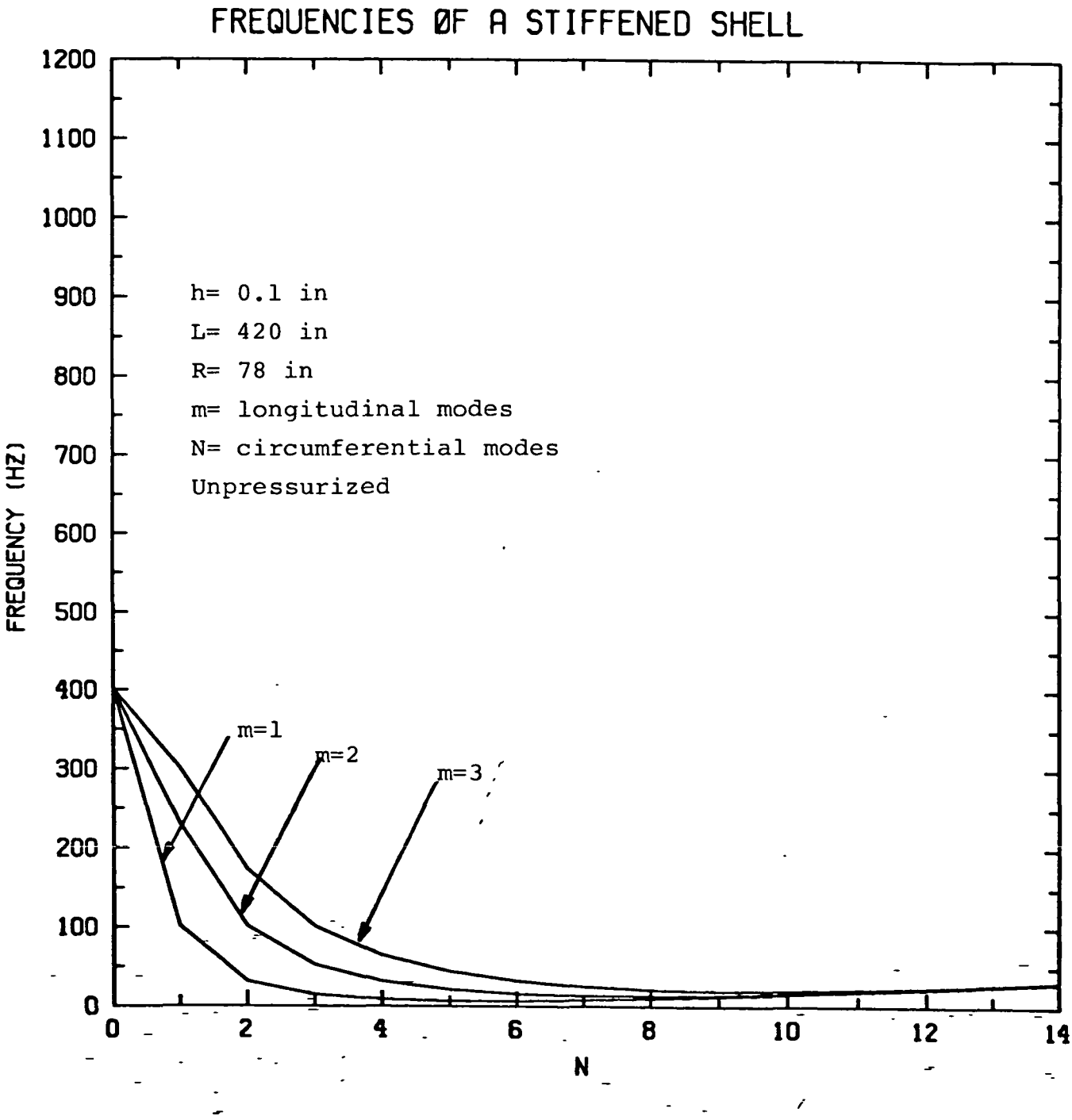

Fig.4 Natural frequencies of a stiffened shell (no rings and no stringers)

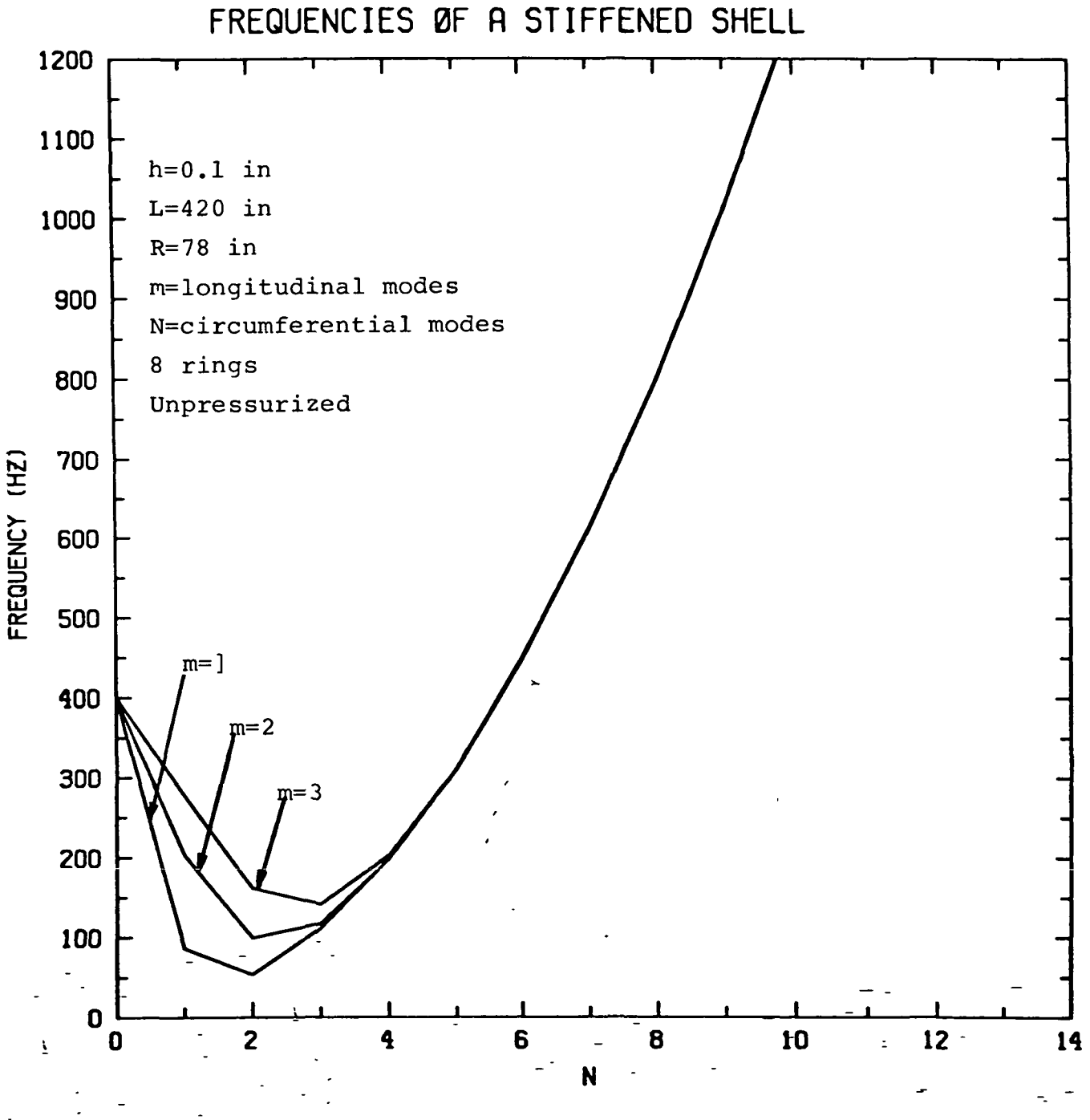

Fig.5 Natural frequencies of a stiffened shell (8 rings and no stringers)

RESPONSE AND NOISE TRANSMISSION OF DOUBLE WALL CIRCULAR PLATES AND LAMINATED COMPOSITE CYLINDRICAL SHELLS

Dimitrios Alexander Bofilios

Submitted in partial fulfillment of the
requirements for the degreee
of Doctor of Philosophy
in the Graduate School of Arts and Sciences

Columbia University
1985

ABSTRACT

RESPONSE AND NOISE TRANSMISSION OF DOUBLE WALL CIRCULAR PLATES AND LAMINATED COMPOSITE CYLINDRICAL SHELLS

Dimitrios Alexander Bofilios

An analytical study is presented to predict the response and noise transmission of double wall circular plates and double wall laminated composite fiber reinforced cylindrical shells to random loads. The core of the double wall construction is taken to be soft so that dilatational motions can be modeled. The analysis of laminated shells is simplified by introducing assumptions similar to those in the Donnell-Mushtari theory for isotropic shells. The theoretical solutions of the governing acoustic-structural equations are obtained using modal decomposition and a Galerkin-like procedure. Numerical results include modal frequencies, deflection response spectral densities and interior sound pressure levels. From the parametric study it was found that by proper selection of dynamic parameters, viscoelastic core characteristics and fiber reinforcement orientation, vibration response can be reduced and specific needs of noise attenuation can be achieved.

TABLE OF CONTENTS

ACKNOWLEDGMENT

I am indebted to Professor R. Vaicaitis for his continuous support and guidance in the preparation of this work and through my stay at Columbia University. I would also like to express my appreciaton to Reva Goldkopf for her typing and editing suggestions. I wish to thank the NASA-Langley Research Center for its financial support.

To my Parents

1. INTRODUCTION

The design of many ground and space structures is impacted by the interaction of functional requirements such as strength, stiffness, weight, passenger and crew comfort, cargo containment protection, reliability, etc. To accommodate many of these requirements, new design concepts for lower weight, extended service life and reduced costs are needed. It has been demonstrated that composite materials could give weight and structural integrity advantages over many commonly used materials [1-3]. However, the low weight composites might not provide any advantages with respect to less response, reduced noise transmission [4] or longer fatigue life. Past studies have demonstrated that sandwich constructions might be an effective way of dissipating vibrational energy [5-7]. Thus, to satisfy the required vibroacoustic environment, designs utilizing composite materials might need to be modified by including the double wall sandwich concept. It is expected that the vibroacoustic environment in the proposed space station might exceed the acceptable vibration and noise levels. Therefore, implementation of sandwich constructions might prove to be useful alternatives in the design process.

Many transportation vehicles involve shell constructions. The greatest impetus to the development of the dynamics and noise transmission of shell-type structures has been for aircraft, missiles, launch vehicles, manned spacecraft, and submercibles [8-22]. Current technological

interest is shifted from simple, single layer, isotropic shells without stiffeners [23-30], to shells made of composite materials, of laminated sandwich type constructions, and shells stiffened with rings and/or stringers. Previous research efforts concerned with the dynamics of laminated shells, neglected the bending-stretching coupling and the concept of an equivalent single-layer special orthotropic shell was used [31-33]. Due to the limiting applicability of the latter formulation, this type of bending-stretching was then incorporated in a Donell-type shell theory for laminated composites and a general solution of free vibration of laminated orthotropic cylindrical shells was presented [34-39]. Similar analyses have been carried out using Love's first approximation theory for an arbitrarily laminated anisotropic shell of moderate length [40-42]. The vibrational analyses of sandwich shells were mainly concerned with simply supported circular cylindrical shells having isotropic facings [43]. Then, it was extended to orthotropic facings and orthotropic core where the in-surface forces were neglected [44]. The forced vibrational analyses of cylindrical orthotropic sandwich shells took into account the transverse shear deformation of the core and the material damping of the core and of the facings [45]. Furthermore, an analysis of sandwich shells with laminated anisotropic facings was presented [46]. In addition, a more complex formulation for the vibration of open and closed sandwich shells was developed [47].

The analytical and experimental studies of noise transmission through shell structures were mostly undertaken in the aerospace industry where models for prediction of sound transmission were developed [8-13,48-50]. The main research efforts were concentrated on the prediction of sound transmission through thin cylindrical shells in an acoustic field [48-50]. A general formulation, using the interaction of structural vibrations and external sound fields, in terms of structural normal modes and acoustic cavity normal modes, has been developed [10]. These procedures have been extended to include a formulation which combines modal methods and statistical energy analysis [11]. Airborne noise transmission through laminated composite cylindrical shells of infinite extent has been considered in Ref. 4. An analysis of the sound transmission through closed sandwich cylindrical shells where the closed ends are taken as acoustically hard walls has been presented [51] as an extension of an earlier investigation on sound transmission through damped sandwich panels [52]. However, studies are needed on response and noise transmission through double wall laminated composite shells separated by a soft core.

This work presents an analytical study on vibration response and noise transmission of double wall laminated composite circular cylindrical shells of finite extent. Each shell is a composite built up of laminae, which in turn consist of unidirectional fibers imbedded in a

supporting matrix. Furthermore, each lamina can be oriented in any arbitrary direction. The shell skins are modeled according to a laminated cylindrical thin shell theory using Love's first approximation theory and the Donnell-Mushtari assumptions for thin shells [53-57]. The end caps are taken as double wall circular isotropic plates [58-66]. The governing differential equations for the vibration of double wall shells and double wall circular plates, shown in Fig. 1, are developed for the case in which the core material is taken to be soft, so that bending and shearing stresses can be neglected and, consequently, the core can be described by a uniaxial constitutive law. Such a core allows in phase (flexural) and out of phase (dilatational) motions of the double wall system [52,67]. The inertia effects of the core follow a linear apportioned mass distribution law. The inputs to the shell and the end caps are either uniformly distributed random pressures or random point loads. The equations for the shell and circular plate systems are analyzed using modal decomposition and a Galerkin-like procedure [68,69], along with power spectal density approaches [70]. It is assumed that the shell and the end plate systems vibrate independently. The noise transmission through the double wall sandwich constructions, of the facings and ends, into the cylindrical enclosure shown in Fig. 1, is analyzed by solving the linearized wave equation for the interior sound pressure field [71]. Time domain and frequency domain

formulations are included. In the time domain approach, the time dependent boundary conditions are transformed into a governing equation and then the solution of the resulting nonhomogeneous partial differential equation with homogeneous boundary conditions is obtained [72,73]. Then, the solutions for the acoustic pressure in the shell interior are obtained in terms of the inner shell and/or the inner circular plate motions. The interior acoustic pressure is ultimately expressed in terms of spectral density functions normalized to a reference pressure, and a quantity is defined called sound pressure level.

This work contains numerical results for response and noise transmission of simply supported double wall cylindrical shells and double wall circular plate systems. Natural frequencies, vibration response spectral densities and transmitted sound pressure levels are calculated. These results are obtained for double wall isotropic (aluminum) and double wall fiber reinforced composite cases. The outer shell is constructed from three laminae and the inner shell from ten laminae. The end caps are taken as flexible double wall constructions capable of structurally inducing noise. It is shown that by proper selection of dynamic parameters, damping characteristics and reinforcing fiber orientation lower response levels can be obtained at some frequencies for a composite shell than those of an equivalent aluminum shell, and a significant amount of noise attenuation might be achieved by a design

composed of two composite shells and a soft viscoelastic core.

2. STRUCTURAL PROBLEM FORMULATION

2.1 Introduction

This section is concerned with the random vibration of a closed double wall cylindrical shell system of finite extent. The sandwich shell system is composed of two simply supported circular cylindrical shells and a soft viscoelastic core as shown in Fig. 1. Each shell is constructed either from isotropic material or from fiber reinforced laminae. The fibers are basically the load carriers. A linear viscoelastic model is chosen to describe the behavior of the core. The thin composite shells separated by the core are modeled according to the theory presented in Refs. 35,42,43,54-56. This theory is appropriate for many arbitrarily oriented layers, each reinforced with unidirectional fibers. The fiber orientation is defined in Fig. 1 with respect to the chosen coordinates. The end plates are taken to be double wall homogeneous isotropic circular plates and modeled according to the theory presented in [58-66]. As in the case of the shell system, a linear viscoelastic model is chosen to describe the behavior of the core. For both, the double wall shell and the end plate systems, the core is assumed relatively soft so bending and shearing stresses can be neglected, and consequently, the core can be described by a uniaxial constitutive law. The double wall homogeneous isotropic shell is considered as a limiting case to the general formulation.

2.2 Random Vibration of a Double Wall Shell

Following the procedures presented in [54,55], the equations of motions of a single cylindrical shell are

$$\partial N_x/\partial x + (1/R)\ \partial N_{\theta x}/\partial\theta + q_x = \rho\ \ddot{u} \tag{2.1}$$

$$(1/R)\partial N_\theta/\partial\theta + \partial N_{x\theta}/\partial x + (1/R)\ ((1/R)\partial M_\theta/\partial\theta + \partial M_{x\theta}/\partial x) + q_\theta = \rho\ \ddot{v} \tag{2.2}$$

$$\partial^2 M_x/\partial x^2 + (2/R)\ \partial^2 M_{x\theta}/\partial x\partial\theta + (1/R^2)\ \partial^2 M_\theta/\partial\theta^2 - N_\theta/R + q_w = \rho\ \ddot{w} \tag{2.3}$$

where a dot indicates a time derivative and

$$\begin{bmatrix} N_x \\ N_\theta \\ N_{x\theta} \\ M_x \\ M_\theta \\ M_{x\theta} \end{bmatrix} = \left[\begin{array}{c|c} [A_{ij}] & [B_{ij}] \\ \hline [B_{ij}] & [D_{ij}] \end{array}\right] \begin{bmatrix} \dfrac{\partial v}{\partial x} \\ (\frac{1}{R})\ (\partial v/\partial\theta + w) \\ (\frac{1}{R})\ \dfrac{\partial u}{\partial\theta} + \dfrac{\partial v}{\partial x} \\ -\dfrac{\partial^2 w}{\partial x^2} \\ -(\frac{1}{R^2})(\partial^2 w/\partial\theta^2 - \partial v/\partial\theta) \\ -(\frac{1}{R})\ (2\partial^2 w/\partial x\partial\theta - \partial v/\partial x) \end{bmatrix} \tag{2.4a}$$

where the submatrices $[A_{ij}]$,$[B_{ij}]$,$[D_{ij}]$ are

$$\left[(A,B,D)_{ij}\right] = \begin{bmatrix} (A,B,D)_{11} & (A,B,D)_{12} & (A,B,D)_{16} \\ (A,B,D)_{12} & (A,B,D)_{22} & (A,B,D)_{26} \\ (A,B,D)_{16} & (A,B,D)_{26} & (A,B,D)_{66} \end{bmatrix} \tag{2.4b}$$

$$\begin{bmatrix} A_{ij} \\ B_{ij} \\ D_{ij} \end{bmatrix} = \sum_{k=1}^{n} \left[C_{ij}^{(k)}\right] \begin{bmatrix} (h_k - h_{k-1}) \\ 1/2\ (h_k^2 - h_{k-1}^2) \\ 1/3\ (h_k^3 - h_{k-1}^3) \end{bmatrix} \tag{2.5}$$

in which $C_{ij}^{(k)}$ are the elastic moduli of the kth lamina and h_k, h_{k-1} are distances measured from the reference surface to outer and inner surfaces of the kth lamina (see Fig. 1). Following Ref. 35, the stiffness coefficients A_{ij}, B_{ij}, D_{ij} can be calculated in terms of directional moduli, Poisson's ratios and fiber orientation angle α. In this approach, the properties of each lamina are functions of volume ratio of fibers to supporting matrix material. A more detailed discussion is given in Appendix I.

The mass density per unit of surface area is calculated from

$$\rho = \sum_{k=1}^{n} \rho_k\ (h_k - h_{k-1}) \tag{2.6}$$

where ρ_k is the material density of the kth lamina and h_k are distances from reference surface to lamina surface.

Using Eqs. (2.4a), (2.5), and (2.1-2.3), the equations of motion of a laminated shell can be written as

$$L_{11}u + L_{12}v + L_{13}w + q_x = \rho \ddot{u} \tag{2.7}$$

$$L_{12}u + L_{22}v + L_{23}w + q_\theta = \rho \ddot{v} \tag{2.8}$$

$$L_{13}u + L_{23}v + L_{33}v + q_w = \rho \ddot{w} \tag{2.9}$$

where the differential operators L_{ij} are given in Appendix II. As can be seen from equations (2.7-2.9) the matrix of differential operators is symmetric. Setting the in-plane loads $q_x = q_\theta = 0$, introducing the Donnell-Mushtari-Vlasov type assumptions [35,54,55] and combining Eqs. (2.7-2.9), a single equation in terms of transverse displacement w can be obtained

$$\{{}_Z\nabla^8 + {}_X\nabla^6 + {}_Y\nabla^4\}\, w + \nabla^4 \{\rho \ddot{w} - q_w\} = 0 \tag{2.10}$$

where

$${}_Z\nabla^8 = Z_1 \partial^8/\partial x^8 + (1/R) Z_2 \partial^8/\partial x^7 \partial\theta$$

$$+ (1/R^2) Z_3 \partial^8/\partial x^6 \partial\theta^2 + (1/R^3) Z_4 \partial^8/\partial x^5 \partial\theta^3$$

$$+ (1/R^4) Z_5 \partial^8/\partial x^4 \partial\theta^4$$

$$+ (1/R^5)Z_6\partial^8/\partial x^3\partial\theta^5 + (1/R^6)Z_7\partial^8/\partial x^2\partial\theta^6$$

$$+ (1/R^7)Z_8\partial^8/\partial x\partial\theta^7 + (1/R^8)Z_4\partial^8/\partial x^8 \qquad (2.11)$$

$${}_X\nabla^6 = (1/R)X_1\partial^6/\partial x^6 + (1/R^2)X_2\partial^6/\partial x^5\partial\theta$$

$$+ (1/R^3)X_3\partial^6/\partial x^4\partial\theta^2 + (1/R^4)X_4\partial^6/\partial x^3\partial\theta^3$$

$$+ (1/R^5)X_5\partial^6/\partial x^2\partial\theta^4$$

$$+ (1/R^6)X_6\partial^6/\partial x\partial\theta^5 + (1/R^7)X_7\partial^6/\partial\theta^6 \qquad (2.12)$$

$${}_Y\nabla^4 = (1/R^2)Y_1\partial^4/\partial x^4 + (1/R^3)Y_2\partial^4/\partial x^3\partial\theta$$

$$+ (1/R^4)Y_3\partial^4/\partial x^2\partial y^2$$

$$+ (1/R^5)Y_4\partial^4/\partial x\partial\theta^3 + (1/R^6)Y_5\partial^4/\partial\theta^4 \qquad (2.13)$$

$$\nabla^4 = \alpha_1\partial^4/\partial x^4 + (2/R)\alpha_2\partial^4/\partial x^3\partial\theta$$

$$+ (1/R^2)\alpha_3\partial^4/\partial x^2\partial\theta^2 \qquad (2.14)$$

$$+ (2/R^3)\alpha_4\partial^4/\partial x\partial\theta^3 + (1/R^4)\alpha_5\partial^4/\partial\theta^4$$

and the coefficients Z_i, X_j, Y_r and α_r ($i = 1,2,\ldots 9$; $j = 1,2,\ldots 7$; $r = 1,2,\ldots 5$) are defined in Appendix II.

Following Ref. 52 and using Eq. (2.10), the double

wall shell motions can be modeled by two coupled partial differential equations for normal deflections w_E and w_I as

$$\{{}_Z\nabla_E^8 + {}_X\nabla_E^6 + {}_Y\nabla_E^4\}w_E + \nabla_E^4\{\rho_E\ddot{w}_E + k_s(w_E - w_I)$$

$$+ c_E\dot{w}_E + (1/3)m_s\ddot{w}_E + (1/6)m_s\ddot{w}_I\} = \nabla_E^4 p^e(x,\theta,t) \qquad (2.15)$$

$$\{{}_Z\nabla_I^8 + {}_X\nabla_I^6 + {}_Y\nabla_I^4\}w_I + \nabla_I^4\{\rho_I\ddot{w}_I + k_s(w_I - w_E)$$

$$+ c_E\dot{w}_I + (1/3)m_s\ddot{w}_I + (1/6)m_s\ddot{w}_E\} = -\nabla_I^4 p^i(x,\theta,t) \qquad (2.16)$$

The subscripts E,I and s denote the external and the internal shells, and the core, respectively. The p^e and p^i are random loads acting on the external and the internal shell. In the present formulation, the acoustic radiation pressure is not included. The stiffness of the core is represented by a linear viscoelastic spring, $k_s = k_o (1 + ig_s)$, where k_o is spring constant and g_s is the loss factor.

The input loads are modeled either as uniformly distributed random pressures or random point loads acting at an arbitrary location on the shell surface as shown in Fig. 2. In the vicinity of point load application some of the assumptions of linear, elastic thin shell theory are violated [54]. However, outside the vicinity of the point load shell response can be calculated with good accuracy. A Dirac delta function is used to define the location of

the point load. The random loads p^e and p^i are expressed in terms of two point loads $F_1^{e,i}$ and $F_2^{e,i}$ as

$$p^e(x,\theta,t) = (1/A_1^e A_2^e)\ \{F_1^e(t)\ \delta(x-x_1^e)\ \delta(\theta-\theta_1^e) + F_2^e(t)\ \delta(x-x_2^e)\ \delta(\theta-\theta_2^e)\} \quad (2.17)$$

$$p^i(x,\theta,t) = (1/A_1^i A_2^i)\ \{F_1^i(t)\ \delta(x-x_1^i)\ \delta(\theta-\theta_1^i) + F_2^i(t)\ \delta(x-x_2^i)\ \delta(\theta-\theta_2^i)\} \quad (2.18)$$

where the superscripts e and i denote the external and the internal loads, δ is the Dirac delta function and for a cylindrical shell [54] $A_1^e = 1$, $A_2^e = R + h_s$, $A_1^i = 1$, $A_2^i = R$. The point loads are assumed to be independent and each characterized by a spectral density.

2.2.1 Frequency Response Functions and Modal Frequencies

The equations of motion of double wall shells are solved by modal expansion methods. To take the advantage of orthogonality of modal functions, the equations of motion are further simplified by neglecting from the operators ${}_Z\nabla^8, {}_X\nabla^6, {}_Y\nabla^4$ and ∇^4 the terms containing odd derivatives of spatial variables x and θ. The various simplifications of shell equations are discussed in Refs. 35,42,54. The general solution of Eqs. (2.15) and (2.16) is expressed in terms of the simply supported shell modes

$$w_E(x,\theta,t) = \sum_{m=1}^{\infty} \sum_{n=0}^{\infty} A^E_{mn} X^S_{mn}(x,\theta) \tag{2.19}$$

$$w_I(x,\theta,t) = \sum_{m=1}^{\infty} \sum_{n=0}^{\infty} A^I_{mn} X^S_{mn}(x,\theta) \tag{2.20}$$

where A^E_{mn} and A^I_{mn} are the generalized coordinates of external and internal shells, and X^S_{mn} are the shell modes. For a simply supported shell, $X^S_{mn} = \sin(m\pi x/L) \cos n\theta$. The input loads p^e and p^i are also expanded in terms of the natural shell modes. Substitution of Eqs. (2.19) and (2.20) into Eqs. (2.15) and (2.16) and use of the orthogonality principle, give a set of coupled differential equations in A^E_{mn} and A^I_{mn}. Taking the Fourier transform of these equations it can be shown that

$$\bar{A}^E_{mn} = H^E_{mn} \{\bar{P}^E_{mn}/\rho_E + A^I_{mn}(k_s + (1/6)m_s\omega^2)/\rho_E\} \tag{2.21}$$

$$\bar{A}^I_{mn} = H^I_{mn} \{\bar{P}^I_{mn}/\rho_I + \bar{A}^E_{mn}(k_s + (1/6)m_s\omega^2)/\rho_I\} \tag{2.22}$$

in which a bar indicates a transformed quantity. The generalized random forces $\bar{P}^E_{mn}$ and $\bar{P}^I_{mn}$ corresponding to point loads given in Eqs. (2.17) and (2.18) are

$$\bar{P}^E_{mn} = \{\bar{F}^e_1 X^S_{mn}(x^e_1, \theta^e_1) + \bar{F}^e_2 X^S_{mn}(x^e_2, \theta^e_2)\}/(R + h_s) \tag{2.23}$$

$$\bar{P}^I_{mn} = \{\bar{F}^i_1 X^S_{mn}(x^i_1,\theta^i_1) + \bar{F}^i_2 X^S_{mn}(x^i_2,\theta^i_2)\}/R \qquad (2.24)$$

The frequency response functions of the external and the internal shells are

$$H^E_{mn} = 1/\{\omega^{E^2}_{mn} - \omega^2\gamma_E/\rho_E + \underset{\sim}{i}\omega c_E/\rho_E + k_s/\rho_E\} \qquad (2.25)$$

$$H^I_{mn} = 1/\{\omega^{I^2}_{mn} - \omega^2\gamma_I/\rho_I + \underset{\sim}{i}\omega c_I/\rho_I + k_s/\rho_I\} \qquad (2.26)$$

where $\gamma_E = \rho_E + 1/3\ m_s$, $\gamma_I = \rho_I + 1/3\ m_s$ and

$$\begin{aligned}\omega^{E,I^2}_{mn} = \{&Z^{E,I}_1(m\pi/L)^8 \\ &+ (m\pi/L)^6\ (Z^{E,I}_3 n^2/R^2_{E,I} - X^{E,I}_1/R_{E,I}) \\ &+ (m\pi/L)^4(Z^{E,I}_5 n^4/R^4_{E,I} - X^{E,I}_3 n^2/R^3_{E,I} + Y^{E,I}_1/R^2_{E,I}) \\ &+ (m\pi/L)^2(Z^{E,I}_7 n^6/R^6_{E,I} - X^{E,I}_5 n^4/R^5_{E,I} + Y^{E,I}_3 n^2/R^4_{E,I}) \\ &+ (n/R_{E,I})^4(Z^{E,I}_9 n^4/R^4_{E,I} - X^{E,I}_7 n^2/R^3_{E,I} \\ &+ Y^{E,I}_5/R^2_{E,I})\}/\{\rho_{E,I}((m\pi/L)^4\ \alpha^{E,I}_1 \\ &+ n^2(m\pi/L)^2\ \alpha^{E,I}_3/R^2_{E,I} + n^4\alpha^{E,I}_5/R^4_{E,I})\}\end{aligned} \qquad (2.27)$$

in which the superscripts or subscripts E,I denote either

the external or the internal shells and $R_E = R + h_s$, $R_I = R$.

Equation (2.27) gives the natural frequencies of uncoupled laminated shell vibrations. The coupled natural frequencies of double wall shell motions can be obtained from Eqs. (2.21) and (2.22) by setting $c_E = c_I = g_s = 0$ and maximizing the solution for generalized coordinates. This yields

$$\omega_{mn}^c = \{[- b_{mn} \pm (b_{mn}^2 - 4ac_{mn})^{1/2}]/2a\}^{1/2} \qquad (2.28)$$

where

$$a = \gamma_E\gamma_I - (1/6\ m_s)^2 \qquad (2.29)$$

$$b_{mn} = (\rho_E\omega_{mn}^{E^2} + k_s)\gamma_I + (\rho_I\omega_{mn}^{I^2} + k_s)\gamma_E + k_s m_s/3 \qquad (2.30)$$

$$c_{mn} = (\rho_E\omega_{mn}^{E^2} + k_s)\ (\rho_I\omega_{mn}^{I^2} + k_s) - k_s^2 \qquad (2.31)$$

Equation (2.28) gives two characteristic values for each set of modal indices (m,n). These roots are associated with in-phase flexural and out-of-phase dilatational vibration frequencies of the sandwich construction.

2.2.2 Response under Random Loads

For the analysis presented herein, it is assumed that the input spectral densities of the uniform pressure or point loads are specified. Thus, the response (shell

deflections) needs to be expressed in the form of a spectral density. Following the procedure given in Ref. 70 it can be shown that the spectral density of normal shell deflections $w_{E,I}$ can be determined from

$$S_w^{E,I}(x,\theta,\omega) = \sum_{m=1}^{\infty} \sum_{n=0}^{\infty} \sum_{r=1}^{\infty} \sum_{s=0}^{\infty} {}_wS_{mnrs}^{E,I}(\omega)\, X_{mn}^{S} \cdot X_{rs}^{S} \tag{2.32}$$

where ${}_wS_{mnrs}^{E,I}(\omega)$ are the cross spectral densities of the generalized coordinates $A_{mn}^{E,I}$. Expanding Eq. (2.32) and assuming that inputs are stationary and independent, it may be shown that

$$S_w^{E,I}(x,\theta,\omega) = \sum_{m=1}^{\infty} \sum_{n=0}^{\infty} \sum_{r=1}^{\infty} \sum_{s=0}^{\infty} \{\Theta_{mn}^{E,I}(\Theta_{rs}^{E,I})^{*} S_{mnrs}^{E,I} + \Lambda_{mn}\Lambda_{rs}^{*} S_{mnrs}^{I,E}\} X_{mn}^{s} \cdot X_{rs}^{s} \tag{2.33}$$

where

$$\Theta_{mn}^{E,I} = (H_{mn}^{E,I}/\rho_{E,I})/\Phi_{mn} \tag{2.34}$$

$$\Lambda_{mn} = (H_{mn}^{E}/\rho_E)\,(H_{mn}^{I}/\rho_I)(k_s + (1/6)m_s\omega^2)/\Phi_{mn} \tag{2.35}$$

$$\Phi_{mn} = 1 - (H_{mn}^{E}/\rho_E)\,(H_{mn}^{I}/\rho_I)(k_s + (1/6)m_s\omega^2)^2 \tag{2.36}$$

and $S_{mnrs}^{E,I}$ are the cross-spectal densities of the generalized random inputs. If the inputs are represented by two independent stationary point loads acting on the external shell, from Eq. (2.23) and Ref. 70, the cross-spectral

density of generalized random forces is

$$S^E_{mnrs} = \{S^e_{F_1}(\omega)\ X^S_{mn}(x^e_1,\theta^e_1)\ X^S_{rs}(x^e_1,\theta^e_1)$$

$$+\ S_{F_2}(\omega)\ X^S_{mn}(x^e_2,\theta^e_2)\ X^S_{rs}(x^e_2,\theta^e_2)\}/(R + h_s)^2 \tag{2.37}$$

where $S^e_{F_1}$ and $S^e_{F_2}$ are the spectral densities of the point loads F^e_1 and F^e_2. Similar expression can be developed for point loads acting on the interior shell.

2.3 Double Wall Homogeneous Isotropic Shell

A special case of the general formulation presented in Section 2.2, is a double wall homogeneous isotropic shell. Using Eqs. (2.1-2.3) and utilizing the Donnel-Mushtari approximations for thin shells [54,55] it may be shown that the coupled governing equations of motion reduce to the following form

$$D_E\nabla^8_E w_E + (E_E h_E/R^2_E)\partial^4 w_E/\partial x^4 + \rho_E\nabla^4_E\ddot{w}_E + \nabla^4_E\{k_s(w_E-w_I)$$

$$+ c_E\dot{w}_E + (1/3)m_s\ddot{w}_E + (1/6)m_s\ddot{w}_I\} = \nabla^4_E\, p^e(x,\theta,t) \tag{2.38}$$

$$D_I\nabla^8_I w_I + (E_I h_I/R^2_I)\partial^4 w_I/\partial x^4 + \rho_I\nabla^4_I\ddot{w}_I + \nabla^4_I\{k_s(w_I-w_E)$$

$$+ c_I\dot{w}_I + (1/3)m_s\ddot{w}_I + (1/6)m_s\ddot{w}_E\} = -\nabla^4_I p^i(x,\theta,t) \tag{2.39}$$

where ρ_E, ρ_I are surface densities of the homogeneous facings and

$$R_{E,I} = (R + h_s), R \tag{2.40}$$

$$m_s = \rho_s h_s \tag{2.41}$$

$$D_{E,I} = E_{E,I} h_{E,I}^3 / 12(1 - \nu_{E,I}^2) \tag{2.42}$$

$$\nabla_{E,I}^4 = \partial^4/\partial x^4 + (2/R_{E,I}^2)\partial^4/\partial x^2 \partial\theta^2 + (1/R_{E,I}^4)\partial^4/\partial\theta^4 \tag{2.43}$$

$$\nabla_{E,I}^8 = \partial^8/\partial x^8 + (4/R_{E,I}^2)\partial^8/\partial x^6 \partial\theta^2 + (6/R_{E,I}^4)\partial^8/\partial x^4 \partial\theta^4 + (4/R_{E,I}^6)\partial^8/\partial x^2 \partial\theta^6 + (1/R_{E,I}^8)\partial^8/\partial\theta^8 \tag{2.44}$$

The uncoupled frequencies of the face shells are given by

$$(\omega_{mn}^{E,I})^2 = \{(D_{E,I}/\rho_{E,I})\ [(m\pi/L)^2 + (n^2/R_{E,I}^2)]^4 + (E_{E,I} h_{E,I}/\rho_{E,I} R_{E,I}^2)(m\pi/L)^4\}/[(m\pi/L)^2 + (n^2/R_{E,I}^2)]^2 \tag{2.45}$$

2.4 Random Vibration of Double Wall Circular Plates

Consider the two circular plates shown in Fig. 1 which are simply supported around the edges. The boundary conditions for deflection and radial bending moment at the edges are

$$w_{T,B}(r,\theta) = 0 \qquad \text{at } r = R^P \tag{2.46}$$

$$M_r(r,\theta) = -D_{T,B}\left\{\frac{\partial^2 w_{T,B}}{\partial r^2} + \nu_{T,B}\left(\frac{1}{r}\frac{\partial w_{T,B}}{\partial r} + \frac{1}{r^2}\frac{\partial^2 w_{T,B}}{\partial \theta^2}\right)\right\} = 0 \text{ at } r = R^P \tag{2.47}$$

where $w_{T,B}$ are the normal displacements of the midsurfaces of the top (exterior) and bottom (interior) circular plates respectively, and superscript P denotes the plate. The governing equations of motion of the two plates, coupled through a linear soft core, can be written as [52,58,59]

$$D_T\nabla^4 w_T + c_T\dot{w}_T + m_T\ddot{w}_T + k_s^P(w_T - w_B) + (1/3)m_s^P\ddot{w}_T + (1/6)m_s^P\ddot{w}_B = -p^T(r,\theta,t) \tag{2.48}$$

$$D_B\nabla^4 w_B + c_B\dot{w}_B + m_B\ddot{w}_B + k_s^P(w_B - w_T) + (1/3)m_s^P\ddot{w}_B + (1/6)m_s^P\ddot{w}_T = p^B(r,\theta,t) \tag{2.49}$$

where

$$D_{T,B} = E_{T,B}h_{T,B}^3/12(1 - \nu_{T,B}^2) \tag{2.50a}$$

$$m_{T,B} = \rho_{T,B}h_{T,B} \tag{2.50b}$$

$$m_s^P = \rho_s^P h_s^P \tag{2.50c}$$

$$\nabla^4 = \left(\frac{\partial^2}{\partial r^2} + \frac{1}{r}\frac{\partial}{\partial r} + \frac{1}{r^2}\frac{\partial^2}{\partial \theta^2}\right)\left(\frac{\partial^2}{\partial r^2} + \frac{1}{r}\frac{\partial}{\partial r} + \frac{1}{r^2}\frac{\partial^2}{\partial \theta^2}\right) \quad (2.50d)$$

The subcripts T,B denote the top and bottom plates and s denotes the core. The pressures $p^T(r,\theta,t)$ and $p^B(r,\theta,t)$ are the random excitations applied to the top and bottom plates. In obtaining Eqs. (2.48) and (2.49) it was assumed that the mass of the core follows an apportioned linear distribution.

The solution to Eqs. (2.48) and (2.49) can be expressed in terms of normal modes

$$w_T(r,\theta,t) = \sum_{s=0}^{\infty} \sum_{q=1}^{\infty} {}_TA_{sq}(t)\, X^P_{sq}(r,\theta) \quad (2.51)$$

$$w_B(r,\theta,t) = \sum_{s=0}^{\infty} \sum_{q=1}^{\infty} {}_BA_{sq}(t)\, X^P_{sq}(r,\theta) \quad (2.52)$$

where ${}_TA_{sq}$ and ${}_BA_{sq}$ are the generalized coordinates of top (exterior) and bottom (interior) circular plates, and $X^P_{sq}(r,\theta)$ are the circular plate modes given by

$$X^P_{sq}(r,\theta) = R_{sq}(r)\cos(s\theta) \quad (2.53a)$$

$$R_{sq}(r) = J_s(k_{sq}r) - \frac{J_s(\lambda^s_{sq})}{I_s(\lambda^s_{sq})} I_s(k_{sq}r) \quad (2.53b)$$

in which J_s and I_s are Bessel functions and modified Bessel functions of the first kind respectively, and λ^s_{sq} is the qth root of the frequency equation

$$\frac{J_{s+1}(\lambda)}{J_s(\lambda)} + \frac{I_{s+1}(\lambda)}{I_s(\lambda)} = \frac{2\lambda}{1-\nu} \tag{2.54}$$

Results given in Eq. (2.54) are obtained by substituting Eqs. (2.53a) and (2.53b) into Eqs. (2.46) and (2.47) and using relationships which relate the derivatives of Bessel functions to high order functions [60,65,69]. In Eq. (2.54) $\lambda = kR^P$, $k^4 = \frac{\omega^2 m}{D}$ and consequently

$$\lambda_{sq}^s = k_{sq} R^P \tag{2.55}$$

$$k_{sq}^4 = {}_{T,B}\omega_{sq}^2 \; m_{T,B}/D_{T,B} \tag{2.56}$$

Substituting Eqs. (2.51) and (2.52) into Eqs. (2.48) and (2.49) and using the orthogonality principle, gives a set of coupled differential equations in ${}_T A_{sq}$ and ${}_B A_{sq}$. Taking the Fourier transform of these equations it can be shown that

$$\begin{aligned} {}_T\bar{A}_{sq}(\omega) = H_{sq}^T(\omega) \; \{ & {}_B\bar{A}_{sq}(\omega) \; (k_s + (1/6)m_s\omega^2) \\ & + {}_T\bar{P}_{sq}(\omega)/\tilde{Q}_{sq}\}/m_T \end{aligned} \tag{2.57}$$

$$\begin{aligned} {}_B\bar{A}_{sq}(\omega) = H_{sq}^B(\omega) \; \{ & {}_T\bar{A}_{sq}(\omega) \; (k_s + (1/6)m_s\omega^2) \\ & + {}_B\bar{P}_{sq}(\omega)/\tilde{Q}_{sq}\}/m_B \end{aligned} \tag{2.58}$$

where

$$H_{sq}^{T,B}(\omega) = 1/\{{}_{T,B}\omega_{sq}^2 - \omega^2\gamma_{T,B}/m_{T,B} + \tilde{i}\omega c_{T,B}/m_{T,B} + k_s/m_{T,B}\} \tag{2.59}$$

$$\gamma_{T,B} = m_{T,B} + (1/3)m_s^P \tag{2.60}$$

$$T,B\bar{P}_{sq}(\omega) = \bar{+} \int_0^{R^P}\int_0^{2\pi} \bar{p}^{T,B}(r,\theta,\omega)\, X_{sq}^P(r,\theta) r dr d\theta \tag{2.61}$$

$$\tilde{Q}_{sq} = \int_0^{R^P}\int_0^{2\pi} \{X_{sq}^P(r,\theta)\}^2 r dr d\theta = \begin{cases} \pi Q_{sq} & \text{if } s \neq 0 \quad (2.62a) \\ 2\pi Q_{0q} & \text{if } s = 0 \quad (2.62b) \end{cases}$$

$$Q_{sq} = \frac{(R^P)^2}{2}\{J_s'^2(\lambda_{sq}^s) + (1 - \frac{s^2}{(\lambda_{sq}^s)^2})\, J_s^2(\lambda_{sq}^s)\}$$

$$- \frac{(R^P)^2}{\lambda_{sq}^s}\frac{J_s(\lambda_{sq}^s)}{I_s(\lambda_{sq}^s)}\{I_s(\lambda_{sq}^s)J_{s+1}(\lambda_{sq}^s) + J_s(\lambda_{sq}^s)I_{s+1}(\lambda_{sq}^s)\}$$

$$+ \frac{(R^P)^2}{2}\frac{J_s^2(\lambda_{sq}^s)}{I_s^2(\lambda_{sq}^s)}\{(1 + \frac{s^2}{(\lambda_{sq}^s)^2})I_s^2(\lambda_{sq}^s) - I_s'^2(\lambda_{sq}^s)\} \tag{2.63}$$

$$T,B\omega_{sq}^2 = k_{sq}^4\, D_{T,B}/m_{T,B} \tag{2.64}$$

Furthermore, a $(\,)'$ indicates differentiation with respect to the spatial variable r and a bar indicates transformed quantity. The coupled natural frequencies can be obtained

from Eqs. (2.28) -(2.31) where the superscripts E,I have to be replaced by T,B.

The excitations applied to the top and/or bottom circular plates are assumed to be uniform random pressure or random point loads as shown in Fig. 2 for which the spectral densities are specified. In the case of uniform pressure input the generalized random forces reduce to

$$ {}_{T,B}\bar{P}_{sq}(\omega) = \begin{cases} 2\pi\mu_{0q}\bar{p}^{T,B}(\omega) & s = 0 \qquad (2.65a) \\ 0 & s \neq 0 \qquad (2.65b) \end{cases} $$

where

$$ \mu_{0q} = \frac{R^P}{k_{0q}} \left\{ J_1(\lambda^s_{0q}) - \frac{J_0(\lambda^s_{0q})}{I_0(\lambda^s_{0q})} I_1(\lambda^s_{0q}) \right\} \qquad (2.66) $$

and $\bar{p}^{T,B}(\omega)$ is the Fourier transform for spatially uniform pressure input $p^{T,B}(r,\theta,t)$.

The random loads acting on the top and bottom plates are expressed in terms of two point loads $F_1^{T,B}$ and $F_2^{T,B}$ as

$$ p^T(r,\theta,t) = (1/A_1^T A_2^T)\{F_1^T(t)\ \delta(\theta-\theta_1^T)\ \delta(r-r_1^T) + F_2^T(t)\ \delta(\theta-\theta_2^T)\ \delta(r-r_2^T)\} \qquad (2.67) $$

$$ p^B(r,\theta,t) = (1/A_1^B A_2^B)\{F_1^B(t)\ \delta(\theta-\theta_1^B)\ \delta(r-r_1^B) + F_2^B(t)\ \delta(\theta-\theta_1^B)\ \delta(r-r_2^B)\} \qquad (2.68) $$

where T,B denote the external and internal loads, δ is the Dirac delta function and for a circular plate [54] $A_1^{B,T} = 1$, $A_2^{B,T} = r$. The generalized random forces corresponding to point loads given in Eqs. (2.67) and (2.68) are

$$ {}_T\bar{P}_{sq}(\omega) = \{\bar{F}_1^T(\omega)\ X_{sq}^P(r_1^T,\theta_1^T) + \bar{F}_2^T(\omega)\ X_{sq}^P(r_2^T,\theta_2^T)\} \quad (2.69) $$

$$ {}_B\bar{P}_{sq}(\omega) = \{\bar{F}_1^B(\omega)\ X_{sq}^P(r_1^B,\theta_1^B) + \bar{F}_2^B(\omega)\ X_{sq}^P(r_2^B,\theta_i^B)\} \quad (2.70) $$

Following the procedures of Ref. 70 and assuming the point loads are stationary and independent, the spectral densities of normal plate deflections w_T, w_B can be determined from

$$ S_w^{T,B}(r,\theta,\omega) = \sum_{s=0}^{\infty}\sum_{q=1}^{\infty}\sum_{j=0}^{\infty}\sum_{k=1}^{\infty} \{{}_{T,B}\Theta_{sq}\ ({}_{T,B}\Theta_{jk}^*)\,{}_{T,B}S_{sqjk}(\omega) + {}_P\Lambda_{sq}({}_P\Lambda_{jk}^*)_{B,T}S_{sqjk}\}\ X_{sq}^P \cdot X_{jk}^P/\tilde{Q}_{sq}\tilde{Q}_{jk} \quad (2.71) $$

where

$$ {}_{T,B}\Theta_{sq}(\omega) = \{H_{sq}^{T,B}(\omega)/m_{T,B}\}/\Phi_{sq}^P(\omega) \quad (2.72) $$

$$ {}_P\Lambda_{sq}(\omega) = {}_T\Theta_{sq}(\omega)\ \{H_{sq}^B(\omega)/m_B\}(k_s + (1/6)m_s\omega^2) \quad (2.73) $$

$$ {}_P\Phi_{sq}(\omega) = 1 - \{H_{sq}^T(\omega)H_{sq}^B(\omega)(k_s + (1/6)m_s\omega^2)^2\}/m_T m_B \quad (2.74) $$

The asterisks in Eq. (2.71) denote complex conjugates and $_{B,T}S_{sqjk}$ are the cross-spectral densities of the generalized random forces.

For two stationary independent point loads acting on the external plate it may be shown that the cross-spectral density of the generalized forces $_{T}S_{sqjk}(\omega)$ may be determined from

$$
\begin{aligned}
{}_{T}S_{sqjk}(\omega) = \{ & S^{T}_{F_1}(\omega)\; X^{P}_{sq}(r^{T}_{1},\theta^{T}_{1})\; X^{P}_{jk}(r^{T}_{1},\theta^{T}_{1}) + \\
& S^{T}_{F_2}(\omega)\; X^{P}_{sq}(r^{T}_{2},\theta^{T}_{2})\; X^{P}_{jk}(r^{T}_{2},\theta^{T}_{2})\}
\end{aligned}
\tag{2.75}
$$

where $S^{T}_{F_1}$ and $S^{T}_{F_2}$ are the spectral densities of the point loads F^{T}_{1} and F^{T}_{2}. Similar expressions can be developed for point loads acting on the interior plate.

3. INTERIOR ACOUSTIC PRESSURE

3.1 Frequency Domain Solution

Consider a closed cylindrical enclosure with volume $V = \pi R^2 L$ shown in Fig. 1. It is assumed that the walls of the multilayered shell and the circular end plates are flexible. However, the motions of the shell and the end plates are taken to be independent. Thus the acoustic pressure inside the enclosure can be obtained from

$$p = p_1 + p_2 \tag{3.1}$$

where p_1 and p_2 are the acoustic pressures due to the inner shell and inner plate motions. The pressure p inside the enclosure satisfies the wave equation in cylindrical polar coordinates

$$\nabla^2 p - \beta \dot{p} = \ddot{p}/c_o^2 \tag{3.2}$$

in which β and c_o are the acoustic damping and speed of sound in the cavity, a dot indicates time derivative, and

$$\nabla^2 = \partial^2/\partial r^2 + (1/r)\partial/\partial r + (1/r^2)\partial^2/\partial\theta^2 + \partial^2/\partial x^2 \tag{3.3}$$

The interior walls ar r = R and x = 0,L are taken to be absorbent with a prescribed point impedance $Z(\omega)$. The boundary conditions to be satisfied are

$$\partial p_1/\partial r = - \rho \ddot{w}_I(x,\theta,t) - (\rho/Z_A)\dot{p}_1 \qquad \text{at } r = R \qquad (3.4)$$

$$\partial p_1/\partial x = 0 \qquad \text{at } x = 0,L \qquad (3.5)$$

$$\partial p_2/\partial x = \rho \ddot{w}_B^L(r,\theta,t) + (\rho/Z_L)\dot{p}_2 \qquad \text{at } x = 0 \qquad (3.6)$$

$$\partial p_2/\partial x = - \rho \ddot{w}_B^R(r,\theta,t) - (\rho/Z_R)\dot{p}_2 \qquad \text{at } x = L \qquad (3.7)$$

$$\partial p_2/\partial r = 0 \qquad \text{at } r = R \qquad (3.8)$$

where ρ is air density, Z_A, Z_L, Z_R are the absorbent wall impedances, w_I, w_B^L and w_B^R are displacements in the normal direction (positive outwards) of the inner shell and the inner end plates respectively. Taking Fourier transformation of Eqs. (3.2) - (3.8) and writing the solution in terms of the orthogonal acoustic modes corresponding to acoustically hard walls yield

$$\bar{p}_1(x,r,\theta,\omega) = \sum_{i=0}^{\infty} \sum_{j=0}^{\infty} P_{ij}(r,\omega) X_{ij}(x,\theta) \qquad (3.9)$$

$$\bar{p}_2(x,r,\theta,\omega) = \sum_{j=0}^{\infty} \sum_{k=1}^{\infty} Q_{jk}(x,\omega) Y_{jk}(r,\theta) \qquad (3.10)$$

where the acoustic modes for a closed cylindrical enclosure are

$$X_{ij} = \sqrt{\frac{2}{\pi L}} \cos (i\pi x/L) \cos j\theta \qquad (3.11)$$

$$Y_{jk} = J_j(\lambda_{jk} r) \cos j\theta \tag{3.12}$$

J_j represents the Bessel function of the first kind of order j and $\lambda_{jk} = \bar{\alpha}_{jk}/R$ where $\bar{\alpha}_{jk}$ is the kth root of the equation $dJ_j/dr = 0$. Substituting Eqs. (3.9) and (3.10) into Eq. (3.2) and using orthogonality condition of acoustic modes, one obtains

$$d^2P_{ij}/dr^2 + (1/r)dP_{ij}/dr + (\sigma_i^2 - j^2/r^2)P_{ij} = 0 \tag{3.13}$$

$$d^2Q_{jk}/dx^2 + \gamma_{jk}^2 Q_{jk} = 0 \tag{3.14}$$

in which

$$\sigma_i^2 = (\omega/c_o)^2 - (i\pi/L)^2 - \underset{\sim}{i}\omega\beta \tag{3.15}$$

$$\gamma_{jk}^2 = (\omega/c_o)^2 - \lambda_{jk}^2 - \underset{\sim}{i}\omega\beta \tag{3.16}$$

and $\underset{\sim}{i} = \sqrt{-1}$. Solving Eqs. (3.13) and (3.14) and imposing the finiteness condition of the pressure $\bar{p}_1$ at r = 0 gives

$$\bar{p}_1(x,r,\theta,\omega) = \sum_{i=0}^{\infty} \sum_{j=0}^{\infty} \alpha_{ij} J_j(\sigma_i r) X_{ij}(x,\theta), \quad \text{for } \sigma_i^2 > 0 \tag{3.17}$$

$$\bar{p}_2(x,r,\theta,\omega) = \sum_{j=0}^{\infty} \sum_{k=1}^{\infty} \{A_{jk} \sin(\gamma_{jk} x) + B_{jk} \cos(\gamma_{jk} x)\} Y_{jk}(r,\theta) \tag{3.18}$$

in which $\alpha_{ij}, A_{jk}, B_{jk}$ are arbitrary constants. For

$\sigma_i^2 < 0$ the Bessel function J_i needs to be replaced with the modified Bessel function I_j. For the special case when $\sigma_i^2 = 0$, the solution for the pressure $\bar{p}_1$ is

$$\bar{p}_1(x,r,\theta,\omega) = \sum_{i=0}^{\infty} \sum_{j=0}^{\infty} C_{ij} r^j X_{ij}(x,\theta) \tag{3.19}$$

where C_{ij} are arbitrary constants. Using the boundary conditions specified in Eqs. (3.4) - (3.8) and expanding the shell, w_I, and the end plate, w_B^L, w_B^R, motions in terms of the acoustic eigenfunctions given in Eq. (3.11) and (3.12), one obtains

$$\bar{p}_1(x,r,\theta,\omega) = \rho\omega^2 \sum_{i=0}^{\infty} \sum_{j=0}^{\infty} \{e_{ij} G_{ij}(r,\omega) \sum_{m=1}^{\infty} \sum_{n=0}^{\infty} \bar{A}^I_{mn} L_{mnij}\} X_{ij}(x,\theta) \tag{3.20}$$

$$\begin{aligned}\bar{p}_2(x,r,\theta,\omega) = & \sum_{j=0}^{\infty} \sum_{k=1}^{\infty} (\varepsilon_{jk}/\Delta_{jk}) \sum_{s=0}^{\infty} \sum_{q=1}^{\infty} [\{(e^{(1)}_{jk} - \underset{\sim}{i} e^{(2)}_{jk}/Z_L)_B A^L_{sq\ L} L^P_{sqjk} \\ & + (\underset{\sim}{i}\rho^2\omega^3/Z_R)_B \bar{A}^R_{sq\ R} L^P_{sqjk}\} \sin(\gamma_{jk}x) + \{\rho\omega\ \gamma^2_{jk\ B} \bar{A}^R_{sq\ R} L^P_{sqjk} \\ & + (e^{(3)}_{jk} + \underset{\sim}{i} e^{(4)}_{jk}/Z_L)_B \bar{A}^L_{sq\ L} L^P_{sqjk}\} \cos(\gamma_{jk}x)] J_j(\lambda_{jk}r) \cos j\theta\end{aligned} \tag{3.21}$$

where

$$e_{ij} = \begin{cases} 1/4 & i = 0, j = 0 \\ 1/2 & i \neq 0, j = 0;\ i = 0, j \neq 0 \\ 1 & i \neq 0, j \neq 0 \end{cases} \tag{3.22}$$

$$G_{ij}(r,\omega) = \begin{cases} r^j/\{jR^{j-1} + i\omega\rho\, R^j/Z_A\} & \sigma_i = 0 \\ J_j(\sigma_i r)/\{\sigma_i J_j'(\sigma_i R) + i\omega\rho J_j(\sigma_i R)/Z_A\} & \sigma_i^2 > 0 \end{cases} \tag{3.23}$$

$$L_{mnij} = \int_0^L \int_0^{2\pi} X_{mn}^s(x,\theta)\, X_{ij}(x,\theta)\, dx d\theta \tag{3.24}$$

$$\varepsilon_{jk} = 1/\{\int_0^R \int_0^{2\pi} rJ_j^2(\lambda_{jk} r)\cos^2 j\theta\, dr d\theta$$

$$= \begin{cases} 2\lambda_{jk}^2/\{\pi(\bar{\alpha}_{jk}^2 - j^2)\,[J_j(\bar{\alpha}_{jk})]^2\} & j \neq 0 \\ 1/\{\pi R^2 [J_0(\bar{\alpha}_{0k})]^2\} & j = 0 \end{cases} \tag{3.25}$$

$$\Delta_{jk} = i\omega\rho\gamma_{jk}\cos(\gamma_{jk}L)\,(1/Z_L + 1/Z_R) - \sin(\gamma_{jk}L)\,(\gamma_{jk}^2 + \rho^2\omega^2/Z_L Z_R) \tag{3.26}$$

$$e_{jk}^{(1)} = \rho\omega^2\gamma_{jk}\sin(\gamma_{jk}L) \tag{3.27a}$$

$$e_{jk}^{(2)} = \rho^2\omega^3\cos(\gamma_{jk}L) \tag{3.27b}$$

$$e_{jk}^{(3)} = \rho\omega^2\gamma_{jk}\cos(\gamma_{jk}L) \tag{3.27c}$$

$$e_{jk}^{(4)} = \rho^2 \omega^3 \sin(\gamma_{jk} L) \tag{3.27d}$$

$$_{L,R}L^{P}_{sqjk} = \int_0^{R^P} \int_0^{2\pi} r \; _{L,R}X^{P}_{sq} \; Y_{jk}(r,\theta) \, dr d\theta \tag{3.28}$$

More explicit expressions for L_{mnij} and $_{L,R}L^{P}_{sqjk}$ are given in Appendix III. The modes of shell and circular end plate vibrations are taken to be

$$X^{s}_{mn}(x,\theta) = \sin(m\pi x/L) \cos n\theta \tag{3.29}$$

$$_{L,R}X^{P}_{sq}(r,\theta)$$

$$= \{J_s(k^{L,R}_{sq} r) - J_s(_{L,R}\lambda^{s}_{sq}) I_S(k^{L,R}_{sq} r)/I_s(_{L,R}\lambda^{s}_{sq})\} \cos(s\theta) \tag{3.30}$$

where $k^{L,R}_{sq} = {}_{L,R}\lambda^{s}_{sq}/R^P$ in which $_{L,R}\lambda^{s}_{sq}$ is the qth root of the characteristic equation of circular plate vibrations and the superscripts L and R denote the end plates at x = 0 and x = L. The generalized deflections responses A^{I}_{mn}, $_{B}A^{L}_{sq}$, $_{B}A^{R}_{sq}$ of the shell and the end plates, respectively, are given in Section 2.

The acoustic resonant frequencies for the cylindrical closed enclosure can be calculated from

$$J_j'(\sigma_i r) = 0 \quad \text{at } r = R \tag{3.31}$$

where $\beta = 0$ is used in Eq. (3.15). For each combination of i,j modal indices there are k zeros of Eq. (3.31). This condition then gives all the modal frequencies ω_{ijk} of the closed cylindrical enclosure shown in Fig. 1.

The total acoustic pressure inside the shell enclosure can be calculated from Eqs. (3.1), (3.20) and (3.21). Assuming the input loads are stationary random processes, the spectral density of the acoustic pressure p can be obtained by taking the Fourier transform and then the mathematical expectation of Eq. (3.1). The result is

$$S_p(x,r,\theta,\omega) = S_{p_1}(x,r,\theta,\omega) + 2S_{p_1p_2}(x,r,\theta,\omega) + S_{p_2}(x,r,\theta,\omega) \qquad (3.32)$$

where S_{p_1}, S_{p_2} and $S_{p_1p_2}$ are the spectral densities and the cross-spectral densities of the acoustic pressures p_1 and p_2, respectively. If the responses of the shell and plates are taken to be independent, the cross-spectral densities $S_{p_1p_2} = 0$. The spectral densities S_{p_1} and S_{p_2}, are calculated from Eqs. (3.20) and (3.21) in terms of the generalized coordinates of the shell, A^I_{mn}, and the end plates, ${}_BA^L_{sq}$, ${}_BA^R_{sq}$. These generalized coordinates are functions of the prescribed random inputs acting on the shell and/or the plate surfaces. Then, the sound pressure levels in the enclosure can be calculated from

$$SPL(x,r,\theta,\omega) = 10 \cdot \log \{S_p(x,r,\theta,\omega)\ \Delta\omega/p_o^2\} \qquad (3.33)$$

where $\Delta\omega$ is the selected frequency bandwidth and p_o is the reference pressure ($p_o = 2.9 \times 10^{-9}$ psi).

3.2 Time Domain Solution

3.2.1 Introduction

In Section 3.2, a frequency domain solution for the perturbation pressure was developed in terms of the system's flexible wall motions for the structural-acoustic problem. Due to the linearity of the structural model, the generalized coordinates $A^I_{mn}, {}_BA^L_{sq}, {}_BA^R_{sq}$ were obtained in closed form. However, when structural and/or material nonlinearities are present, the frequency domain approach is no longer feasible. Structural response solutions have to be determined in time domain using numerical procedures. In such a case, it may be advantageous to develop a solution for the acoustic perturbation pressure in time domain. The time domain solutions for the sound pressure in the enclosure due to the double wall shell and end plate motions are presented separately. Then, the total perturbation pressure inside the acoustic cavity is obtained by the superposition of the individual contributions. Validity of the latter statement stems from the assumption of an independently vibrating shell and end plate systems.

3.2.2 Acoustic Pressure due to Vibrating Shell

The perturbation pressure, p_1 due to the shell system motions, satisfies the linear acoustic wave, Eq. (3.2)

$$\nabla^2 p_1 - \beta \dot{p}_1 = \ddot{p}_1 / c_o^2 \tag{3.34}$$

On the rigid boundaries of the acoustic region, i.e., at the end plates, it is assumed that there exists no acoustic energy dissipation and therefore

$$\partial p_1/\partial x = 0 \qquad \text{at } x = 0,L \tag{3.35}$$

Furthermore, by taking into account the effect of acoustic absorption at the flexible surface of the shell system and assuming that at the interface the fluid velocity and the wall motions are equal, p_1 must also satisfy the following boundary condition

$$\partial p_1/\partial r = - \rho\ddot{w}_I - (\rho/Z_A)\dot{p}_1 \qquad \text{at } r = R \tag{3.36}$$

Equation (3.36) demonstrates that the boundary condition for pressure p_1 is nonhomogeneous at r = R. Solution of this boundary value problem can be obtained by employing a linear transformation which renders the boundary conditions homogeneous [72]. Hence,

$$p_1(x,r,\theta,t) = q_1(x,r,\theta,t) + G_1(r)\rho\ddot{w}_I(x,\theta,t) \tag{3.37}$$

where $G_1(r)$ is a function chosen to modify the given boundary conditions. Therefore a boundary value problem of an inhomogeneous differential eguation in q_1 is established, which can be solved using the resulting homogeneous boundary conditions.

Substituting Eq. (3.37) into Eqs. (3.34-3.36) yields

$$\nabla^2 q_1 - \beta \dot{q}_1 + \ddot{q}_1/c_o^2 = \rho \ddot{f}_1(x,r,\theta,t) \tag{3.38}$$

$$\partial q_1/\partial x = 0 \qquad \text{at } x = 0,L \tag{3.39}$$

$$\partial q_1/\partial r = -(\rho/Z_A)\dot{q}_1 \qquad \text{at } r = R \tag{3.40}$$

where the function $G_1(r)$ has been chosen to have the following form

$$G_1(r) = \frac{r^4}{R^3} - \frac{3r^3}{R^2} + \frac{2r^2}{R} \tag{3.41}$$

The linear transformation introduced by Eq. (3.37) requires for the function $G_1(r)$ to be defined at the boundaries. Furthermore, $G_1(r)$ is subject only to the conditions of continuity and differentiability within the domain and may be chosen arbitrarily [71]. The forcing function $f_1(x,r,\theta,t)$ is given by

$$f_1(x,r,\theta,t) = G_1(r)\left\{\frac{\ddot{w}_I}{c_o^2} + \beta \dot{w}_I - \frac{\partial^2 w_I}{\partial x^2} - \left(\frac{1}{r^2}\right)\frac{\partial^2 w_I}{\partial \theta^2}\right\} - w_I\left\{\frac{d^2 G_1}{dr^2} + \frac{1}{r}\frac{dG_1}{dr}\right\} \tag{3.42}$$

Equations (3.38-3.40) constitute the new boundary value problem. In obtaining the boundary condition given by

Eq. (3.39) at the end caps x = 0,L, it was assumed that the shell motions w_I do not extend to these boundaries. Thus, the flexible shell is located in the region $\varepsilon_o < x < L-\varepsilon_o$, where ε_o could be a small positive number but $\varepsilon_o \neq 0$.

The acoustic hard wall modes $\tilde{Y}_{ijk}$ satisfy the equations

$$\nabla^2\tilde{Y}_{ijk} + (\omega_{ijk}/c_o)^2 \tilde{Y}_{ijk} = 0 \qquad (3.43)$$

in the enclosure, and

$$\partial\tilde{Y}_{ijk}/\partial r = 0 \qquad \text{at } r = R \qquad (3.44)$$

where

$$\tilde{Y}_{ijk} = \cos(i\pi x/L) \cos j\theta \, J_j(\lambda_{jk} r) \qquad (3.45)$$

ω_{ijk} are the corresponding modal frequencies given by

$$\omega_{ijk}^2 = c_o^2 \{\lambda_{jk}^2 + (i\pi/L)^2\} \qquad (3.46)$$

The effect of acoustic absorption in Eq. (3.40) can be transferred into the governing differential euqation by making use of Green's theorem [12], which states the following

$$\int_V (q_1 \nabla^2\tilde{Y}_{ijk} - \tilde{Y}_{ijk}\nabla^2 q_1)dV = \int_S (q_1 \frac{\partial\tilde{Y}_{ijk}}{\partial r} - \tilde{Y}_{ijk} \frac{\partial q_1}{\partial r})dS \qquad (3.47)$$

where V and S indicate volume and surface integrals, respectively. Substituting Eqs. (3.38), (3.40), (3.43) and (3.44) into Eq. (3.47) it can be shown that

$$ {}_1\ddot{Q}_{ijk}(t) + 2\zeta_{ijk}\omega_{ijk}\,{}_1\dot{Q}_{ijk}(t) + \omega_{ijk}^2\,{}_1Q_{ijk}(t) + \rho c_o^2\,{}_1\ddot{F}_{ijk}(t) + (\rho c_o^2/Z_A)\frac{\partial}{\partial t}\int_A q_1\,\tilde{Y}_{ijk}\,dA = 0 \tag{3.48} $$

where

$$ {}_1Q_{ijk}(t) = \int_V q_1\,\tilde{Y}_{ijk}\,dV \tag{3.49} $$

$$ {}_1F_{ijk} = \int_V f_1\,\tilde{Y}_{ijk}\,dV \tag{3.50} $$

$$ \zeta_{ijk} = \beta c_o^2/2\omega_{ijk} \tag{3.51} $$

and A indicates that the integration is taken over the interior absorbing surface [12]. Upon expanding q_1 in terms of acoustic modes, utilizing the orthogonality principle and using Eq. (3.49), gives

$$ q_1(x,r,\theta,t) = \sum_{i=0}^{\infty}\sum_{j=0}^{\infty}\sum_{k=1}^{\infty}\tilde{\varepsilon}_{ijk}\,{}_1Q_{ijk}(t)\,\tilde{Y}_{ijk}(x,r,\theta) \tag{3.52} $$

where

$$ \tilde{\varepsilon}_{ijk} = \begin{cases} (L/2)\varepsilon_{jk} & i \neq 0 \\ L\varepsilon_{jk} & i = 0 \end{cases} \tag{3.53} $$

and ε_{jk} is given by Eq. (3.25). Substitution of Eq. (3.52) into Eq. (3.48) results in

$$\ddot{{}_1Q}_{ijk}(t) + 2\zeta_{ijk}\omega_{ijk}\,\dot{{}_1Q}_{ijk}(t) + \omega_{ijk}^2\,{}_1Q_{ijk}(t) + \rho c_o^2\,\ddot{{}_1F}_{ijk}(t)$$

$$+ \pi RL(\rho c_o^2/Z_A)\tilde{\delta}_{ij}J_j(\bar{\alpha}_{jk})\left\{\sum_{q=1}^{\infty}\tilde{\varepsilon}_{ijq}J_j(\bar{\alpha}_{jq})\,\dot{{}_1Q}_{ijq}(t)\right\} = 0 \tag{3.54}$$

where

$$\tilde{\delta}_{ij} = \begin{cases} 2 & i = 0, j = 0 \\ 1 & i = 0, j \neq 0;\ i \neq 0, j = 0 \\ 1/2 & i \neq 0, j \neq 0 \end{cases}$$

The modal forcing functions ${}_1F_{ijk}$ can be obtained from Eqs. (3.42), (3.50) and the modal solutions of the shell system motion w_I are presented in Section 2. Hence

$${}_1F_{ijk}(t) =$$

$$\sum_{m=0}^{\infty}\sum_{n=1}^{\infty} B_{mnij}\{R^3[\phi_j(5,k) - 3\phi_j(4,k) + 2\phi_j(3,k)]$$

$$[\ddot{A}^I_{mn}/c_o^2 + 2\zeta_{ijk}\omega_{ijk}\dot{A}^I_{mn}/c_o^2]$$

$$+ \{(\tfrac{m\pi}{L})^2R^3[\phi_j(5,k) - 3\phi_j(4,k) + 2\phi_j(3,k)]$$

$$+ n^2R[\phi_j(3,k) - 3\phi_j(2,k) + 2\phi_j(1,k)]$$

$$+ [16\phi_j(2,k) - 27\phi_j(1,k) + 8\phi_j(0,k)]\}A^I_{mn}\} \tag{3.55}$$

where B_{mnij} is given by

$$B_{mnij} = \begin{cases} 0 & n \neq j \\ \frac{L}{m}\{1-(-1)^m\} & m \neq 0, i = 0, n = j \neq 0 \\ \frac{2L}{m}\{1-(-1)^m\} & m \neq 0, i = 0, n = j = 0 \\ L\{\frac{1-(-1)^{m+1}}{m+i} + \frac{1-(-1)^{m-i}}{m-i}\} & m \neq i, i \neq 0, n = j = 0 \\ 0 & m = i, i \neq 0, n = j \neq 0 \\ \frac{L}{2}\{\frac{(1-(-1)^{m+i}}{m+i} + \frac{1-(-1)^{m-i}}{m-i}\} & m \neq i, i \neq 0, n = j \neq 0 \\ 0 & m = i, i \neq 0, n = j \neq 0 \end{cases} \tag{3.56}$$

and $\phi_j(\mu,k)$ is defined as

$$\phi_j(\mu,k) = \int_0^1 r^\mu J_j(\bar{\alpha}_{jk} r)dr = \bar{\alpha}_{jk}^{-(\mu+1)}[(j+\mu-1)\bar{\alpha}_{jk} J_j(\bar{\alpha}_{jk}) + S_{\mu-1,j-1}(\bar{\alpha}_{jk})$$

$$- \bar{\alpha}_{jk} J_{j-1}(\bar{\alpha}_{jk}) S_{\mu,j}(\bar{\alpha}_{jk}) + 2^\mu \frac{\Gamma(1/2 + 1/2\mu + 1/2j)}{\Gamma(1/2 + 1/2j - 1/2\mu)} \tag{3.57}$$

In Eq. (3.57) $\Gamma, S_{\mu,j}$ represent Gamma and Lommel functions, respectively [73]. A^I_{mn} are the generalized coordinates corresponding to the inner shell motions of the double wall system described in Section 2. Finally, combining Eqs. (3.32) and (3.52), the solution for the perturbation pressure inside the enclosure due to the inner shell

motions is given by

$$p_1(x,r,\theta,t)$$

$$= \sum_{i=0}^{\infty} \sum_{j=0}^{\infty} \sum_{k=1}^{\infty} \tilde{\varepsilon}_{ijk}\, {}_1Q_{ijk}(t)\tilde{Y}_{ijk}(x,r,\theta) + G_1(r)\rho\ddot{w}_I(x,\theta,t) \tag{3.58}$$

where the solutions to ${}_1Q_{ijk}$ are determined from Eq. (3.54).

3.2.3 Acoustic Pressure due to Vibrating End Plates

The perturbation pressure, p_2, due to the end plates motion, satisfies the linear acoustic wave equation

$$\nabla^2 p_2 - \beta\dot{p}_2 = \ddot{p}_2/c_o^2 \tag{3.59}$$

and the boundary condtions

$$\partial p_2/\partial x = \rho\ddot{w}_B^L + (\rho/Z_L)\dot{p}_2 \quad \text{at } x = 0 \tag{3.60}$$

$$\partial p_2/\partial x = -\rho\ddot{w}_B^R - (\rho/Z_R)\dot{p}_2 \quad \text{at } x = L \tag{3.61}$$

$$\partial p_2/\partial r = 0 \quad \text{at } r = R \tag{3.62}$$

Equations (3.60) and (3.61) show that the boundary conditions for p_2 are nonhomogeneous at $x = 0,L$. Therefore, proceeding as in Section 3.2.2 we introduce a solution for p_2 of the following form

$$p_2(x,r,\theta,t) = q_2(x,r,\theta,t) - G_L(x)\rho\ddot{w}_B^L + G_R(x)\rho\ddot{w}_B^R \tag{3.63}$$

where G_L and G_R are functions chosen to modify the given boundary conditions. Substituting Eq. (3.63) into Eqs. (3.59-3.62) yields

$$\nabla^2 q_2 - \beta \dot{q}_2 - \ddot{q}_2/c_o^2 = \rho \ddot{f}_2(x,r,\theta,t) \tag{3.64}$$

$$\partial q_2/\partial x = (\rho/Z_L)\dot{q}_2 \qquad \text{at } x = 0 \tag{3.65}$$

$$\partial q_2/\partial x = -(\rho/Z_R)\dot{q}_2 \qquad \text{at } x = L \tag{3.66}$$

$$\partial q_2/\partial r = 0 \qquad \text{at } r = R \tag{3.67}$$

where the modifying functions $G_L(x)$ and $G_R(x)$ are chosen as

$$G_L(x) = \frac{2x^2}{L} - \frac{x^3}{L^2} - x \tag{3.68}$$

$$G_R(x) = \frac{x^2}{L} - \frac{x^3}{L^2} \tag{3.69}$$

where $G_L(x)$ and $G_R(x)$ must satisfy the requirements of continuity and differentiability as discussed in Section 3.2.2. The forcing function $f_2(x,r,\theta,t)$ is

$$\begin{aligned} f_2(x,r,\theta,t) = {} & G_L(x)\{\nabla_s^2 w_B^L - \beta \dot{w}_B^L - \ddot{w}_B^L/c_o^2\} \\ & - G_R(x)\{\nabla_s^2 w_B^R - \beta \dot{w}_B^R - \ddot{w}_B^R/c_o^2\} \\ & + d^2/dx^2\{w_B^L G_L(x) - w_B^R G_R(x)\} \end{aligned} \tag{3.70}$$

and ∇_s^2 is the two-dimensional Laplacian operator in polar coordinates. Equations (3.64-3.67) constitute the new boundary value problem. In obtaining the boundary condition given by Eq. (3.61) it was assumed that the flexible end plate motions at x = 0,L do not extend at this boundary. Thus, the flexible end plates are located in the region defined by $r < R^P - \varepsilon_o$ where ε_o is a small positive number but $\varepsilon_o \neq 0$.

Using the property of the acoustic hard wall modes $\tilde{Y}_{ijk}$ given by Eq. (3.43), and utilizing Green's theorem in the same manner as in Section 3.2.2, it may be shown that

$$\ddot{2Q}_{ijk}(t)+2\zeta_{ijk}\omega_{ijk}\,\dot{2Q}_{ijk}(t)+\omega_{ijk}^2\,{}_2Q_{ijk}(t)+\rho c_o^2\,\ddot{2F}_{ijk}(t)$$

$$+\rho c_o^2\frac{\partial}{\partial t}\left\{\frac{1}{Z_R}\int_{A_R} q_2\,\tilde{Y}_{ijk}\,dA_R-\frac{1}{Z_L}\int_{A_L} q_2\,\tilde{Y}_{ijk}\,dA_L\right\}=0 \tag{3.71}$$

with ${}_2Q_{ijk}$, ${}_2F_{ijk}$, ζ_{ijk} defined in Eqs. (3.49)-(3.51) where the subscript 1 is replaced with 2. A_R and A_L are the acoustic absorbing surfaces of the end plates at x = 0,L. The function q_2 may be expanded in terms of the acoustic hard wall modes resulting in

$$q_2(x,r,\theta,t)=\sum_{i=0}^{\infty}\sum_{j=0}^{\infty}\sum_{k=1}^{\infty}\tilde{\varepsilon}_{ijk}\,{}_2Q_{ijk}(t)\,\tilde{Y}_{ijk}(x,r,\theta) \tag{3.72}$$

where $\tilde{\varepsilon}_{ijk}$ is given by Eq. (3.53). Substitution of Eq. (3.72) into Eq. (3.71) yields

$$ {}_2\ddot{Q}_{ijk}(t) + 2\zeta_{ijk}\omega_{ijk}\,{}_2\dot{Q}_{ijk}(t)+\omega_{ijk}^2\,{}_2Q_{ijk}(t)+\rho c_o^2\,{}_2\ddot{F}_{ijk}(t) $$

$$ + \rho c_o^2\{\frac{R\varepsilon_{jk}^P}{Z_R}\sum_{r=0}^{\infty}(-1)^{i+r}\,\tilde{\varepsilon}_{rjk}\,{}_2\dot{Q}_{rjk} - \frac{L\varepsilon_{jk}^P}{Z_L}\sum_{r=0}^{\infty}\tilde{\varepsilon}_{rjk}\,{}_2\dot{Q}_{rjk}\} = 0 \qquad (3.73) $$

where

$$ {}_{L,R}\varepsilon_{jk}^P = \begin{cases} \frac{\pi}{2\lambda_{jk}^2}\,[\bar{\alpha}_{jk}^2\xi^2 - j^2][J_j(\bar{\alpha}_{jk}\xi)]^2 & j \neq 0 \\ \pi(R^P)^2\,[J_0(\bar{\alpha}_{0k}\xi)]^2 & j = 0 \end{cases} \qquad (3.74a) $$

$$ \xi = R^P/R \qquad (3.74b) $$

The modal forcing functions ${}_2F_{ijk}$ can be obtained from Eqs. (3.70) and (3.50) and the modal solutions of the end plates motions given in Section 2. Therefore

$$ {}_2F_{ijk}(t) = \tau_j[\{\chi_i(1) - 2\chi_i(2) + \chi_i(3)\}\{\sum_{q=1}^{\infty}[{}_Lk_{jq}^2 A_{jq}^L \cdot $$

$$ \cdot \{\phi_{jkq}^L + \frac{J_j({}_L\lambda_{jq}^S)}{I_j({}_L\lambda_{jq}^S)}\,\tilde{\phi}_{jkq}^L\} + \{\beta\,\dot{A}_{jq}^L + \ddot{A}_{jq}^L/c_o^2\} \cdot $$

$$ \cdot \{\phi_{jkq}^L - \frac{J_j({}_L\lambda_{jq}^S)}{I_j({}_L\lambda_{jq}^S)}\,\tilde{\phi}_{jkq}^L\}] + \{\chi_i(2) - \chi_i(3)\} \cdot $$

$$\cdot \left\{ \sum_{q=1}^{\infty} {}_R k_{jq}^2 \, A_{jq}^R \left\{ \psi_{jkq}^R + \frac{J_j({}_R\lambda_{jq}^s)}{I_j({}_R\lambda_{jq}^s)} \tilde{\psi}_{jkq}^R \right\} \right.$$

$$\left. + \left\{ \beta \, \dot{A}_{jq}^R + \ddot{A}_{jq}^R / c_o^2 \right\} \left\{ \psi_{jkq}^R - \frac{J_j({}_R\lambda_{jq}^s)}{I_j({}_R\lambda_{jq}^s)} \tilde{\psi}_{jkq}^R \right\} \right]$$

$$+ \left\{ 4\kappa_i - 6\tilde{\chi}_i(1) \right\} \sum_{q=1}^{\infty} A_{jq}^L \left\{ \psi_{jkq}^L - \frac{J_j({}_L\lambda_{jq}^s)}{I_j({}_L\lambda_{jq}^s)} \tilde{\psi}_{jkq}^L \right\}$$

$$- \left\{ 4\kappa_i - 6\tilde{\chi}_i(1) \right\} \sum_{q=1}^{\infty} A_{jq}^R \left\{ \psi_{jkq}^R - \frac{J_j({}_R\lambda_{jq}^s)}{I_j({}_R\lambda_{jq}^s)} \tilde{\psi}_{jkq}^R \right\} \qquad (3.75)$$

where

$$\chi_i(n) = \begin{cases} L^2/(n+1) & i = 0, \; n = 1,2,\ldots \\ \dfrac{L^2}{2(n+1)} \left[{}_1F_1(n+1;n+2;\underset{\sim}{i}\eta_i) \right. & \\ \qquad \left. + \, {}_1F_1(n+1;n+2;-\underset{\sim}{i}\eta_i) \right] & i \neq 0, \; n = 1,2,\ldots \end{cases} \qquad (3.76a)$$

$$\tilde{\chi}_i(n) = \chi_i(n)/L^2 \qquad (3.76b)$$

$$\eta_i = i\pi/L \qquad (3.77)$$

$$\tau_j = \begin{cases} 2\pi & j = 0 \\ \pi & j \neq 0 \end{cases} \qquad (3.78)$$

$$\kappa_i = \begin{cases} 0 & i \neq 0 \\ 1 & i = 0 \end{cases} \tag{3.79}$$

$$\phi^{L,R}_{jkq} = \int_0^{R^P} J_j(k^{L,R}_{sq} r)\, J_j(\lambda_{jk} r) r dr$$

$$= (R^P)^2 \left\{ \frac{{}_{L,R}\lambda^s_{jq} J_j(\bar{\alpha}_{jk}\xi)\, J_j'({}_{L,R}\lambda^s_{jq}) - \bar{\alpha}_{jk}\xi\, J_j({}_{L,R}\lambda^s_{jq}) J_j'(\bar{\alpha}_{jk}\xi)}{(\bar{\alpha}_{jk}\xi)^2 - ({}_{L,R}\lambda^s_{jq})^2} \right\} \tag{3.80}$$

$$\tilde{\phi}^{L,R}_{jkq} = \int_0^{R^P} I_j(k^{L,R}_{sq} r)\, J_j(\lambda_{jk} r) r dr$$

$$= (R^P)^2 \left\{ \frac{{}_{L,R}\lambda^s_{jq} J_j(\bar{\alpha}_{jk}\xi)\, I_j'({}_{L,R}\lambda^s_{jq}) - \bar{\alpha}_{jk}\xi\, I_j({}_{L,R}\lambda^s_{jq}) J_j'(\bar{\alpha}_{jk}\xi)}{(\bar{\alpha}_{jk}\xi)^2 + ({}_{L,R}\lambda^s_{jq})^2} \right\} \tag{3.81}$$

${}_1F_1(u;v;z)$ represent degenerate hypergeometric functions [73], J_j and I_j are Bessel and modified Bessel functions of the first kind, respectively, λ^s_{jq} are solutions of the frequency equation for circular plate vibrations described in Section 2, and $\bar{\alpha}_{jk}$ is the kth root of the equation $dJ_i/dr = 0$. In Eqs. (3.80), (3.81) a $(\,)'$ indicates differentiation with respect to the spatial variable r. Furthermore, A^L_{sq}, A^R_{sq} are the generalized coordinates of the inner plates motion described in Section 2.

Finally, combining Eqs. (3.63) and (3.72) the solution for the perturbation pressure inside the enclosure due to

the inner plates motion is given by

$$p_2(x,r,\theta,t) = \sum_{i=0}^{\infty} \sum_{j=0}^{\infty} \sum_{k=1}^{\infty} \tilde{\varepsilon}_{ijk}\, {}_2Q_{ijk}(t)\tilde{Y}_{ijk} - G_L(x)\rho\ddot{w}_B^L + G_R(x)\rho\ddot{w}_B^R \qquad (3.82)$$

where ${}_2Q_{ijk}$ are determined from Eq. (3.73).

Due to the assumption of independently vibrating shell and end plate systems, the complete solution for the acoustic pressure inside the acoustic cavity can be obtained by combining Eq. (3.58) and (3.82). Hence

$$p(x,r,\theta,t) = \sum_{i=0}^{\infty} \sum_{j=0}^{\infty} \sum_{k=1}^{\infty} \tilde{\varepsilon}_{ijk}\{{}_1Q_{ijk}(t) + {}_2Q_{ijk}(t)\}\tilde{Y}_{ijk}(x,r,\theta) + G_l(r)\rho\ddot{w}_I(x,\theta,t) - G_L(x)\rho\ddot{w}_B^L(r,\theta,t) + G_r(x)\rho\ddot{w}_B^R(r,\theta,t) \qquad (3.83)$$

4. NUMERICAL RESULTS

4.1 General

Numerical results presented herein correspond to the double wall sandwich shell and circular plate systems shown in Fig. 1. The following set of parameters are selected for the study: The dimensions of the double wall shell are L = 25 ft, R = 58 in, h_s = 2 in. The shell response is computed at x = L/2 and θ = 45°. The thicknesses of the external and internal shells are h_E = 0.032 in. and h_I = 0.1 in. The stiffness and material density of the core are k_s = 4.17 lb_f/in^3 and ρ_s = 3.4 x 10^{-6} lb_f-sec^2/in^4. The outer shell consists of three laminae while the inner shell is composed of ten laminae. Fiberglass and graphite fibers are used to reinforce the plexiglass material. The ratio of fibers volume to the plexiglass volume is 0.2. The fiber orientation is prescribed by angle α as shown in Fig. 1. The elastic moduli, Poisson's ratios and material densities are E_f = 7.75 x 10^6 psi, ν_f = 0.33, ρ_f = 0.0002 lb_f-sec^2/in^4, E_g = 10.5 x 10^7 psi, ν_g = 0.33, ρ_g = 0.00015 lb_f-sec^2/in^4, E_p = 2.35 x 10^5 psi, ν_p = 0.35, ρ_p = 0.00011 lb_f-sec^2/in^4 where the subscripts f,p,g denote fiberglass, graphite and plexiglass, respectively. The fiber reinforcement--same pattern is used for internal and external shell--is arranged as follows: 1st layer fiberglass, 2nd layer graphite, 3rd layer fiberglass, and so on. For the aluminum shell, E_a = 10.5 x 10^6 psi, ν_a = 0.30, ρ_a = 0.000259 lb_f-sec^2/in^4.

The viscous damping coefficient c_E and c_I are expressed in terms of modal damping ratios ζ^E_{mn} and ζ^I_{mn} corresponding to the external and internal shells. Damping in the soft core is introducted through the loss factor g_s for which values ranging from 0.02 to 0.1 are selected.

The input random pressures, p^e, p^i, and the point loads F^e_j, F^i_j $(j = 1,2)$ are assumed to be characterized by truncated Gaussian white noise spectral densities

$$S_{p^e,p^i} = \begin{cases} 8.41 \times 10^{-5} & (\text{psi})^2/\text{Hz} \quad 0 < f < 1000 \text{ Hz} \\ 0 & \text{otherwise} \end{cases} \tag{4.1}$$

$$S^{e,i}_{F_1,F_2} = \begin{cases} 0.84 & \text{lb}^2_f/\text{Hz} \quad 0 < f < 1000 \text{ Hz} \\ 0 & \text{otherwise} \end{cases} \tag{4.2}$$

The spectral densities given in Eq. (4.1) correspond to a 130 dB sound level. Numerical computations were performed using the same value of spectral density for the external and the internal loads. The frequency bandwidth was selected to be $\Delta\omega = 2\pi$ rad/sec with the upper frequency cutoff 6280 rad/sec for the aluminum shell and 8164 rad/sec for the composite shell. The random point loads were located at $x^e_1 = x^e_2 = 12.5$ ft, $x^i_1 = x^i_2 = 12.5$ ft, $\theta^e_1 = -90°$, $\theta^e_2 = 90°$, $\theta^i_1 = -90°$, $\theta^i_2 = 90°$.

The dimensions of the double wall circular plates located at x = 0,L are taken to be R^P = 58 in, $h_s^P = h_s$. The thicknesses of the inner and outer plates are $h_T = h_B$ = 0.25 in. The stiffness and material density of the core are the same as in the shell system, i.e., k_s = 4.17 lb_f/in^3 and $\rho_s = 3.4 \times 10^{-6}$ $lb_f\text{-}sec^2/in^4$. Both end plate systems are composed of aluminum, with elastic moduli $E_T = E_B = 10.5 \times 10^6$ psi, Poisson's ratios $\nu_T = \nu_B$ = 0.3 and material densities $\rho_T = \rho_B$ = 0.000259 $lb_f\text{-}sec^2/in^4$. The viscous damping coefficients c_T and c_B are expressed in terms of modal damping ratios ζ_{sq}^T and ζ_{sq}^B corresponding to the outer (top) and inner (bottom) plates, respectively. The loss factor accounting for damping in the soft core of the double wall plate systems is taken to be g_s = 0.02.

The input random pressures p^T, p^B, and the point loads F_j^T, F_j^B (j = 1,2) are assumed to be characterized by truncated Gaussian white noise spectral densities

$$S_{p^T,p^B} = \begin{cases} 8.41 \times 10^{-7} \ (psi)^2 \ Hz & 0 < f < 1000 \ Hz \\ 0 & \text{otherwise} \end{cases} \qquad (4.3)$$

$$S_{F_1,F_2}^{T,B} = \begin{cases} 0.84 \ lb_f^2/Hz & 0 < f < 1000 \ Hz \\ 0 & \text{otherwise} \end{cases} \qquad (4.4)$$

The spectral densities given in Eq. (4.3) correspond to a

110 dB sound level. The noise levels and the magnitudes of input point loads characterized by spectral densities given in Eqs. (4.1-4.4) were selected in such a way that the resulting maximum shell or plate response is linear and equal to about one half value of the outer shell or outer plate thicknesses.

Numerical results are presented for noise transmitted and noise generated by vibrations of the cylindrical shell and circular plate systems. However, the vibrations and noise transmission of the shell and circular plates are assumed to be independent. Then, the total transmitted noise into the enclosure due to shell and end caps (circular plates) can be obtained by superposition of the individual contributions.

The speed of sound, c_o, in the enclosure, the air density ρ and flow resistivity of porous acoustic material lining, R_1, of the interior surfaces, are taken to be c_o = 13540 in/sec, $\rho = 1.147 \times 10^{-7}$ lb_f-sec^2/in^4, $R_1 = 3.74 \times 10^{-3}$ lb_f-sec/in^4. The sound pressure levels are computed at x = L/2, r = 28 in and $\theta = 45°$. To save computation time, only one location inside the shell was selected for sound pressure calculations. The acoustic impedance of porous materials was calculated from [71]

$$Z_A = Z_L = Z_R = -\rho c_o \{(1 + 0.0571\ (2\pi R_1/\rho\omega)^{0.754}) + i(0.087\ (2\pi R_1/\rho\omega)^{0.732})\}$$

The equivalent acoustic damping parameter β due to viscous

air damping and wall absorption was obtained from

$$\beta = 2\zeta_o^a \omega^{\ell}/c_o^2 \tag{4.6}$$

where ω^{ℓ} is the lowest acoustic modal frequency in the enclosure. In using Eq. (4.6), the acoustic modal damping ratios are taken as $\zeta_{ijk} = \zeta_o^a(\omega^{\ell}/\omega_{ijk})$ with ω_{ijk} representing the modal frequencies and ζ_o^a the damping coefficient corresponding to the first lowest acoustic modal frequency in the cylindrical enclosure.

Numerical results are obtained for aluminum and fiber reinforced laminated double wall shells and aluminum double wall circular plates. The frequency range considered is 0-1300 Hz. The results are presented for uniform random pressure and for random point load inputs.

4.1.1 Deflection Response of the Double Wall Shell

The introduction of soft core in the system's formulation allows for in phase (flexural) and out of phase (dilatational) motions of the double wall shell. The modal frequencies of double wall aluminum and double wall composite shells are presented in Figs. 3-5. The fiber reinforcement pattern fiberglass/graphite is repeated for the interior and the exterior shells. The fiber orientation for the three laminae of the exterior shell are α = -45°,45°,-45° (Fig. 4) and α = 90°,0°,90° (Fig. 5). The fiber orientation for the ten laminae of the interior shell

is arranged in an alternating order with α = - 45°,45°, -45°,45°, etc., (Fig. 4) and α = 90°,0°,90°,0°, etc., (Fig. 5). The results are presented for half axial wavelengths m = 1,2,...10 and for circumferential waves n = 0,1,...20. Results plotted in Figs. 3-5 indicate that for the large shell dimensions and the ratio radius/length = 0.1933 chosen in this study, the modal frequencies at n = 0 seem to converge to a single point for all values of m = 1,2,...10. A comparison of modal frequencies of aluminum and composite shells shows that depending on fiber reinforcement orientation, significantly higher modal frequencies can be obtained for a composite shell. However, the mass of the composite shell is about 50% less than that of the aluminum shell while all the other geometric parameters remain the same. For an orthogonal orientation of fiber reinforcement, the stiffness of the composite shell is reduced. Furtheremore, a direct comparison of the results given in Fig. 4 to those in Fig. 5 indicate a different modal behavior in the latter case. For the results that follow, the fiber orientation, except when stated, of the composite shell will be the same as that given for Fig. 4.

The deflection response spectral densities for the external and internal shells due to uniform random pressure acting on the external shell are given in Fig. 6. The abscissa is a logarithmic scale, called response level (RL), in units of decibels (dB)

$$RL^{E,I}(x,\theta,\omega) = 10 \log [S_w^{E,I}(x,\theta,\omega)\Delta\omega/w_{ref}^2] \quad (4.7)$$

where the reference deflection w_{ref} is taken to be $w_{ref} = h_E = 0.032$ in. The modes that are excited by the random pressure are indicated in Fig. 6 by the symbols F and D, which refer to the flexural and dilatational, respectively, of the double wall system. For a uniform pressure distribution, only the circumferential modes for which n = 0 are excited. As can be seen from Fig. 6, only two peaks are observed in each case. Response levels for the internal shell are lower at the flexural frequencies when compared to the response levels of the external shell. However, at the dilatational frequency the trend is reversed. Vibration response at the dilatational frequencies is a function of damping, stiffness and coupling effects of the viscoelastic core. Response peaks of the composite shell are about 6dB lower than those of an aluminum shell.

The deflection response levels due to two random point loads acting on the external shell are shown in Figs. 7 and 8. As can be seen from these results, a large number of flexural and dilatational modes are excited by point loads. Due to the large number of participating modes and modal frequency overlaps as shown in Figs. 3-5, it is difficult to identify the response peaks corresponding to dilatational frequencies. However, for n = 0 the flexural and dilatational frequencies are well separated. A direct comparison of these results indicates that at most

frequencies the response levels of the composite shells are lower when compared to the response levels of the aluminum shells. However, at some frequency values the opposite is true. Similar results are presented in Fig. 9 but for the point loads acting on the interior shell. As can be seen from Figs. 8 and 9, response levels at the first three peaks are about the same for both of these cases. However, significantly different vibration levels might be observed at other frequencies when the input point loads are moved from external to internal shells. The location and magnitude of these loads are the same for both cases.

To demonstrate the effect of shell and core damping, results are presented in Figs. 10 and 11 for constant modal damping ratios, $\zeta^{E}_{mn} = \zeta^{I}_{mn} = \zeta_{o} = 0.04$ and $g_{s} = 0.1$. The point loads are acting on the interior shell for both of these cases. By increasing modal damping of the interior and exterior shell from 0.01 to 0.04, about 12 dB of response reduction can be gained at most modal frequencies. As can be seen from Figs. 9 and 11, only about 2-4 dB of the response reduction is achieved at some peaks when damping in the core is increased from 0.02 to 0.1. However, the shells forming a double wall construction are bonded to the core. Thus, the cumulative effect of damping on vibration response would be similar to the combined results given in Figs. 10 and 11.

The deflection response levels of the external and internal shells are presented in Fig. 12 for a fiber

orientation $\alpha = 0°,90°,0°$, etc. The modal frequencies corresponding to this case were given in Fig. 5. A direct comparison of these results to the results given in Fig. 9 indicate that the response levels are significantly higher at some frequencies when the fiber reinforcement orientation is orthogonal.

4.1.2 Deflection Response of the End Plates

The core separating the double wall end plate construction is taken to be relatively soft in order to allow for dilatational modes to be present. The coupled modal *frequencies of the double wall aluminum caps* for $s = 0,1,2,3$ (number of nodal diameters) and $q = 1,2,...10$ (number of nodal circles) are given in Table 1 where F,D represent the in phase (flexural) and out of phase (dilatational) motions of the double wall circular plates, respectively. The first three structural modes for zero number of diametrical nodes are shown in Fig. 13.

The response levels, as given by Eq. (4.7), of the inner plate of the double wall end cap construction are illustrated in Fig. 14 for various thicknesses of the outer plate. These results are for a uniform random pressure input, as given by Eq. (4.3), acting on the outer plate. The modal damping ratios are assumed to be constant, $\zeta^T_{sq} = \zeta^B_{sq} = \zeta_o = 0.06$, and the loss factor in the core $g_s = 0.02$. The thickness of the inner plate was taken to be $h_B = 0.25$ in. For a uniform random pressure excitation,

only the modes with s = 0 (i.e., no nodal diameters) are excited. As can be seen from Fig. 14, the response levels of the inner plate are significantly higher at most values of the lower frequency range when the thickness of the outer plate is h_T = 0.05 in. However, the trend is reversed when the thickness of the outer plate increases to h_T = 0.25 in. and h_T = 0.5 in. It should be noted that for h_T = 0.05 in., the response level of the inner plates almost reaches the nonlinear range and therefore assumptions made in the formulation of the theory may be violated. At higher frequency values and h_T = 0.5 in., significantly lower response levels for the inner plate are observed.

The effect on structural response due to changes in location of point loads is presented in Figs. 15 and 16. In this case, the thicknesses of the plates are taken to be $h_T = h_B$ = 0.25 in. The two point loads are acting on the outer plate and characterized by the spectral densities given in Eq. (4.4). The response levels for both the inner and outer plates are calculated at r = 0 in. (i.e., at the center of the plate) and θ = 45°. In Fig. 15 results are presented for the outer plate response due to two point loads acting on $r_1^T = r_2^T$ = 28 in. θ_1^T = - 90°, θ_2^T= 90° and $r_1^T = r_2^T$ = 10 in and θ_1^T = 0°, θ_2^T = 180°. As can be seen from these results, response levels are significantly higher at most modal frequencies when the point

loads are located at $r_1^T = r_2^T = 10$ in. and $\theta_1^T = 0°$, $\theta_2^T = 180°$. Furthermore, the number of participating modes in the response calculation is increased. However, the response level at the fundamental modal frequency (3.73 Hz) is approximately the same for both of these cases. In Fig. 16, results are presented for the vibration response of the inner plate. From the results shown in Fig. 15 and 16 it can be said that at the first two modal frequencies the response levels for both the inner and outer plates are about the same and not strongly dependent on the location of point load application.

4.1.3 Interior Noise Due to Shell Vibrations

The first sixty-four acoustic resonant frequencies for the cylindrical closed enclosure were obtained by solving Eq. (3.31) and given in Table 2. The lowest modal frequency in the enclosure is 22.56 Hz which corresponds to the first longitudinal mode (x-dimension) in the shell.

In Fig. 17, the sound pressure levels normalized to the highest peak for reverberant ($Z_A \to \infty, \beta = 0$) and highly absorbent conditions (Z_A given in Eq. (4.5), $\beta = 1 \times 10^{-7}$ rad-sec/in^2) are presented. In obtaininig these results, the following data were used: uniform random pressure corresponding to a 130 dB sound pressure level acting on the exterior shell, both shells are made of aluminum with densities $\rho_E = \rho_I = 0.000259$ lb$_f$-sec^2/in^4, elastic moduli $E_E = E_I = 10.5 \times 10^6$ psi, Poisson's ratios $\nu_E = \nu_I = 0.3$,

structural modal damping coefficients $\zeta^E_{mn} = \zeta^I_{mn} = 0.03$. The structural loss factor in the core was taken to be $g_s = 0.02$. Up to ten structural modes are included for each of the circumferential and the longitudinal directions. However, for a uniformly distributed input of an axially symmetric shell only the modes for which n = 0 are excited. As can be seen from Fig. 17, a large number of acoustic modes is excited for reverberant conditions. For highly absorbent interiors, peaks are observed only at the structural modal frequencies. The modal frequencies corresponding to the breathing mode of the flexural and dilatational motions of the double wall structure are at 490 and 600 Hz. Sound pressure levels at these frequencies are significantly higher when compared to other response peaks.

In Fig. 18, the same shell configuration is used, but the inputs are two point loads located on the exterior shell surface at $x^e_1 = x^e_2 = L/2$, $\theta^e_1 = -90°$ and $\theta^e_2 = 90°$. The structural and acoustic damping parameters are $\zeta^E_{mn} = \zeta^I_{mn} = 0.01$ and $\beta = 1 \times 10^{-8}$ rad-sec/in^2. The results of Figs. 17 and 18 indicate that many more structural modes are excited for point load inputs. Even though the sound pressure levels in a shell with large acoustic absorption are dominated by the flexural vibration mode, the sound pressure levels at other structural modes excited by point loads are relatively high. The results presented in these figures clearly illustrate the difference between

the noise transmitted due to a uniformly distributed acoustic pressure input and sound generated (structureborne noise) by point loads.

The results shown in Fig. 19 are for the same shell and identical point load excitation, but higher modal and core damping. It is seen from Fig. 19 that for higher damping in the shell and the core the sound pressure levels are significantly lower at the modal response peaks.

Figure 20 depicts sound pressure levels for an aluminum and fiber reinforced laminated shell under exterior point load inputs, with $\zeta^E_{mn} = \zeta^I_{mn} = 0.01$, $g_s = .02$ and $\beta = 1. \times 10^8$ rad-sec/in^2. As can be observed from these results, the noise levels generated by a composite shell are higher than the noise levels for an aluminum shell at most frequencies. The mass of the composite shell is about one half of the mass of the aluminum shell. However, the composite shell is much stiffer than the aluminum one. For a shell structure, a shift in modal frequency could induce different coupling between structural and acoustic modes. The effect of structural and acoustic damping on sound generation is illustrated in Fig. 21. These results correspond to $\beta = 1 \times 10^{-8}$ rad-sec/in^2. As can be seen from these results, a significant amount of noise reduction can be achieved in a composite shell by increasing structural and acoustic damping. The results shown in Fig. 21 indicate that for acoustically hard interior walls ($Z_A \to \infty$), the noise levels in the cylinder become

relatively large.

A direct comparison of interior sound pressure levels in the cylinder excited by exterior and interior point loads is given in Fig. 22. The loading conditions are the same for both cases. Since vibration coupling is provided by the viscoelastic core, the noise generated in the interior is a function of how the point loads are acting on the double wall shell. The results presented in Fig. 22 correspond to point loads acting on the interior shell at $x_1^i = x_2^i = L/2$, $\theta_1^i = -90°$ and $\theta_2^i = 90°$. The fiber orientation of the three layers (Fig. 1) at the exterior shell is described in Fig. 23. The fiber orientation for the ten layers of the interior shell are: (A) 0°,22.5°, 45°,45°,22.5°,0°,90°,90°,90°,90° (B) 90°,0°,90°,0°,90°,0°, 90°,0°,90°,0° (c) -45°,45°,-45°,45°,-45°,45°,-45°,45°, -45°,45°. These results show that shell response and interior noise are functions of fiber orientation in a composite shell. The interior noise levels might be tailored to meet specific needs by selecting a suitable fiber orientation. However, interior noise is a function of frequency and only specific frequency bands might be affected by this procedure.

4.1.4 Interior Noise Due to End Plate Vibrations

In Fig. 24, the first three radial acoustic modes are illustrated. These results were obtained from Eq. (3.12) for zero number of nodal diameters (i.e., j = 0, no

variation in θ-direction) and k = 1,2,3, where k represents number of nodal circles (r-direction).

The sound pressure levels at x = L/2, r = 23 in. and θ = 45° due to noise transmitted through the double wall circular end plates located at x = L, are shown in Fig. 25 for reverberant and absorbent interiors. The input is a uniform 120 dB acoustic pressure acting on the exterior end plate. In this case, the end plate located at x = 0 is assumed to be rigid. The reverberant and absorbent conditions are simulated by selecting $Z_L, Z_R \to \infty$, $\beta = 0$, and Z_L, Z_r as given in Eq. (4.5) and $\beta = 1 \times 10^{-7}$ rad-sec/in^2, respectively. As can be seen from Fig. 25, a large number of acoustic modes are excited by the vibration of the end plates for reverberant conditions. Modal plate damping is taken to be constant and equal to $\zeta^T_{sq} = \zeta^B_{sq} = 0.06$. The structural loss factor of the core $g^p_s = 0.02$. The noise transmission of the end caps is predominantly low frequency. The fundamental circular plate frequency is 3.73 Hz while the lowest acoustic modal frequency in the shell enclosure is 22.56 Hz. From these results and the results presented in Fig. 17 it can be seen that under uniform random pressure input, the noise transmitted by the double wall shell and circular end plates could be relatively large over the selected frequency range.

The results presented in Fig. 26 illustrate the difference between the noise tranmsmitted due to a uniformly distributed acoustic pressure input and sound

generated by point loads. In both cases, the random excitations are acting on the exterior plate of the double wall construction located at x = L and the end plate located at x = 0 is assumed to be rigid. The uniform input is 120 dB acoustic pressure and the two point loads are characterized by a truncated Gaussian white noise spectral density given by Eq. (4.2) and are located at $r_1^T = r_2^T = 28$ in. and $\theta_1^T = -90°$ $\theta_2^T = 90°$. The absorbent conditions are described in Eq. (4.5) and the equivalent acoustic camping parameter is $\beta = 1 \times 10^{-7}$ rad-sec/in^2. The modal damping ratios are taken to be constant and equal to 0.06. The loss factor of the core $g_s^p = 0.02$. The sound pressure levels are calculated at x =L/2, r = 23 in, $\beta = 45°$. From Fig. 26 it can be seen that the uniform acoustic pressure tends to generate more noise in the low frequency region while the sound generated by point loads inside the enclosure is about 10-15 dB higher in the high frequency region.

4.1.5 Total Interior Noise

Due to the assumption of independently vibrating double wall shell and end plate systems, the total interior pressure can be calculated by a superpositon of the individual contributions. In Fig. 27 results are shown of noise generated inside the enclosure due to uniform random pressure applied on the exterior surfaces of the double wall shell and double wall end plates. It can be seen that

transmitted noise is dominated by end plate vibrations for frequencies up to 200 Hz and by shell vibrations for frequencies above 200Hz. Then, the total interior pressure is presented in Fig. 28. These results indicate that neglecting noise transmitted by the end caps would underestimate interior sound pressure levels for the low frequency region. Similar results are presented in Figs. 29 and 30 but for random point load inputs. These loads were applied on the exterior surfaces of the shell and end plate systems. As can be observed from these results, low frequency noise is dominated by end plate motions.

5. CONCLUDING REMARKS

An analytical model has been developed to predict vibration response and noise transmission of double wall circular plates and double wall laminated composite shells to random inputs. Results indicate that the shell response is strongly dependent on damping characteristics of the shell material and the core, location of the point load action, and reinforcing fiber orientation of the different laminae. In general, the response levels for a composite double wall shell are lower at most frequencies than those of an equivalent aluminum shell. The vibration response of the end caps (circular plates) are predominantly low frequency with the largest peak occuring at the fundamental mode.

The interior noise is strongly dependent on damping characteristics of the shell and the core, location of the point load action, fiber orientation of the different laminae and wall absorption of the interior walls. A fiber reinforced composite double wall shell tends to generate more noise than an equivalent aluminum shell. This is due to the fact that the mass of the composite shell is about one half of the mass of the aluminum shell and increase of the modal frequencies of the stiffer composite shell could induce different coupling of the structural-acoustic modes. The noise transmitted by the end caps is predominantly low frequency. Thus, neglecting noise transmitted by the end caps could underestimate interior sound pressure

levels for the low frequency region. Furthermore, by a proper selection of structural damping, reinforcing fiber orientation, acoustic absorption and core stiffness, a significant amount of lower response and higher noise attenuation can be achieved by a design consisting of double wall laminated fiber reinforced composite shells and a soft viscoelastic core.

REFERENCES

1. Davis, G.W. and Sakata, I.F., "Design Considerations for Composite Fuselage Structure of Commercial Transport Aircraft," NASA CR-159296, March 1981.

2. Yang, J.C.S. and Tsui, C.Y., "Optimum Design of Structures and Composite Materials in Response to Aerodynamic Noise and Noise Transmission," NASA CR-155332, December 1977.

3. Durchlaub, E.C., "Minimized Fuselage Vibrations Using Advanced Composites," 33rd Annual National Forum of the American Helicopter Society, Paper No. 77.33-84, Washington, D.C., May 1977.

4. Koval, L.R., "Sound Transmission into a Laminated Composite Shell," Journal of Sound and Vibration, Vol. 71, 1980, pp. 523-530.

5. Bieniek, M.P. and Freudenthal, M.A., "Frequency Response Functions of Orthotropic Sandwich Plates," Journal of Aerospace Sciences, Vol. 28, No. 9, Sept. 1961.

6. Freudenthal, M.A. and Bieniek, M.P., "Forced Vibrations of Sandwich Structures," WADD Technical Report 60-307, U.S. Air Force, Jan. 1961.

7. Narayanan, S. and Shanbhag, R.L., "Acoustoelasticity of a Damped Sandwich Panel Backed by a Cavity," Journal of Sound and Vibration, Vol. 78, 1981, pp. 453-473.

8. Koval, L.R., "On Sound Transmission into a Thin Cylindrical Shell under Flight Conditions," Journal of Sound and Vibration, Vol. 48, 1976, pp. 265-275.

9. Vaicaitis, R., "Noise Transmission into a Light Aircraft," Journal of Aircraft, Vol. 17, 1980, pp. 81-86.

10. White, P.H., "Sound Transmission through a Finite Closed Cylindrical Shell," Journal of the Acoustical Society of America, Vol. 40, 1966, pp. 1121-1130.

11. Pope, L.D., "On the Transmission of Sound through Finite Closed Shells Statistical Analysis, Modal Coupling, and Non-Resonant Transmission," Journal of the Acoustical Society of America, Vol. 50, 1971, pp. 1004-1018.

12. Dowell, E.H., Gorman, G.F. and Smith, D.A., "Acousto-elasticity: General Theory, Acoustic Natural Modes and Forced Response to Sinusoidal Excitations including Comparisons with Experiment," Journal of Sound and Vibration, Vol. 52, 1977, pp. 519-542.

13. Dowell, E.H., "Interior Noise Studies for Single and and Double Walled Cylindrical Shells," Journal of Aircraft, Vol. 17, 1980, pp. 690-699.

14. Ungar, E.E., "A Guide for Estimation of Aeroacoustic Loads on Flight Vehicle Surfaces," AFFDL-TR-76-91, Vol. 1, 1977.

15. Bhat, R.B. and Mixson, J.S., "A Theoretical Investigation of Noise Reduction through the Cylindrical Fuselage of a Twin-Engine, Propeller-Driven Aircraft," NASA Technical Paper 1325, 1978.

16. Unruh, J.F., "Structure-Borne Noise Prediction for Single-Engine General Aviation Aircraft," Journal of Aircraft, Vol. 18, No. 8, 1981, pp. 687-694.

17. Wilby, J.F. and Pope, L.D., "Prediction of the Acoustic Environment in the Space Suttle Payload Bay," Journal of Spacecraft and Rockets, Vol. 17, No. 3, 1979, pp. 232-239.

18. Pope, L.D., Rennison, D.C., Willis, C.M. and Mayes, W.H., "Development and Validation of Preliminary Analytical Models for Aircraft Interior Noise Prediction," Journal of Sound and Vibration, Vol. 82, No. 4, 1982, pp. 541-575.

19. Pope, L.D. and Wilby, E.G., "Analytical Prediction of the Interior Noise for Cylindrical Models of Aircraft Fuselages for Prescribed Exterior Noise Fields, Phase II, Models for Sidewall Trim, Stiffened Structures, and Cabin Acoustics with Floor Partition," NASA CR-165869, 1982.

20. Balena, F. and Prydz, R., "Experimental and Predicted Noise Reduction of Stiffened and Unstiffened Cylinders With and Without a Limp Inner Wall," AIAA Paper 81-1968, 1981.

21. Dym, C.L. and Lang, M.S., "Transmission of Sound through Sandwich Panels," Journal of the Acoustical Society of America, Vol. 56, No. 5, November 1974, pp. 1523-1532.

22. Wilby, J.F., "The Prediction of Interior Noise of Propeller-Driven Aircraft: A Review," SAE Technical

Paper Series, Paper No. 830737, 1983.

23. Weingarten , V.I., "Free Vibration of Thin Cylindrical Shells," Vol. 2, No. 4, April 1964, pp. 717-721.

24. Yu, Y.-Y., "Free Vibrations of Thin Cylindrical Shells having Finite Lengths with Freely Supported and Clamped Edges," Transactions of the ASME, Journal of Applied Mechanics, Vol. 77, 1955, pp. 547-552.

25. Forsberg, K., "Influence of Boundary Conditions on the Modal Response of Thin Cylindrical Shells," AIAA Journal, Vol. 2, No. 12, Dec. 1964, pp. 2150-2157.

26. Arnold, R.N. and Warburton, G.B., "The Flexural Vibrations of Thin Cylinders," Proceedings of the Institution of Mechanical Engineers, Vol. 167, 1953, pp. 62-74.

27. Warburton, G.B., "Vibration of Thin Cylindrical Shells," Mechanical Engineering Science Journal, Vol. 7, No. 4, 1965, pp. 399-407.

28. Leissa, A.W. and Iyer, K.M., "Modal Response of Circular Cylindrical Shells with Structural Damping," Journal of Sound and Vibration, Vol. 77, No. 1, 1981, pp. 1-10.

29. Das, Y.C., "Vibrations of Orthotropic Cylindrical Shells," Applied Scientific Research, Vol. A12, 1964, pp. 317-326.

30. Gottis, M.G., "On the Dynamic Response of an Orthotropic Finite Cylindrical Shell to an Arbitrary Pressure Field," Journal of Sound and Vibration, Vol. 7, No. 1, Jan. 1968 pp. 31-38.

31. Jones, R.M. and Klein, S., "Equivalence Between Single Layered and Certain Multilayered Shells," AIAA Journal, Vol. 6, No. 12, Dec. 1968, pp. 2295-2300.

32. White, J.C., "The Flexural Vibrations of Thin Laminated Cylinders," Transactions of the ASME, Series B: Journal of Engineering for Industry, Vol. 83, No. 4, Nov. 1961, pp. 397-402.

33. Weingarten, V.I., "Free Vibrations of Multilayered Cylindrical Shells," Experimental Mechanics, Vol. 4, No. 7, July 1964, pp. 200-205.

34. Dong, S.B., "Free Vibrations of Laminated Orthotropic Cylindrical Shells," The Journal of the Acoustical Society of America, Vol. 44, No. 6, Dec. 1968, pp. 1628-1635.

35. Soedel, W., "Simplified Equations and Solutions for the

Vibration of Orthotropic Cylindrical Shells," Journal of Sound and Vibration, Vol. 87, No. 4, 1983, pp. 555-566.

36. Hsu, T.- M. and Wang, J. Ting-Shun, "Rotationally Symmetric Vibrations of Orthotropic Layered Cylindrical Shells," Journal of Sound and Vibration, Vol. 16. No. 4, 1971, pp.473-487.

37. Bushnell, D., "Dynamic Response of Two Layered Cylindrical Shells to Time-Dependent Loads," AIAA Journal, Vol. 3, No. 9, Sept. 1965, pp. 1698-1703.

38. Reck, R.J. and McClymonds, K.A., "An Analysis for the Dynamic Response of Multilayered Orthotropic Cylindrical Shells," Rept. No. SM-47851, April 1965, Missile and Space Systems Div., Douglas Aircraft Co. Inc.

39. Keeffe, R.E. and Windholz, W.M., "Dynamic Analysis of Multilayered Cylinder," AIAA Paper 68-350, Palm Springs, Calif., 1968.

40. Dong, R.M., Pister, K.S. and Taylor, R.L., "On the Theory of Laminated Anisotropic Shells and Plates," Journal of Aerospace Sciences, Vol. 29, No. 8, Aug. 1962, pp. 969-975.

41. Bert, C.W., "Structural Theory for Laminated Anisotropic Shells," Journal of Composite Materials, Vol. 1, No. 4, Oct. 1967, pp. 414-423.

42. Bert, C.W., Baker, J.L. and Eagle, D.M., "Free Vibrations of Multilayered Anisotropic Cylindrical Shells," Journal of Composite Materials, Vol. 3, No. 4, July 1969, pp. 480-499.

43. Yu. Y.-Y., "Vibrations of Elastic Sandwich Cylindrical Shells," Transactions of the ASME, Series E: Journal of Applied Mechanics, Vol. 82, No. 4, Dec. 1960, pp. 653-662.

44. Baker, E.H. and Hermann, G., "Vibrations of Orthotropic Cylindrical Sandwich Shells under Initial Stress," AIAA Journal, Vol. 4, No. 6, June 1966, pp. 1063-1070.

45. Bieniek, M.P. and Freudenthal, A.M., "Forced Vibrations of Cylindrical Sandwich Shells," Journal of the Aerospace Sciences, Vol. 29, No. 2, Feb. 1962, pp. 180-184.

46. Martin, R.E., "Theory of Sandwich Shells with Laminated Anisotropic Facings," AIAA Journal, Vol. 6, No. 11, Nov. 1968, pp. 2232-2235.

47. Padoran, J. and Koplik, B., "Vibrations of Closed and Open Sandwich Cylindrical Shells Using Refined Theory," The Journal of the Acoustical Society of America, Vol. 47, No. 3(Part 2),1970, pp. 862-869.

48. Smith, P.W., "Sound Transmission through Thin Cylindrical Shells," Journal of the Acoustical Society of America, Vol. 29, 1957, pp. 721-729.

49. Foxwell, J.M. and Franklin, R.E., "The Vibrations of a Thin-Walled Stiffened Cylinder in an Acoustic Field," The Aeronautical Quarterly, Vol. 10, 1959, pp. 47-64.

50. Koval, L.R., "Effect of Cavity Resonances on Sound Transmission into a Thin Cylindrical Shell," Journal of Sound and Vibration, Vol. 59, 1978, pp. 23-33.

51. Narayanan, S. and Shanbhag, R.L., "Sound Transmission through Layered Cylindrical Shells with Applied damping Treatment," Journal of Sound and Vibration, Vol. 92, 1984, pp. 541-558.

52. Vaicaitis, R., "Noise Transmission by Viscoelastic Sandwich Panels," NASA-TND-8516, 1977.

53. Bert, C.W. and Eagle, M.D., "Dynamics of Composite, Sandwich, and Stiffened Shell-Type Structures," Journal of Spacecraft and Rockets, Vol. 6, No. 12, Dec. 1969, pp. 1345-1361.

54. Soedel, W., Vibrations of Shells and Plates, Marcell Dekker Inc., 1981.

55. Kraus, H., Thin Elastic Shells, Wiley, New York, 1967.

56. Calcotte, W., Composite Structures, Wiley, New York, 1967.

57. Timoshenko, S., Woinowsky-Krieger, S., Theory of Plates and Shells, McGraw-Hill, 2nd ed., New York, 1959.

58. Kunukkasseril, V.X. and Swamidas, A.S.J., "Normal Modes of Elastically Connected Circular Plates," Journal of Sound and Vibration, Vol. 30, No. 1, 1973, pp. 99-108.

59. Chonan, S., "The Free Vibrations of Elastically Connected Circular Plate Systems with Elastically Restrained Edges and Radial Tensions," Journal of Sound and Vibration, Vol. 49, No. 1, 1976, pp. 129-136.

60. Schlack Jr., A.L., Kessel, W.N. and Dong, W.N., "Dynamic Response of Elastically Supported Circular Plates

to a General Surface Load," AIAA Journal, Vol. 10, No. 6, June 1972, pp. 733-738.

61. Reismann, H., "Forced Vibrations of a Circular Plate," Journal of Applied Mechanics, Vol. 26, 1959, pp. 526-527.

62. Wah, T., "Vibration of Circular Plates," Journal of the Acoustical Society of America, Vol. 34, No. 3, 1962, pp. 275-281.

63. Anderson, G., "On the Determination of Finite Integral Transforms for Forced Vibrations of Circular Plates," Journal of Sound and Vibration, Vol. 9, 1969, pp. 126-144.

64. Weiner, R.S., "Forced Axisymmetric Motions of Circular Elastic Plates," Journal of Applied Mechanics, Vol. 4 1965, pp. 893-989.

65. Leissa, A.W. and Narita, Y., "Natural Frequencies of Simply Supported Circular Plates," Journal of Sound and Vibration, Vol. 70, No. 2, 1980, pp. 221-229.

66. Jacquot, R.G. and Lindsay, J.E., "On the Influence of Poisson's ratio on Circular Plate Natural Frequencies," Journal of Sound and Vibration,Vol. 52, 1977, pp. 603-605.

67. Smolenski, C.P. and Krokosky, E.M., "Dilatational Mode Transmission in Sandwich Panels," Journal of the Acoustical Society of America, Vol. 54, No. 6, 1973, pp. 1449-1457.

68. Meirovitch, L., Analytical Methods in Vibrations, MacMillan, New York, 1967.

69. McLachlan, N.W., Bessel Functions for Engineers, 2nd ed., Clarendon Press, Oxford, England, 1955.

70. Lin, Y.K., Probabilistic Theory of Structural Dynamics, McGraw-Hill Inc., 1967.

71. Beranek, L.L., Noise and Vibration Control, McGraw-Hill, New York, 1971.

72. Mindlin, R.D. and Goodman, L.E., "Beam Vibrations with Time Dependent Boundary Conditions," Journal of Applied Mechanics, Vol. 50, pp. 377-380.

73. Gradshteyn, I.S. and Ryzhik, I.M., Table of Integrals, Series and Products, Academic Press, New York, 1965.

APPENDIX I - ELASTIC MODULI

Following Refs. 34,54 the elements of $[C^{(k)}]$ for the kth lamina are given by

$$C_{11} = Q_{11}\cos^4\alpha + 2(Q_{12}+ 2Q_{66})\sin^2\alpha \cos^2\alpha + Q_{22}\sin^4\alpha \quad (I-1)$$

$$C_{12} = (Q_{11}+Q_{22}-4Q_{66})\sin^2\alpha \cos^2\alpha + Q_{12}(\sin^4\alpha+\cos^4\alpha) \quad (I-2)$$

$$C_{22} = Q_{11}\sin^4\alpha + 2(Q_{12}+2Q_{66})\sin^2\alpha \cos^2\alpha + Q_{22}\cos^4\alpha \quad (I-3)$$

$$C_{16} = (Q_{11}-Q_{12}-2Q_{66})\sin \alpha \cos^3\alpha + (Q_{12}-Q_{22}+2Q_{66})\sin^3\alpha \cos \alpha \quad (I-4)$$

$$C_{26} = (Q_{11}-Q_{12}-2Q_{66})\sin^3\alpha \cos \alpha+(Q_{12}-Q_{22}+2Q_{66})\sin \alpha \cos^3\alpha \quad (I-5)$$

$$C_{66} = (Q_{11}+Q_{22}-2Q_{12}-2Q_{66})\sin^2\alpha \cos^2\alpha +Q_{66}(\sin^4\alpha + \cos^4\alpha) \quad (I-6)$$

where α is the angle between the fiber direction and the cylindrical shell axis in the kth lamina and Q_{ij} (ij = 11,12,22,66) are given by [54]

$$Q_{11} = \frac{E_{11}}{1-\nu_{12}\nu_{21}} \quad (I-7)$$

$$Q_{22} = \frac{E_{22}}{1-\nu_{12}\nu_{21}} \quad (I-8)$$

$$Q_{12} = \frac{\nu_{12}E_{11}}{1-\nu_{12}\nu_{11}} \qquad \text{(I-9)}$$

$$Q_{66} = G_{12} \qquad \text{(I-10)}$$

Furthermore, the directional moduli E_{11},E_{22},G_{12} and Poisson's ratios, ν_{12},ν_{21} can be expressed in the terms of the volume ratio of fiber and matrix material [54]

$$E_{11} = E_f V_f + E_m V_M \qquad \text{(I-11)}$$

$$E_{22} = E_m(1 + \alpha' V_f)/V_m \qquad \text{(I-12)}$$

$$\nu_{12} = \nu_f V_v + \nu_m V_m \qquad \text{(I-13)}$$

$$\nu_{21} = \nu_{12}E_{11}/E_{22} \qquad \text{(I-14)}$$

$$G_{12} = G_m(1 + \beta' V_f)/V_m \qquad \text{(I-15)}$$

where

$$\alpha' = [E_f/E_m) - 1]/[(E_f/E_m) + 1] \qquad \text{(I-16)}$$

$$\beta' [(G_f/G_m)-1]/(G_f/G_m) + 1] \qquad \text{(I-17)}$$

The subscripts m,f refer to matrix and fiber material, V refers to volume fraction and E,G,ν represent the modulus

of elasticity, shear modulus and Poisson's ratio, respectively. Finally, using Eqs.(II-7)-(II-17) into Eqs. (II-1)-(II-6) the elastic moduli $C_{ij}^{(k)}$ can be expressed in terms of directional moduli E_{11},E_{22},E_{12}, angle α, and volume fractions V_F,V_m. It should be noted that the subscripts 1,2 in directional moduli and Poisson's ratios notation refer to fiber direction and should not be confused with subscripts indicating position of element in elastic moduli matrix $[C^{(k)}]$.

APPENDIX II

(a) Differential operators L_{ij}

The differential operators used in equations (2.7-2.9) are

$$L_{11} = A_{11} \frac{\partial^2}{\partial x^2} + \frac{2A_{16}}{R} \frac{\partial^2}{\partial \theta \partial x} + \frac{A_{66}}{R^2} \frac{\partial^2}{\partial \theta^2} - \rho \frac{\partial^2}{\partial t^2}$$

$$L_{12} = \bar{A}_{16} \frac{\partial^2}{\partial x^2} + \frac{\bar{A}_{12}}{R} \frac{\partial^2}{\partial \theta \partial x} + \frac{\bar{A}_{26}}{R^2} \frac{\partial^2}{\partial \theta^2}$$

$$L_{13} = \frac{A_{12}}{R} \frac{\partial}{\partial x} + \frac{A_{26}}{R^2} \frac{\partial}{\partial \theta} - B_{11} \frac{\partial^3}{\partial x^3} - \frac{3}{R} B_{16} \frac{\partial^3}{\partial x^2 \partial \theta} - \frac{B_{17}}{R^2} \frac{\partial^3}{\partial x \partial \theta^2} - \frac{B_{26}}{R^3} \frac{\partial^3}{\partial \theta^3}$$

$$L_{22} = A'_{66} \frac{\partial^2}{\partial x^2} + \frac{2}{R} A'_{26} \frac{\partial^2}{\partial x \partial \theta} + \frac{1}{R^2} A'_{22} \frac{\partial^2}{\partial \theta^2} - \rho \frac{\partial^2}{\partial t^2}$$

$$L_{23} = \frac{1}{R} \bar{A}_{26} \frac{\partial}{\partial x} + \frac{1}{R^2} \bar{A}_{22} \frac{\partial}{\partial \theta} - \bar{B}_{16} \frac{\partial^3}{\partial x^3} - \frac{1}{R} \bar{B}_{17} \frac{\partial^3}{\partial x^2 \partial \theta} - \frac{3}{R^2} \bar{B}_{26} \frac{\partial^3}{\partial x \partial \theta^2} - \frac{1}{R^3} \bar{B}_{22} \frac{\partial^3}{\partial \theta^3}$$

$$L_{33} = \frac{1}{R^2} A_{22} - \frac{2}{R} B_{12} \frac{\partial^2}{\partial x^2} - \frac{4}{R^2} B_{26} \frac{\partial^2}{\partial \theta \partial x} - \frac{2}{R^3} B_{22} \frac{\partial^2}{\partial \theta^2} + D_{11} \frac{\partial^4}{\partial x^4} + \frac{4}{R} D_{16} \frac{\partial^4}{\partial x^3 \partial \theta} + \frac{\partial^2}{\partial t^2} + \frac{2}{R^2} D_{17} \frac{\partial^4}{\partial x^2 \partial \theta} + \frac{4}{R^3} D_{26} \frac{\partial^4}{\partial x \partial \theta^3} + \frac{1}{R^4} D_{22} \frac{\partial^4}{\partial \theta^4} + \rho \frac{\partial^2}{\partial t^2} \quad \text{(II-1)}$$

where

$$\bar{A}_{12} = A_{12} + \frac{B_{12}}{R} + A_{66} + \frac{B_{66}}{R}$$

$$\bar{A}_{ij} = A_{ij} + \frac{B_{ij}}{R} \qquad (ij = 16,22,26,66)$$

$$B_{17} = B_{12} + 2B_{66}$$

$$\bar{B}_{ij} = B_{ij} + \frac{D_{ij}}{R} \qquad (ij = 16,17,22,26)$$

$$A'_{ij} = \bar{A}_{ij} + \frac{\bar{B}_{ij}}{R} \qquad (ij = 22,26,66)$$

$$D_{17} = D_{12} + 2D_{66} \qquad \text{(II-2)}$$

(b) Stiffness parameters

The coefficients Z_i, X_i, Y_r, α_r in eqs. (2.11-2.14) are as follows

$$Z_1 = D_{11}\alpha_1 + B_{11}\beta_1 + \bar{B}_{16}\gamma_1$$

$$Z_2 = 2D_{11}\alpha_2 + 4D_{16}\alpha_1 + B_{11}\beta_2 + 3B_{16}\beta_1 + \bar{B}_{16}\gamma_2 + \bar{B}_{17}\gamma_1$$

$$Z_3 = D_{11}\alpha_3 + 8D_{16}\alpha_2 + 2D_{17}\alpha_1 + B_{11}\beta_3 + 3B_{16}\beta_2 + B_{17}\beta_1 + \bar{B}_{16}\gamma_3 + \bar{B}_{17}\gamma_2 + 3\bar{B}_{26}\gamma_1$$

$$Z_4 = 2D_{11}\alpha_4 + 4D_{16}\alpha_3 + 4D_{17}\alpha_2 + 4D_{26}\alpha_1$$

$$+ B_{11}\beta_4 + 3B_{16}\beta_3 + B_{17}\beta_2 + B_{26}\beta_1$$

$$+ \bar{B}_{16}\gamma_4 + \bar{B}_{17}\gamma_3 + 3\bar{B}_{26}\gamma_2 + \bar{B}_{22}\gamma_1$$

$$Z_5 = D_{11}\alpha_5 + 8D_{16}\alpha_4 + 2D_{17}\alpha_3 + 8D_{26}\alpha_2$$

$$+ D_{22}\alpha_1 + B_{11}\beta_5 + 3B_{16}\beta_4 + B_{17}\beta_3 + B_{26}\beta_2$$

$$+ \bar{B}_{16}\gamma_5 + \bar{B}_{17}\gamma_4 + 3\bar{B}_{26}\gamma_3 + \bar{B}_{22}\gamma_2$$

$$Z_6 = 4D_{16}\alpha_5 + 4D_{17}\alpha_4 + 4D_{26}\alpha_3 + 2D_{22}\alpha_2$$

$$+ B_{11}\beta_6 + 3B_{16}\beta_5 + B_{17}\beta_4 + B_{26}\beta_3$$

$$+ \bar{B}_{16}\gamma_6 + \bar{B}_{17}\gamma_5 + 3\bar{B}_{26}\gamma_4 + \bar{B}_{22}\gamma_3$$

$$Z_7 = 2D_{17}\alpha_5 + 8D_{26}\alpha_4 + D_{22}\alpha_3 + 3B_{16}\beta_6 + B_{17}\beta_5$$

$$+ B_{26}\beta_4 + \bar{B}_{17}\gamma_6 + 3\bar{B}_{26}\gamma_5 + \bar{B}_{22}\gamma_4$$

$$Z_8 = 4D_{26}\alpha_5 + 2D_{22}\alpha_4 + B_{17}\beta_6 + B_{26}\beta_5$$

$$+ 3\bar{B}_{26}\gamma_6 + \bar{B}_{22}\gamma_5$$

$$Z_9 = D_{22}\alpha_5 + B_{26}\beta_6 + \bar{B}_{22}\gamma_6 \qquad \text{(II-3)}$$

$$X_1 = -(2B_{12}\alpha_1 + A_{12}\beta_1 + B_{11}\beta_7 + \bar{A}_{26}\gamma_1 + \bar{B}_{16}\gamma_7)$$

$$X_2 = -(4B_{12}\alpha_2 + 4B_{26}\alpha_1 + A_{12}\beta_2 + A_{26}\beta_1 + B_{11}\beta_8 + 3B_{16}\beta_7 + \bar{A}_{26}\gamma_2 + \bar{A}_{22}\gamma_1 + \bar{B}_{16}\gamma_8 + \bar{B}_{17}\gamma_7)$$

$$X_3 = -(2B_{12}\alpha_3 + 8B_{26}\alpha_2 + 2B_{22}\alpha_1 + A_{12}\beta_3 + A_{26}\beta_2 + B_{11}\beta_9 + 3B_{16}\beta_8 + B_{17}\beta_7 + \bar{A}_{26}\gamma_3 + \bar{A}_{22}\gamma_2 + \bar{B}_{17}\gamma_8 + 3\bar{B}_{26}\gamma_7 + \bar{B}_{16}\gamma_9)$$

$$X_4 = -(4B_{12}\alpha_4 + 4B_{26}\alpha_3 + 4B_{22}\alpha_2 + A_{12}\beta_4 + A_{26}\beta_3 + 3B_{16}\beta_9 + B_{17}\beta_8 + B_{26}\beta_7 + B_{11}\beta_{10} + \bar{A}_{26}\gamma_4 + \bar{A}_{22}\gamma_3 + \bar{B}_{16}\gamma_{10} + \bar{B}_{17}\gamma_9 + 3\bar{B}_{26}\gamma_3 + \bar{B}_{22}\gamma_7)$$

$$X_5 = -(2B_{12}\alpha_5 + 8B_{26}\alpha_4 + 2B_{22}\alpha_3 + A_{12}\beta_5 + A_{26}\beta_4 + B_{17}\beta_9 + B_{26}\beta_8 + 3B_{16}\beta_{10} + \bar{A}_{26}\gamma_5 + \bar{A}_{22}\gamma_4 + \bar{B}_{17}\gamma_{10} + 3\bar{B}_{26}\gamma_9 + \bar{B}_{22}\gamma_8)$$

$$X_6 = -(4B_{26}\alpha_5 + 4B_{22}\alpha_4 + A_{12}\beta_6 + A_{26}\beta_5 + B_{26}\beta_9 + B_{17}\beta_{10} + \bar{A}_{26}\gamma_6 + \bar{A}_{22}\gamma_5 + 3\bar{B}_{26}\gamma_{10} + \bar{B}_{22}\gamma_9)$$

$$X_7 = -(2B_{22}\alpha_5 + A_{26}\beta_6 + B_{26}\beta_{10} + \bar{A}_{26}\gamma_6 + \bar{B}_{22}\gamma_{10}) \quad \text{(II-4)}$$

$$Y_1 = A_{22}\alpha_1 + A_{12}\beta_7 + \bar{A}_{26}\gamma_7$$

$$Y_2 = 2A_{22}\alpha_2 + A_{12}\beta_8 + A_{26}\beta_7 + \bar{A}_{26}\gamma_8 + \bar{A}_{22}\gamma_7$$

$$Y_3 = A_{22}\alpha_3 + A_{12}\beta_9 + A_{26}\beta_8 + \bar{A}_{26}\gamma_9 + \bar{A}_{22}\gamma_8$$

$$Y_4 = 2A_{22}\alpha_4 + A_{12}\beta_{10} + A_{26}\beta_9 + \bar{A}_{26}\gamma_{10} + \bar{A}_{22}\gamma_9$$

$$Y_5 = A_{22}\alpha_5 + A_{26}\beta_{10} + \bar{A}_{22}\gamma_{10} \quad \text{(II-5)}$$

$$\alpha_1 = \bar{A}_{16}^2 - A_{11}A_{66}'$$

$$\alpha_2 = \bar{A}_{16}\bar{A}_{12} - A_{11}A_{26}' - A_{16}A_{66}'$$

$$\alpha_3 = 2\bar{A}_{16}\bar{A}_{26} + \bar{A}_{12}^2 - A_{11}A_{22}' - 4A_{16}A_{26}' - A_{66}A_{66}'$$

$$\alpha_4 = \bar{A}_{12}\bar{A}_{26} - A_{16}A_{22}' - A_{66}A_{26}'$$

$$\alpha_5 = \bar{A}_{26}^2 - A_{66}A_{22}' \quad \text{(II-6)}$$

$$\beta_1 = B_{11}A_{66}' - \bar{A}_{16}\bar{B}_{16}$$

$$\beta_2 = 2B_{11}A_{26}' + 3B_{16}A_{66}' - \bar{A}_{16}\bar{B}_{17} - \bar{A}_{12}\bar{B}_{16}$$

$$\beta_3 = B_{11}A'_{22} + 6B_{16}A'_{26} + B_{17}A'_{66} - 3\bar{A}_{16}\bar{B}_{26} - \bar{A}_{12}\bar{B}_{17} - \bar{A}_{26}\bar{B}_{16}$$

$$\beta_4 = 3B_{16}A'_{22} + B_{17}A'_{26} + B_{26}A'_{66} - \bar{A}_{16}\bar{B}_{22} - 3\bar{A}_{12}\bar{B}_{26} - \bar{A}_{26}\bar{B}_{17}$$

$$\beta_5 = B_{17}A'_{22} + 2B_{26}A'_{26} - \bar{A}_{12}\bar{B}_{22} - 3\bar{A}_{26}\bar{B}_{26}$$

$$\beta_6 = B_{26}A'_{22} - \bar{A}_{26}\bar{B}_{22}$$

$$\beta_7 = A_{12}A'_{66} - \bar{A}_{16}\bar{A}_{26}$$

$$\beta_8 = 2A_{12}A'_{26} + A_{26}A'_{66} - \bar{A}_{16}\bar{A}_{22} - \bar{A}_{12}\bar{A}_{26}$$

$$\beta_9 = A_{12}A'_{22} + 2A_{26}A'_{26} - \bar{A}_{12}\bar{A}_{22} - \bar{A}_{26}^2$$

$$\beta_{10} = A_{16}A'_{22} - \bar{A}_{26}\bar{A}_{22} \qquad \text{(II-7)}$$

$$\gamma_1 = A_{11}\bar{B}_{16} - \bar{A}_{16}B_{11}$$

$$\gamma_2 = A_{11}\bar{B}_{17} + 2A_{16}\bar{B}_{16} - 3\bar{A}_{16}B_{16} - \bar{A}_{12}B_{11}$$

$$\gamma_3 = 3\bar{B}_{26}A_{11} + 2\bar{B}_{17}A_{16} + A_{66}\bar{B}_{16} - \bar{A}_{16}B_{17} - 3\bar{A}_{12}B_{16} - \bar{A}_{26}B_{11}$$

$$\gamma_4 = A_{11}\bar{B}_{22} + 6A_{16}\bar{B}_{26} + A_{66}\bar{B}_{17} - \bar{A}_{16}B_{26}$$

$$- \bar{A}_{12}B_{17} - 3\bar{A}_{26}B_{16}$$

$$\gamma_5 = 2A_{16}\bar{B}_{22} + 3A_{66}\bar{B}_{26} - \bar{A}_{12}B_{26} - \bar{A}_{26}B_{17}$$

$$\gamma_6 = A_{66}\bar{B}_{22} - \bar{A}_{26}B_{26}$$

$$\gamma_7 = A_{11}\bar{A}_{26} - \bar{A}_{16}A_{12}$$

$$\gamma_8 = A_{11}\bar{A}_{22} + 2A_{16}\bar{A}_{26} - \bar{A}_{16}A_{26} - A_{12}\bar{A}_{12}$$

$$\gamma_9 = 2A_{16}\bar{A}_{22} + \bar{A}_{26}A_{66} - \bar{A}_{12}A_{26} - \bar{A}_{26}A_{12} \qquad \text{(II-8)}$$

$$\gamma_{10} = A_{66}\bar{A}_{22} - A_{26}\bar{A}_{26}$$

APPENDIX III

The structural-acoustic coupling terms are

$$
{}_{L,R}L^{P}_{sqjk} = \begin{cases}
0 & s \neq j \\
\pi(R^{P})^{2}\left\{\dfrac{1}{[\bar{\alpha}_{jk}\xi]^{2}-({}_{L,R}\lambda^{s}_{jq})^{2}}\left[{}_{L,R}\lambda^{s}_{jq}J_{j}(\bar{\alpha}_{jk}\xi)J_{j}'({}_{L,R}\lambda^{s}_{jq})\right.\right. & \\
\left. - \bar{\alpha}_{jk}\xi\, J_{j}({}_{L,R}\lambda^{s}_{jq})\, J_{j}'(\bar{\alpha}_{jk}\xi)\right] + & \\
+ \dfrac{1}{[\bar{\alpha}_{jk}\xi]^{2}+({}_{L,R}\lambda^{s}_{jq})^{2}}\dfrac{J_{j}({}_{L,R}\lambda^{s}_{jq})}{I_{j}({}_{L,R}\lambda^{s}_{jq})}\left[\bar{\alpha}_{jk}\xi\, I_{j}({}_{L,R}\lambda^{s}_{jq})\cdot\right. & \\
\left.\left.\cdot J_{j}'(\bar{\alpha}_{jk}\xi) - {}_{L,R}\lambda^{s}_{jq}\, J_{j}(\bar{\alpha}_{jk}\xi)\, I_{j}'({}_{L,R}\lambda^{s}_{jq})\right]\right\} & j \neq 0 \\
2\pi(R^{P})^{2}\left\{\dfrac{1}{[\bar{\alpha}_{0k}\xi]^{2}-({}_{L,R}\lambda^{s}_{0q})^{2}}\left[{}_{L,R}\lambda^{s}_{0q}J_{0}(\bar{\alpha}_{0k}\xi)\, J_{0}'({}_{L,R}\lambda^{s}_{0q})\right.\right. & \\
\left. - \bar{\alpha}_{0k}\xi\, J_{0}({}_{L,R}\lambda^{s}_{0q})\, J_{0}'(\bar{\alpha}_{0k}\xi)\right] & \\
+ \dfrac{1}{[\bar{\alpha}_{0k}\xi]^{2}+({}_{L,R}\lambda^{s}_{0q})^{2}}\dfrac{J_{0}({}_{L,R}\lambda^{s}_{0q})}{I_{0}({}_{L,R}\lambda^{s}_{0q})}\left[\bar{\alpha}_{0k}\xi\, I_{0}({}_{L,R}\lambda^{s}_{0q})\right. & \\
\left.\left.\cdot J_{0}'(\bar{\alpha}_{0k}\xi) - {}_{L,R}\lambda^{s}_{0q}J_{0}(\bar{\alpha}^{s}_{0k}\xi)I_{0}'({}_{L,R}\lambda^{s}_{0q})\right]\right\} & j = 0
\end{cases}
\qquad \text{(III-1)}
$$

$$L_{mnij} = \sqrt{\frac{2}{\pi L}} \begin{cases} 0 & s \neq j \\ 0 & m = i, i \neq 0, n = j = 0 \\ 0 & m = i, i \neq 0, n = j \neq 0 \\ \frac{L}{m}\left\{1-(-1)^m\right\} & m \neq 0, i = 0, n = j \neq 0 \\ \frac{2L}{m}\left\{1-(-1)^m\right\} & m \neq 0, i = 0, n = j = 0 \\ L\left\{\frac{1-(-1)^{m+i}}{m+i} + \frac{1-(-1)^{m-i}}{m-i}\right\} & m \neq i, i \neq 0, n = j = 0 \\ \frac{L}{2}\left\{\frac{1-(-1)^{m+i}}{m+i} + \frac{1-(-1)^{m-i}}{m-i}\right\} & m \neq i, i \neq 0, n = j \neq 0 \end{cases} \qquad \text{(III-2)}$$

APPENDIX IV - LIST OF SYMBOLS

A_{ij}, B_{ij}, D_{ij}	stiffness coefficients
$A_{mn}^{E,I}$	shell generalized deflection coordinates
${}_{T,B}A_{sq}^{L,R}$	end plates generalized deflection coordinates
c_E, c_I	shell damping coefficients
c_T, c_B	end plates damping coefficients
$C_{ij}^{(k)}$	elastic moduli defined in Appendix I
c_o	speed of sound
E_E, E_I	Young's moduli of external and internal shells
E_T, E_B	Young's moduli of outer and inner end plates
h_E, h_I	thicknesses of external and internal shells
h_K	distance from reference surface to lamina surface
h_s, h_s^P	thicknesses of shell and end plate cores
h_T, h_B	thicknesses of outer and inner end plates
$H_{mn}^{E,I}$	frequency response functions of external and internal shells
$H_{sq}^{T,B}$	frequency response functions of outer and inner end plates
$\underset{\sim}{i}$	$\sqrt{-1}$
k_o	core stiffness
k_s	$k_o(1+g_s)$
L	length of shell

L_{ij}	differential operators given in Appendix II
m_s, m_s^P	core surface densities for shell and end plates
m_E, m_I	surface densities of external and internal shells
m_T, m_B	surface densities of outer and inner end plates
M	number of laminae of internal shell
$M_x, M_\theta, M_{x\theta}$	loading moments
N	number of laminae of external shell
$N_x, N_\theta, N_{x\theta}$	membrane forces
p	acoustic pressure
p_1, p_2	acoustic pressures due to vibrating shell and end plate systems
p^e, p^i	external and internal random pressures applied on shell surface
p^T, p^B	outer and inner random pressures applied on end plate surfaces
$\bar{P}_{mn}^{E,I}$	shell generalized random forces
$T,B\bar{P}_{sq}$	end plate generalized random forces
q_x, q_w, q_θ	shell loading
r, θ	polar coordinates
R_1	porous material flow resistivity
R	shell radius
R^P	plate radius
$RL^{E,I}$	shell deflection response levels

$S_{F_j}^{e,i}, S_{F_j}^{T,B}$	spectral densities of shell and end plate point loads j=1,2
$S_{mnrs}^{E,I}$	shell cross-spectral densities of generalized random forces
$T,B S_{sqjk}$	end plate cross-spectral densities of generalized random forces
S_p	spectral density of acoustic pressure
SPL	sound pressure levels
$S_w^{E,I}$	spectral densities of shell deflections
$S_w^{T,B}$	spectral densities of end plate deflections
u,v,w	shell displacements
w_E, w_I	transverse displacement of external and internal shells
w_T, w_B	displacement of outer and inner plates
x,θ	cylindrical coordinates
$x_j^e, x_j^i, \theta_j^e, \theta_j^i$	coordinates of shell point loads location, j = 1,2
X_j	coefficients given in Appendix II
Y_r	coefficients given in Appendix II
Z_A	shell acoustic impedance
Z_i	coefficients given in Appendix II
Z_R, Z_L	end plate acoustic impedances
α	angle between fiber direction and shell axis
α_r	coefficients defined in Appendix II

β	acoustic damping coefficient
ζ_{mn}	critical damping ratios
ζ_o	a constant value of damping coefficient
ω	frequency
$\omega^c_{mn,sq}$	coupled modal frequency
$\omega_{mn,sq}$	uncoupled modal frequency
ω_{ijk}	acoustic modal frequencies

superscripts and subscripts:

E	external shell
I	internal shell
E,I	external or internal shell
T	outer plate (top)
B	inner plate (bottom)
T,B	outer or inner plate
R,L	right (x=L), left (x = 0) end plates

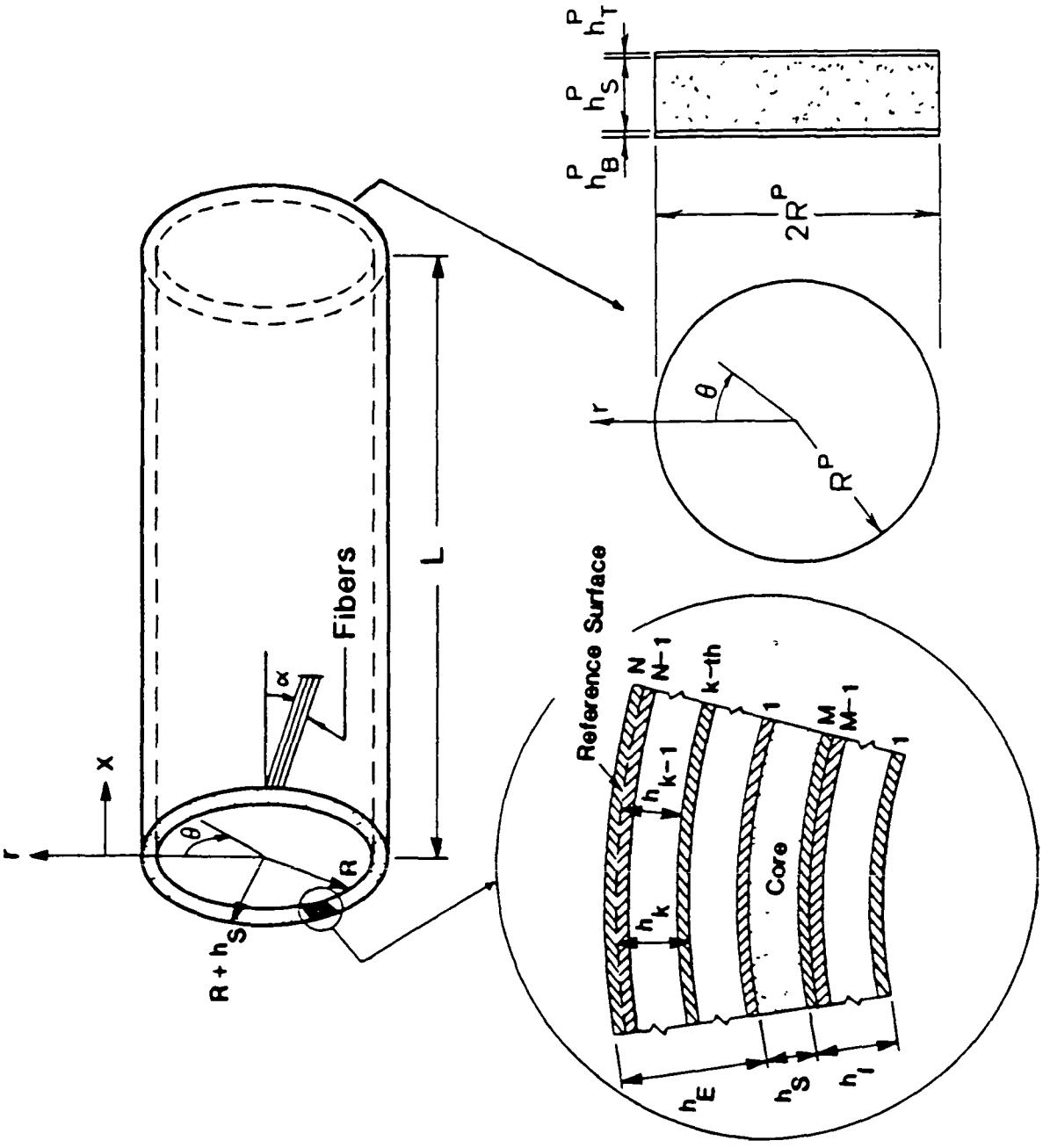

Figure 1. System's Geometry

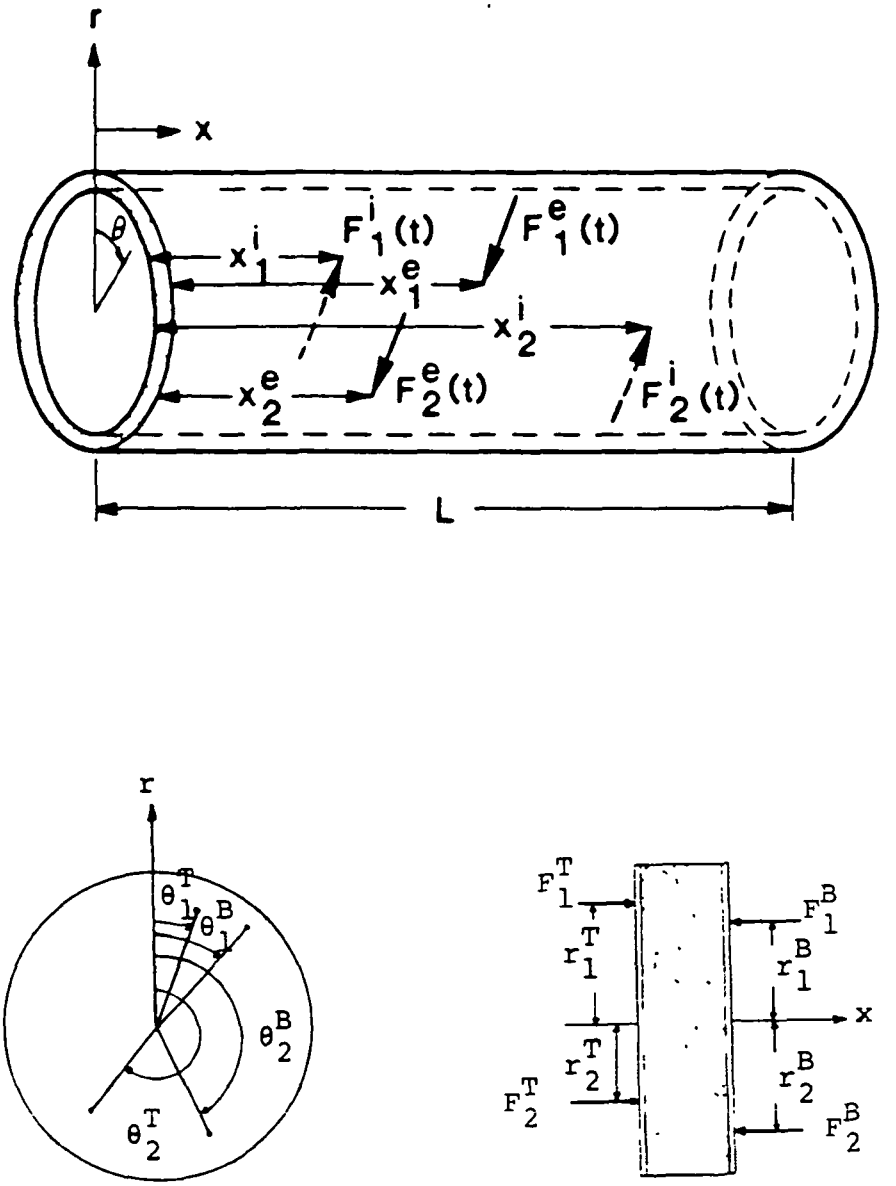

Figure 2. Location of Random Point Loads.

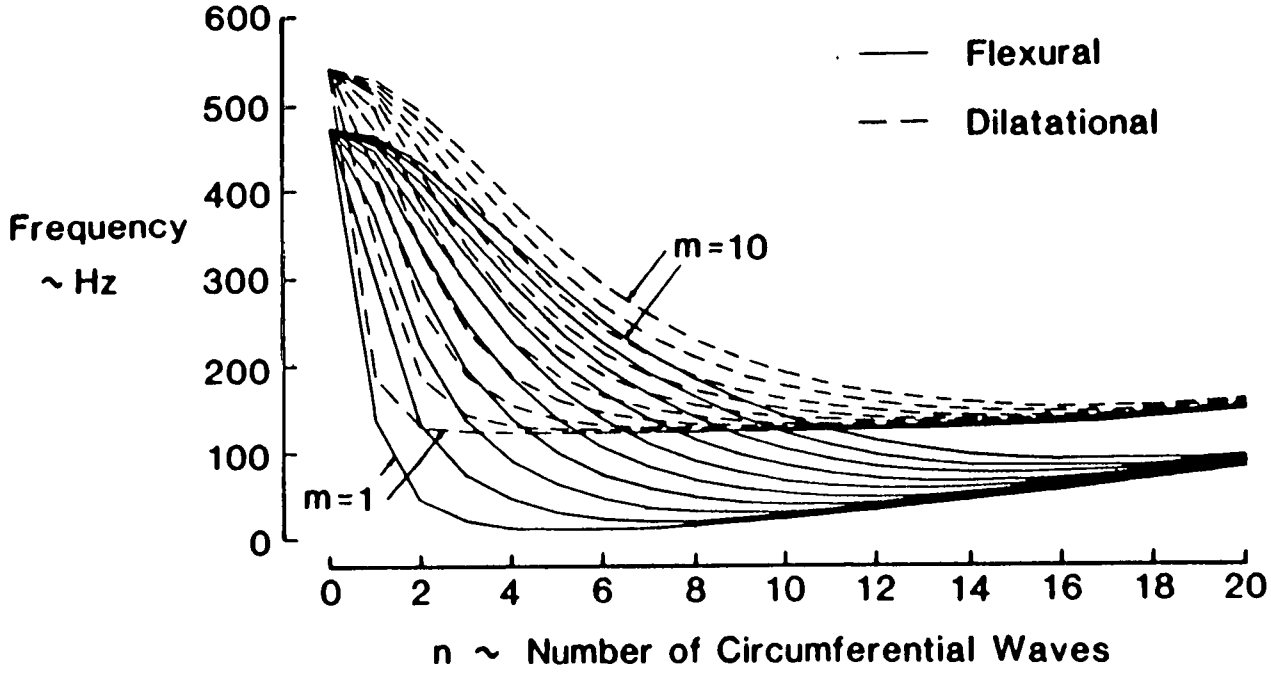

Figure 3. Natural Frequencies for Double Wall Aluminum Shell

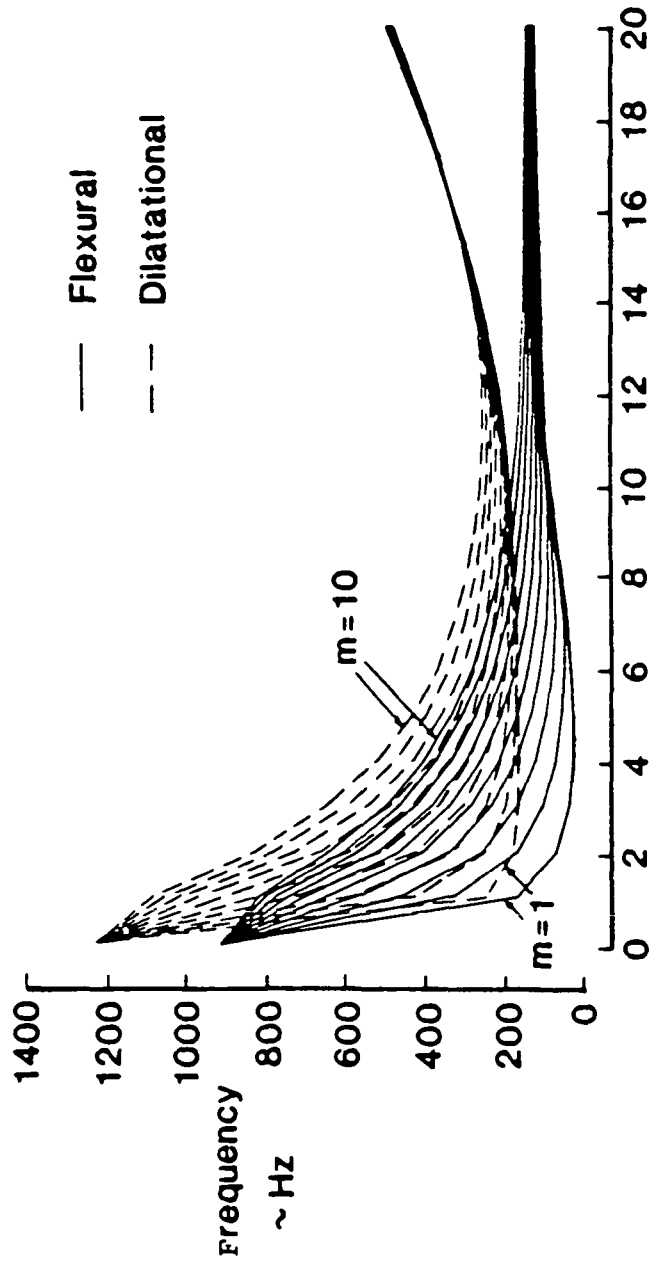

Figure 4. Natural Frequencies for Double Wall Composite Shell

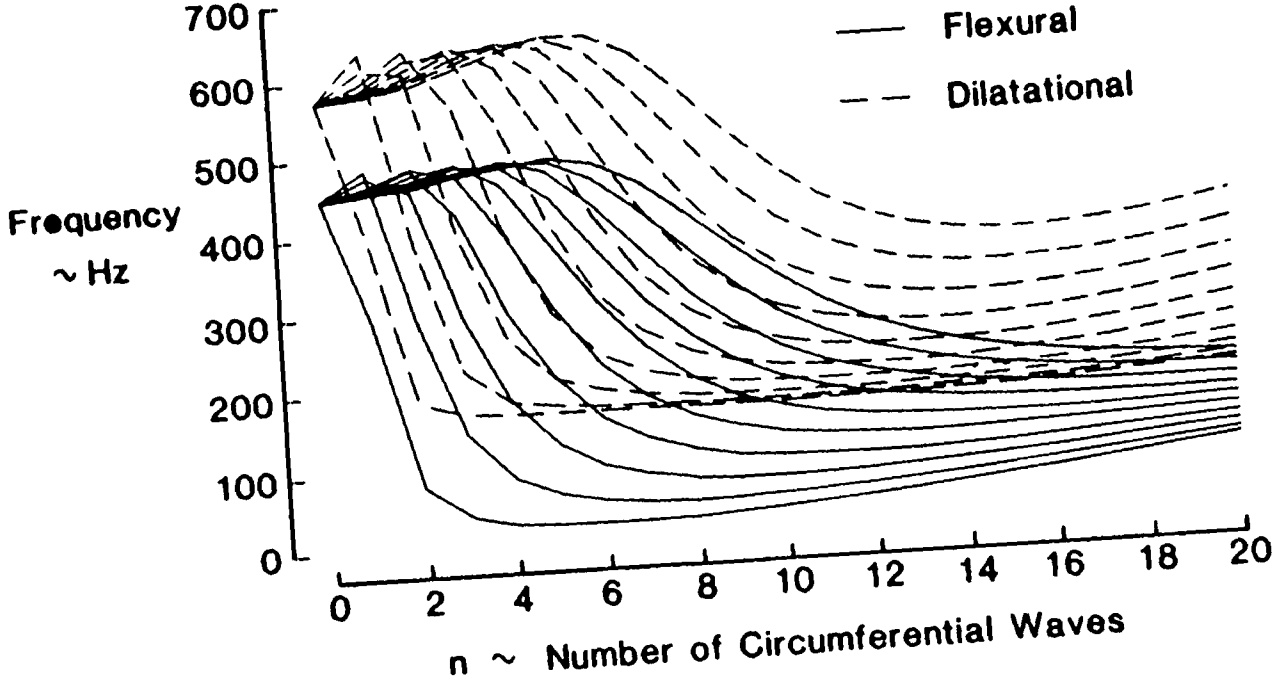

Figure 5. Natural Frequencies for Double Wall Composite Shell with Orthogonal Fiber Reinforcement

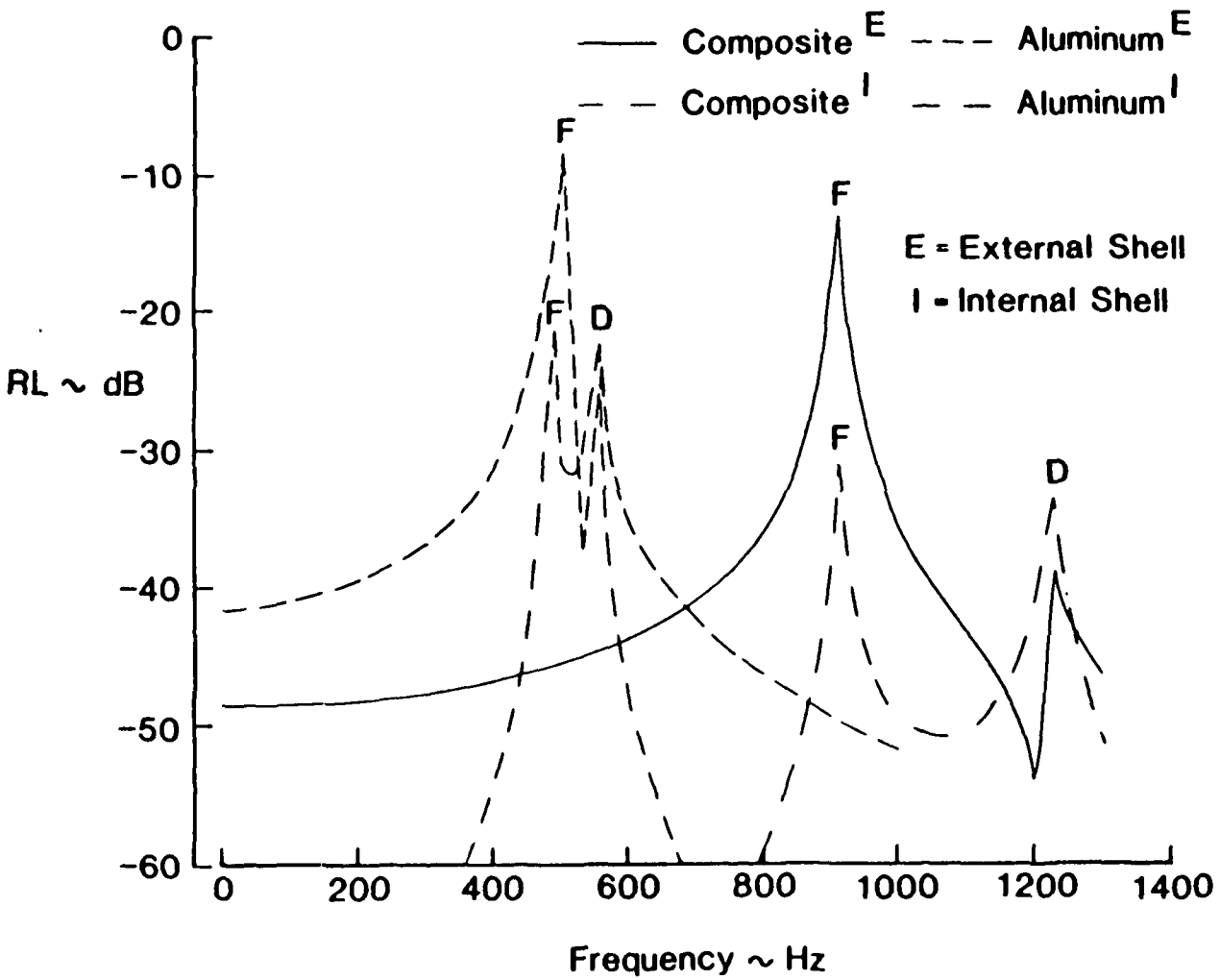

Figure 6. Shell Deflection Levels for Uniform External Pressure

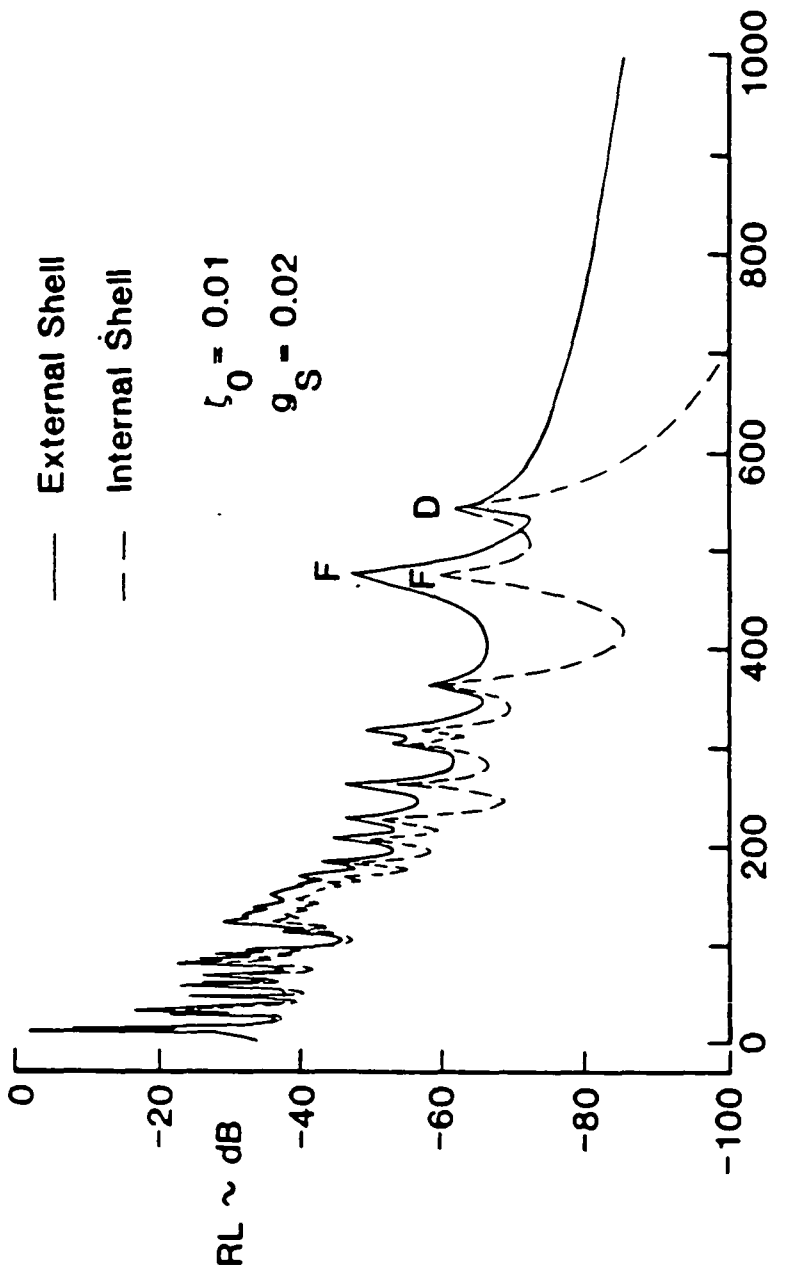

Figure 7. Aluminum Shell Deflection Levels for Point Loads

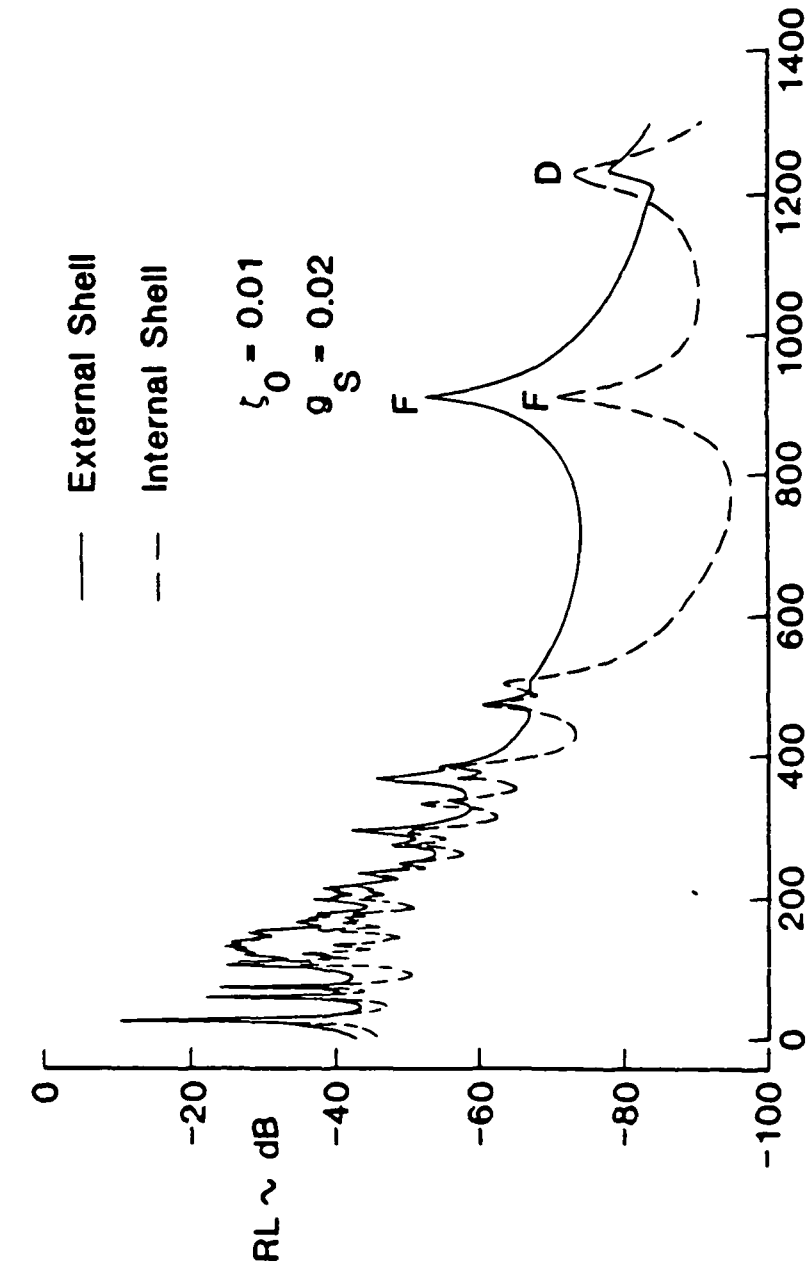

Figure 8. Composite Shell Deflection Levels for Point Loads Acting on the Exterior Surface

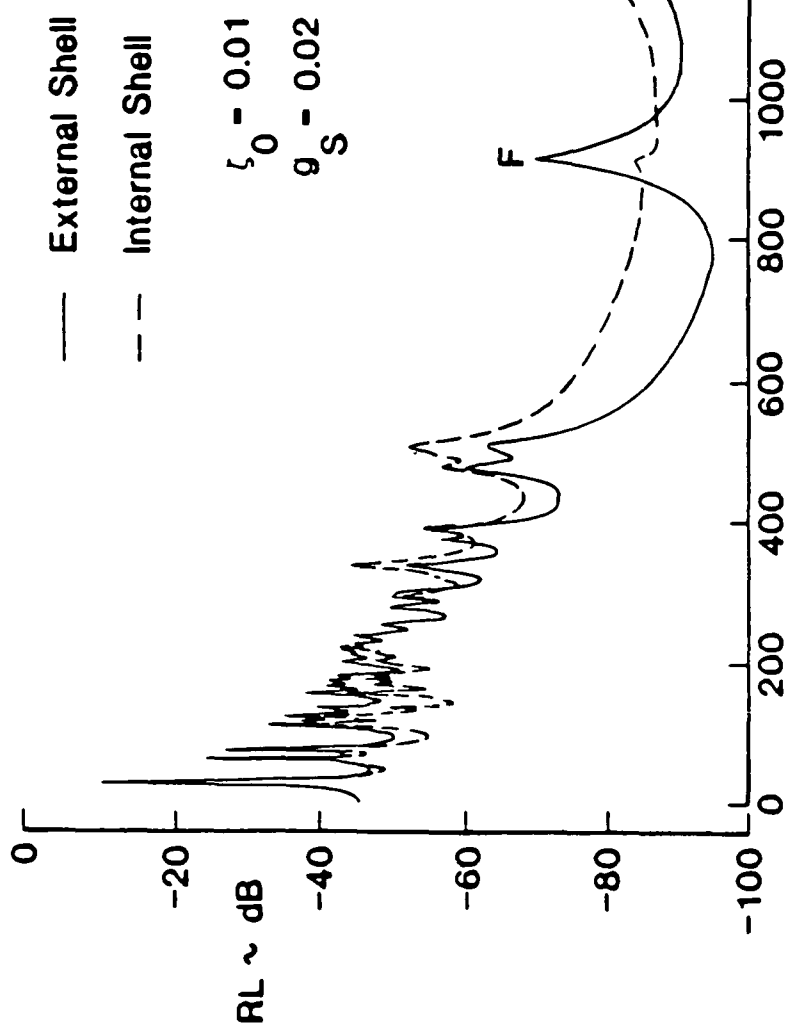

Figure 9. Composite Shell Deflection Levels for Point Loads Acting on the Interior Surface

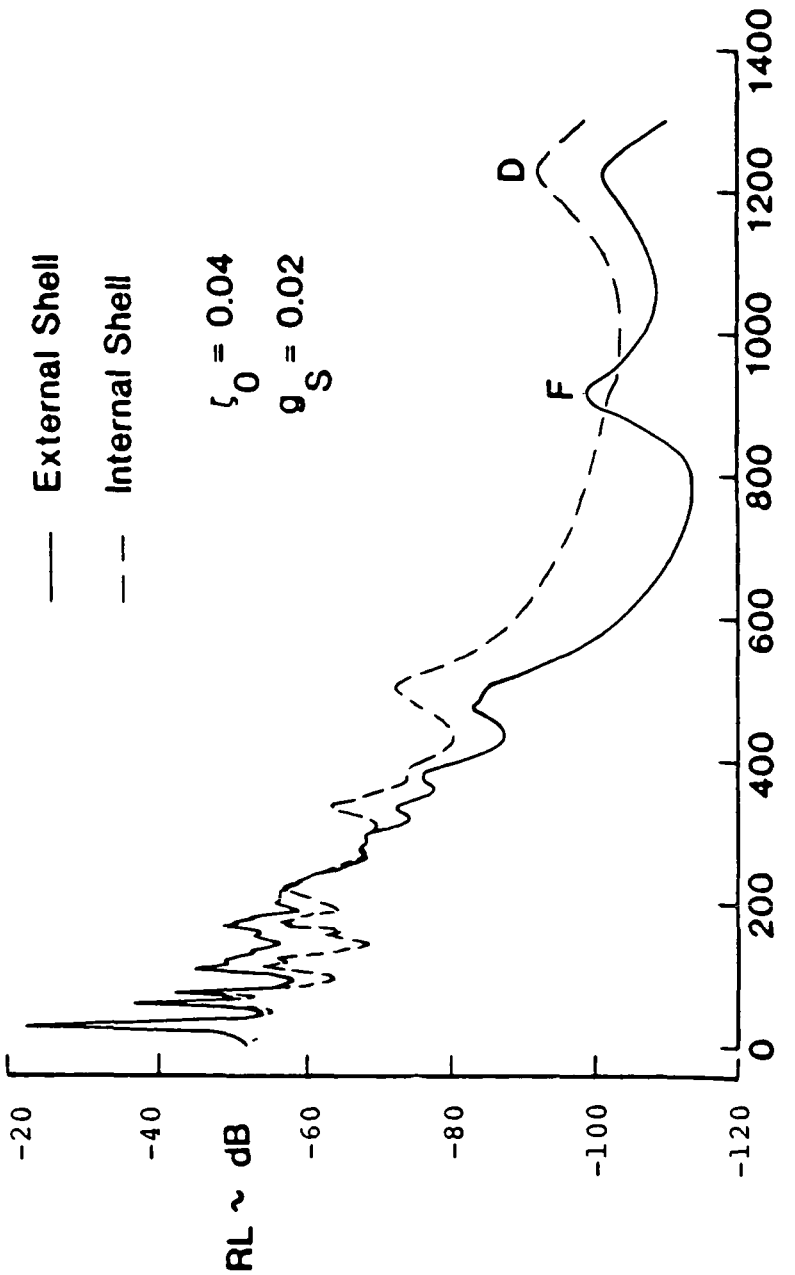

Figure 10. Composite Shell Deflection Levels for Point Loads Acting on the Interior Surface and Critical Damping ζ_o = 0.04

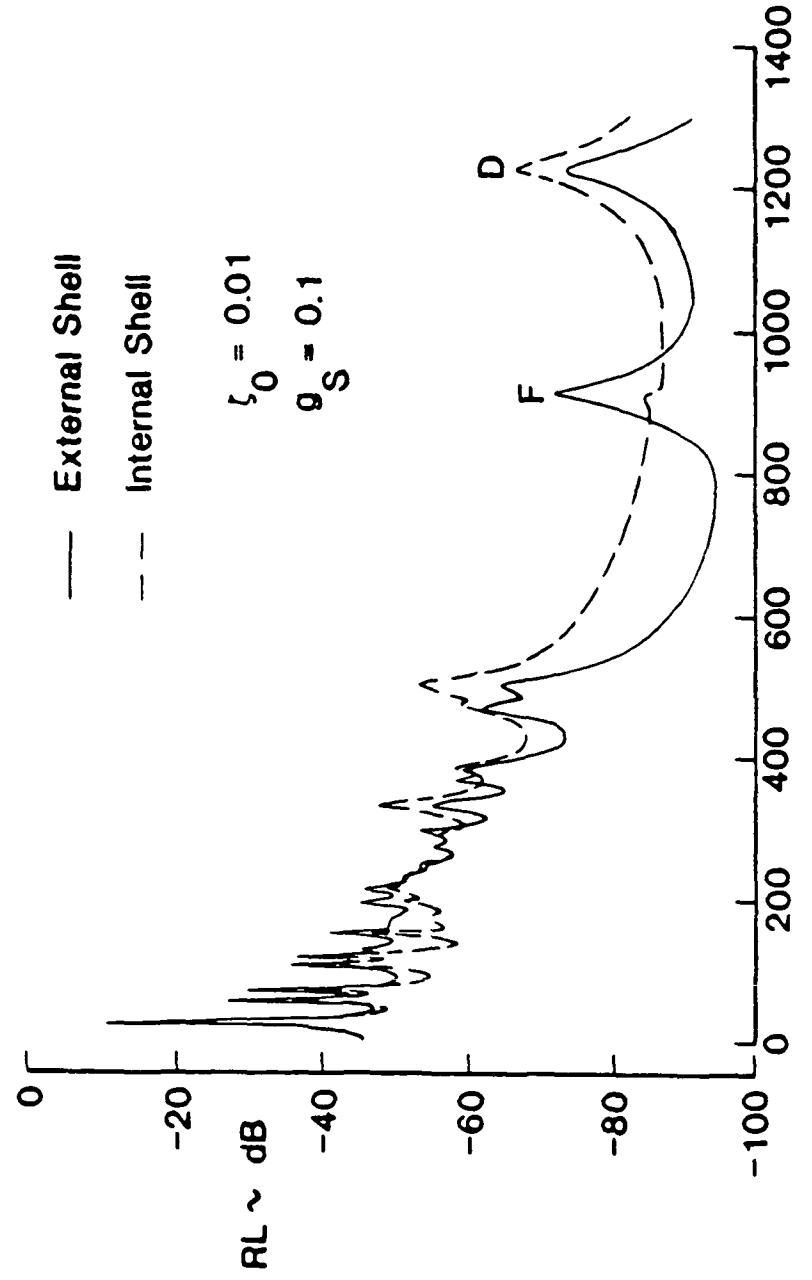

Figure 11. Composite Shell Deflection Levels for Point Loads Acting on the Interior Surface and Core Damping g_s=0.1

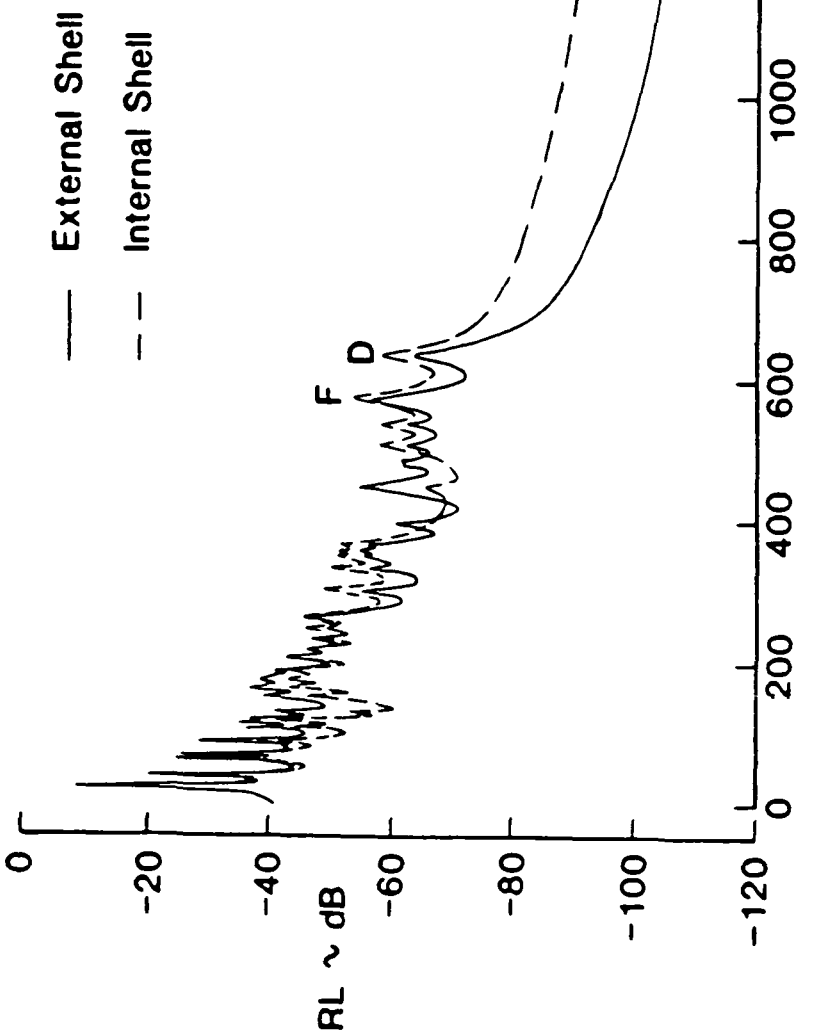

Figure 12. Composite Shell Deflection Levels for Point Loads Acting on the Interior Surface and Orthogonal Orientation of Fiber Reinforcement

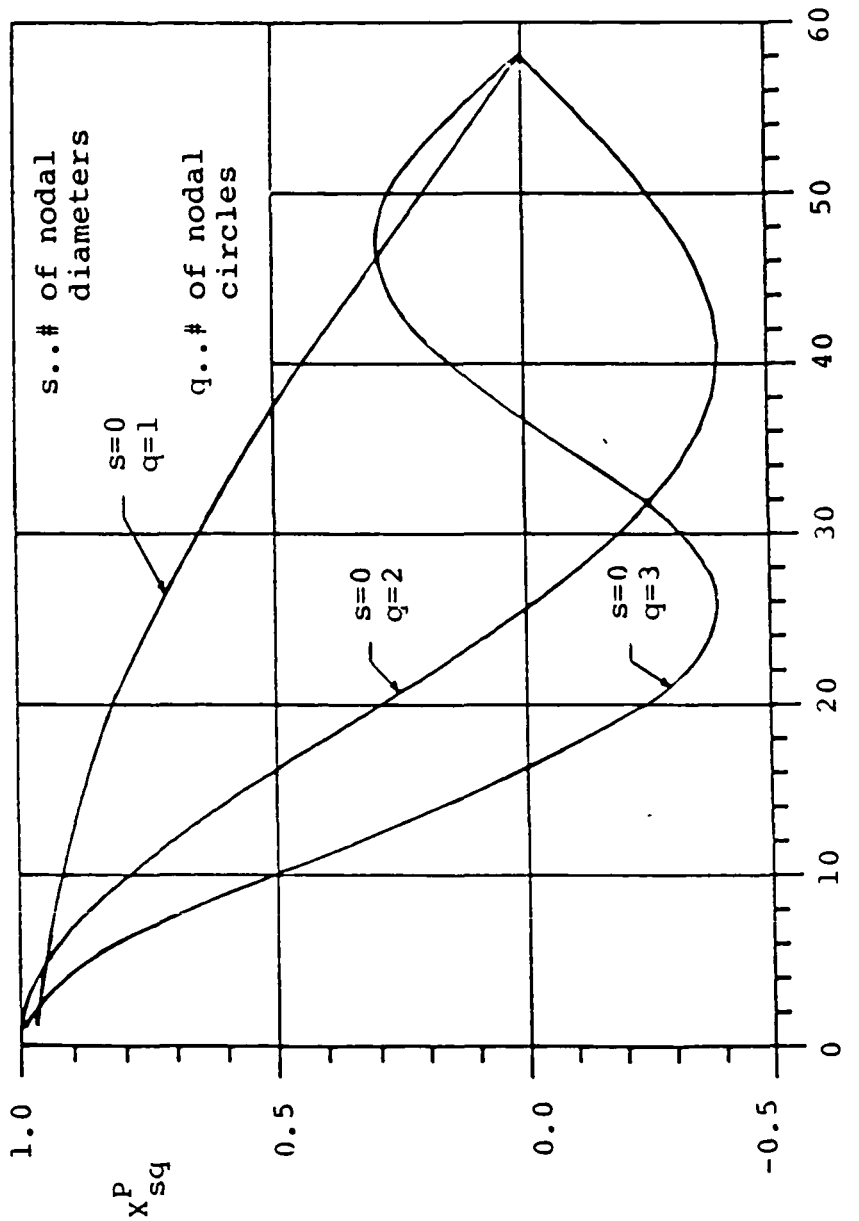

Figure 13. Structural Modes of End Plates

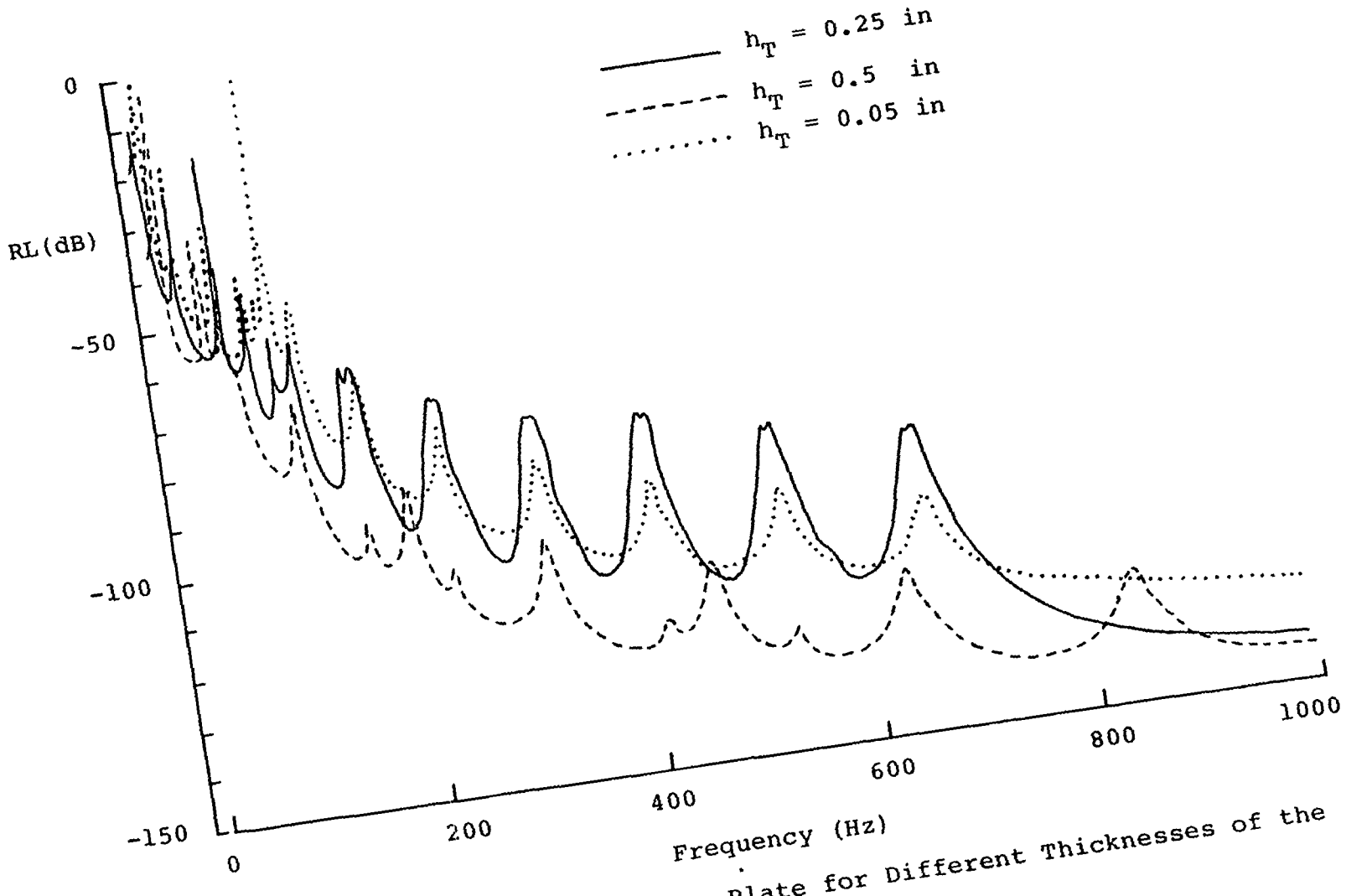

Figure 14. Deflection of Inner Plate for Different Thicknesses of the Outer Plate

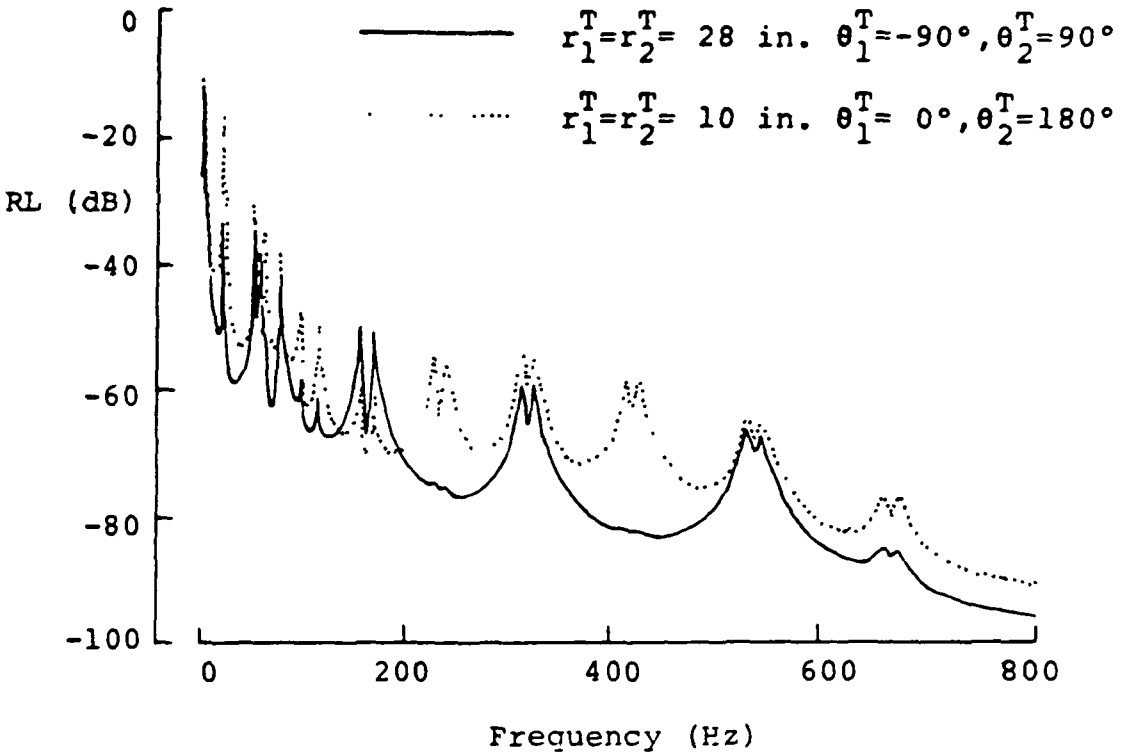

Figure 15. Response Levels of Outer Plate for Different Location of Point Loads(Exterior)

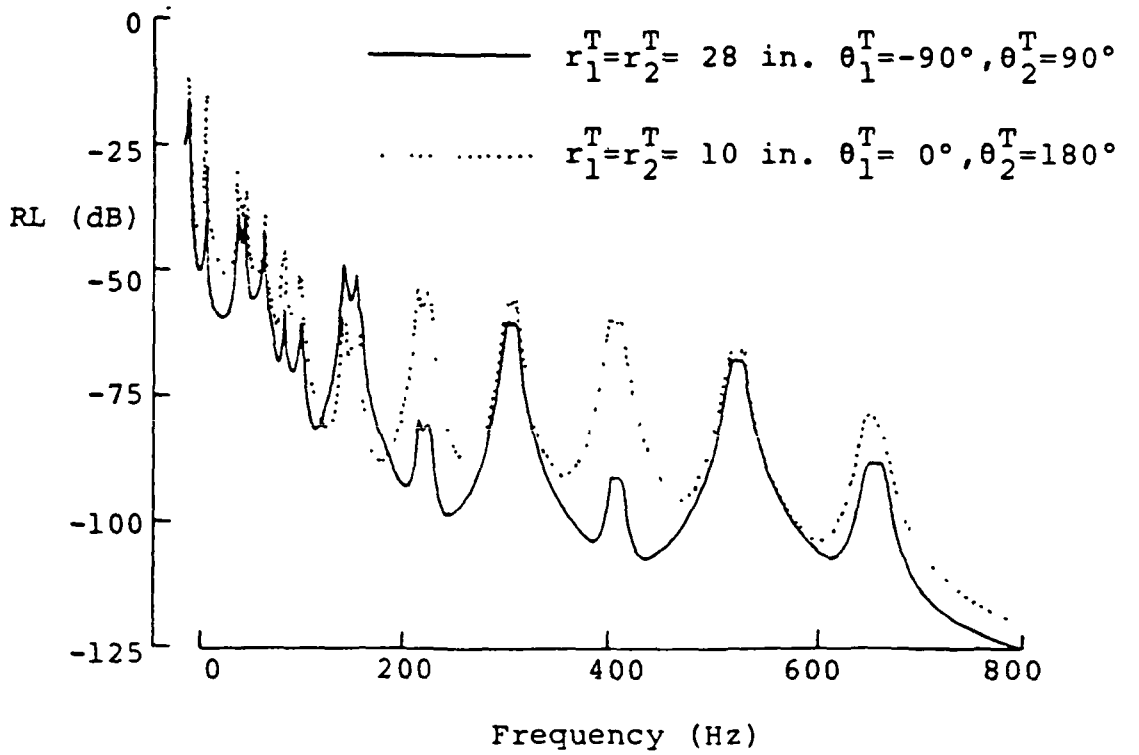

Figure 16. Response Levels of Inner Plate for Different Location of Point Loads(Exterior)

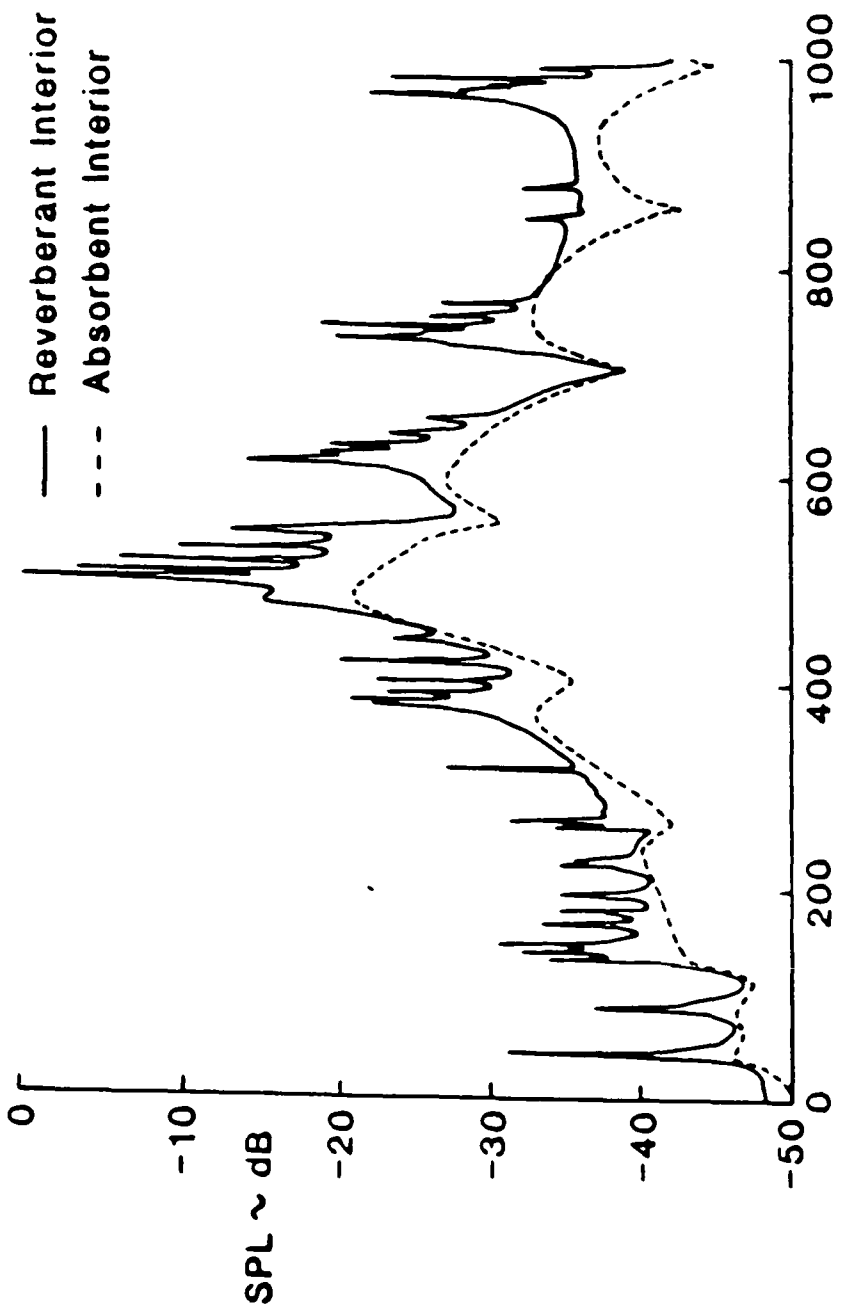

Figure 17. Normalized Sound Pressure Levels in a Double Wall Aluminum Shell(Uniform Exterior Pressure)

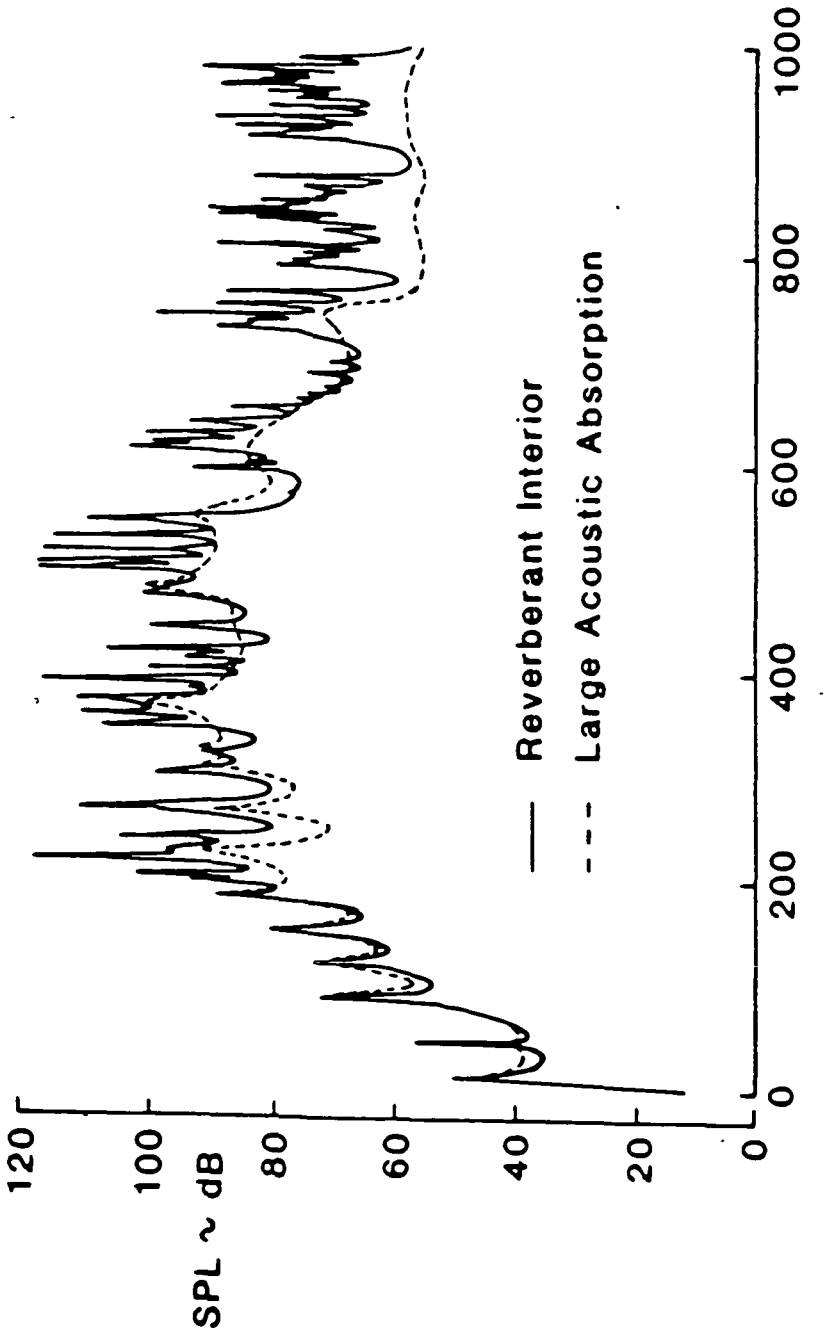

Figure 18. Sound Pressure Levels of a Double Wall Aluminum Shell (Exterior Point Loads)

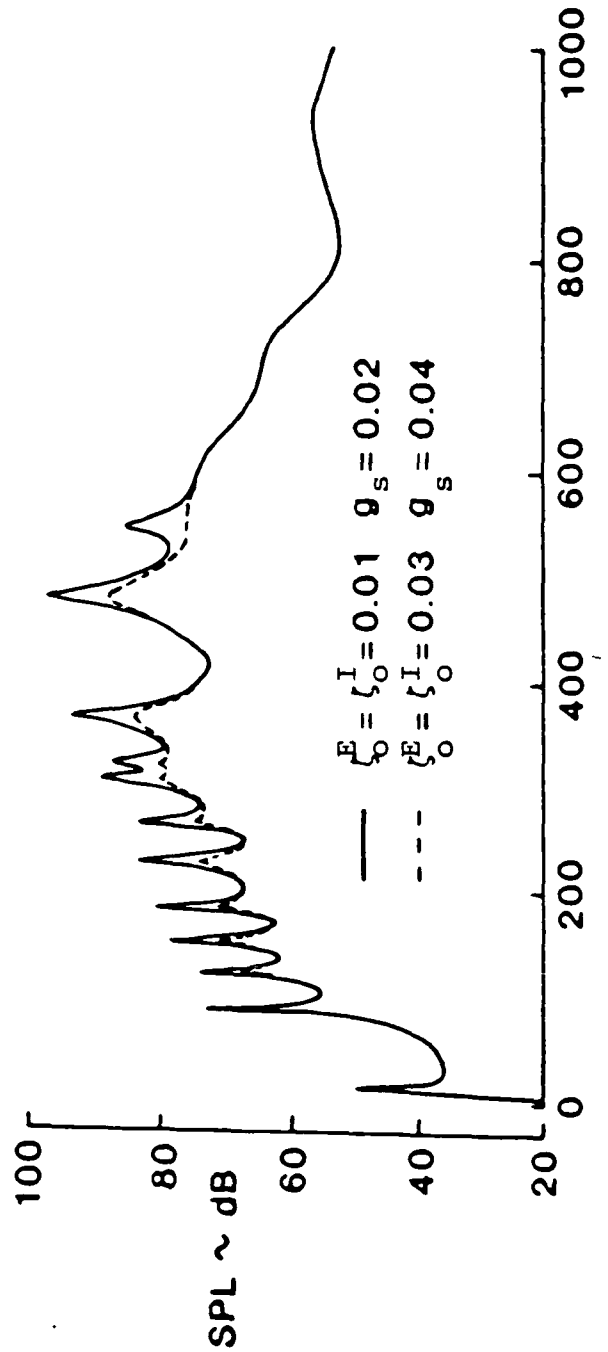

Figure 19. Sound Pressure Levels in a Shell for Low and High Structural Damping Values(Exterior Point Loads)

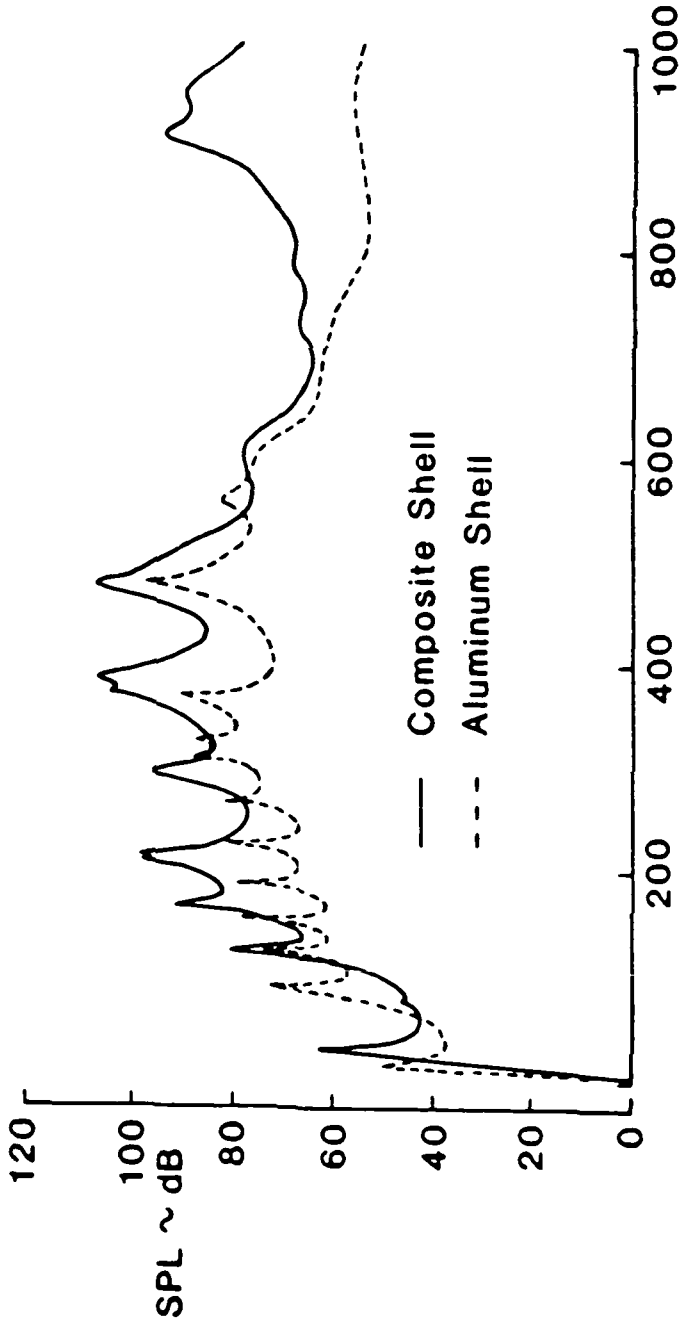

Figure 20. Sound Pressure Levels for Aluminum and Composite Shells(Exterior Point Loads)

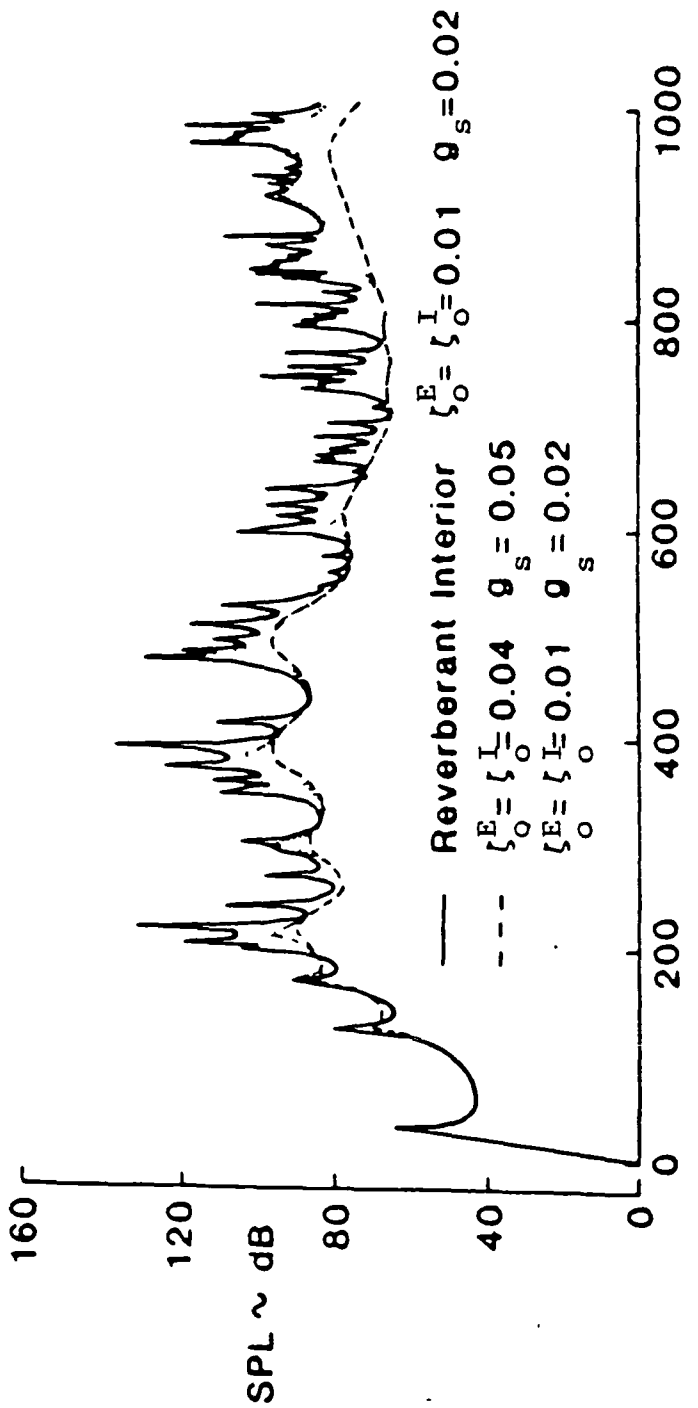

Figure 21. Sound Pressure Levels for Different Structural and Acousting Damping Conditions(Exterior Point Loads)

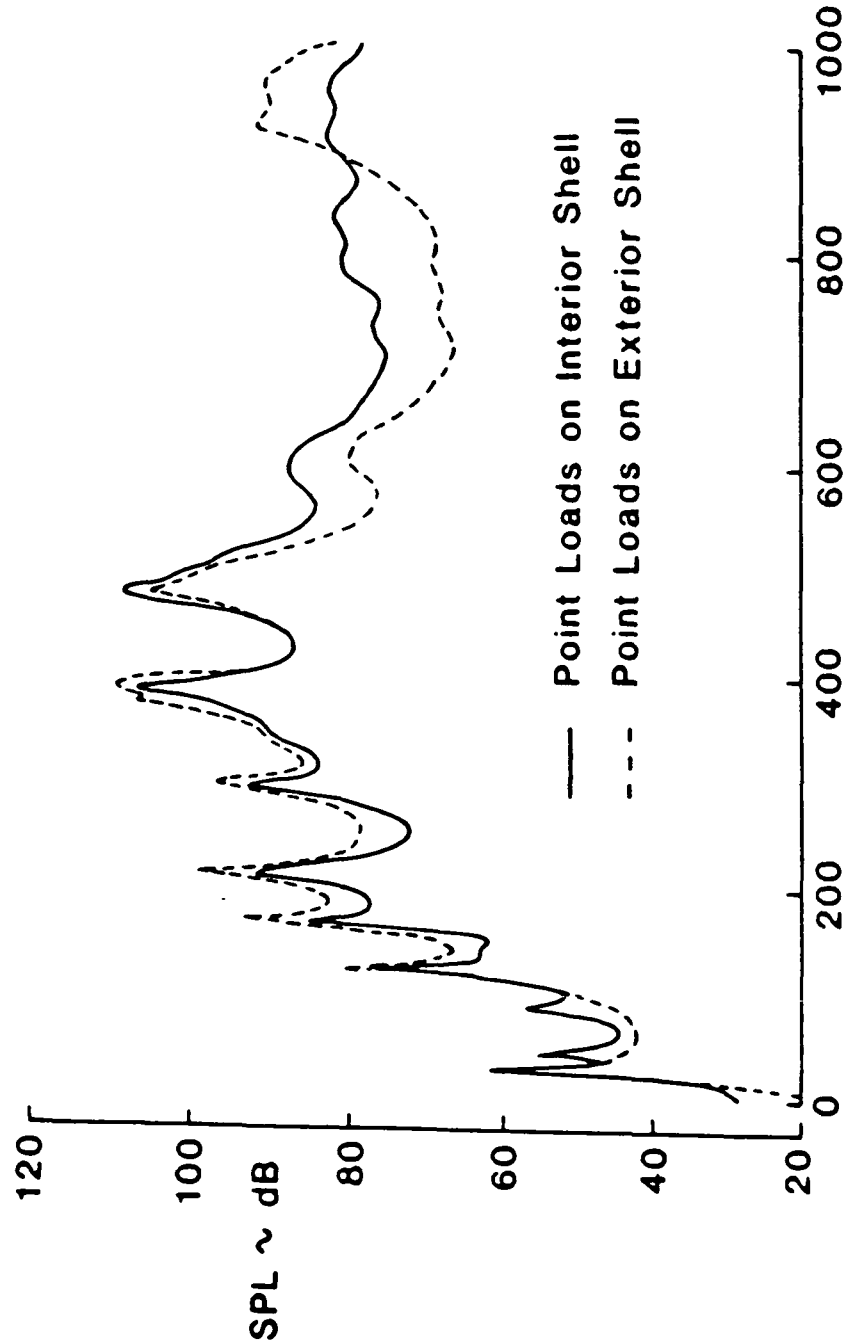

Figure 22. Sound Pressure Levels in a Composite Shell for Different Loading Conditions.

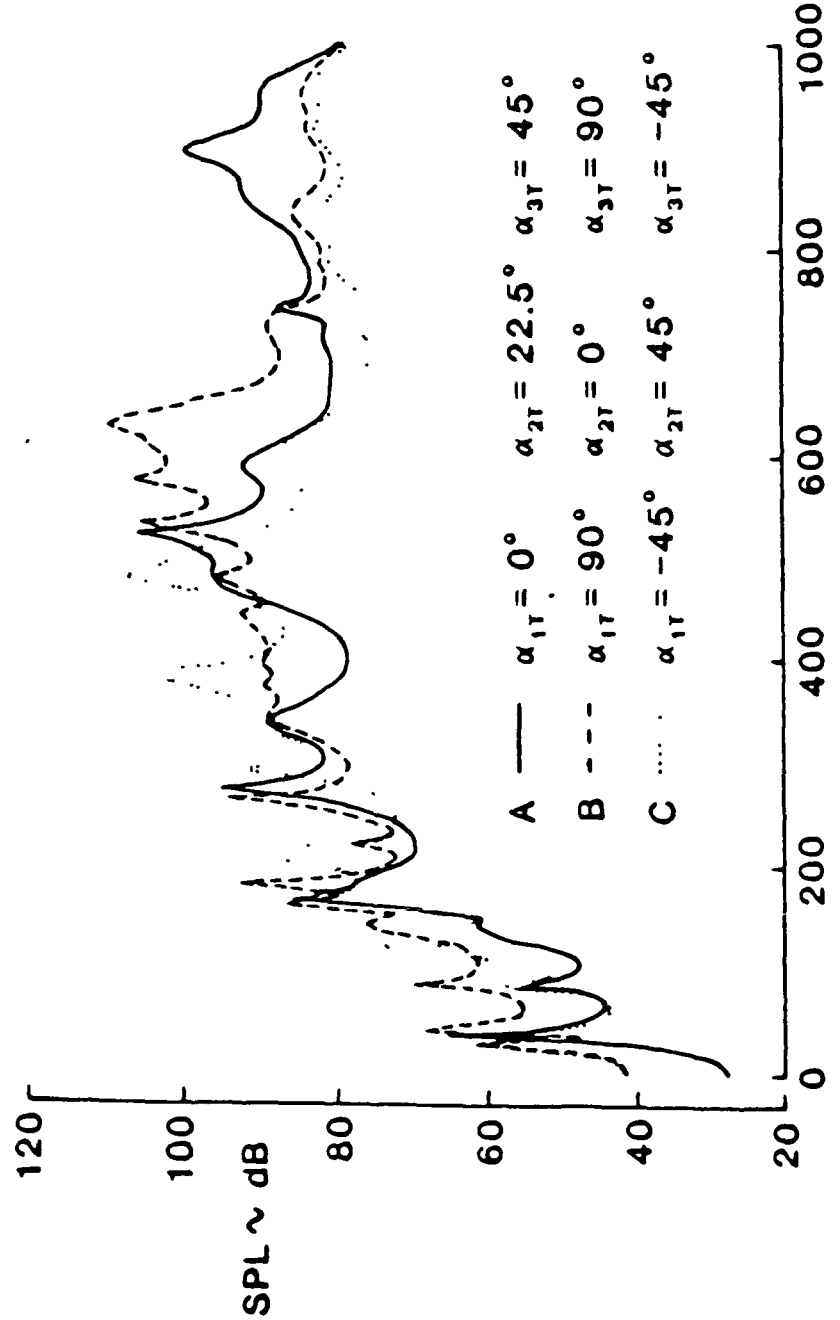

Figure 23. Sound Pressure Levels in a Composite Shell for Different Fiber Orientations(Interior Point Loads)

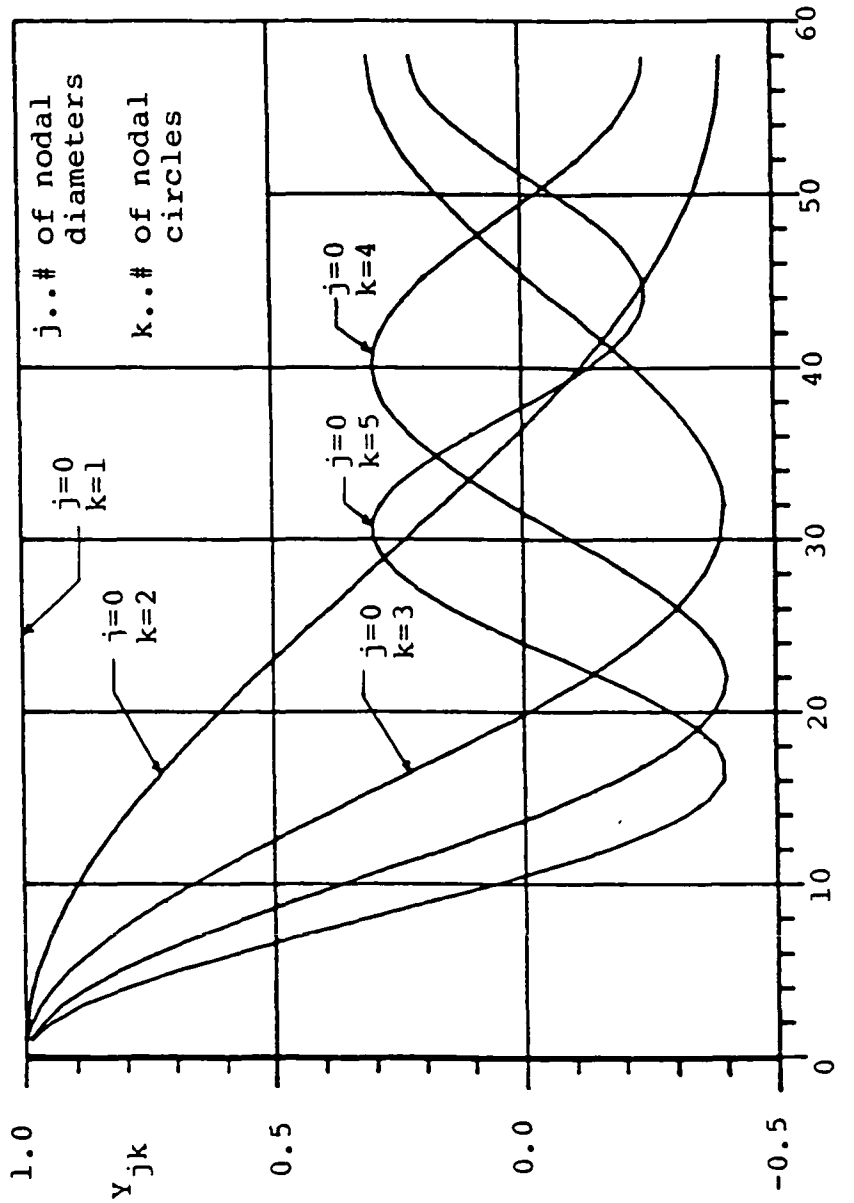

Figure 24. Radial Acoustic Modes

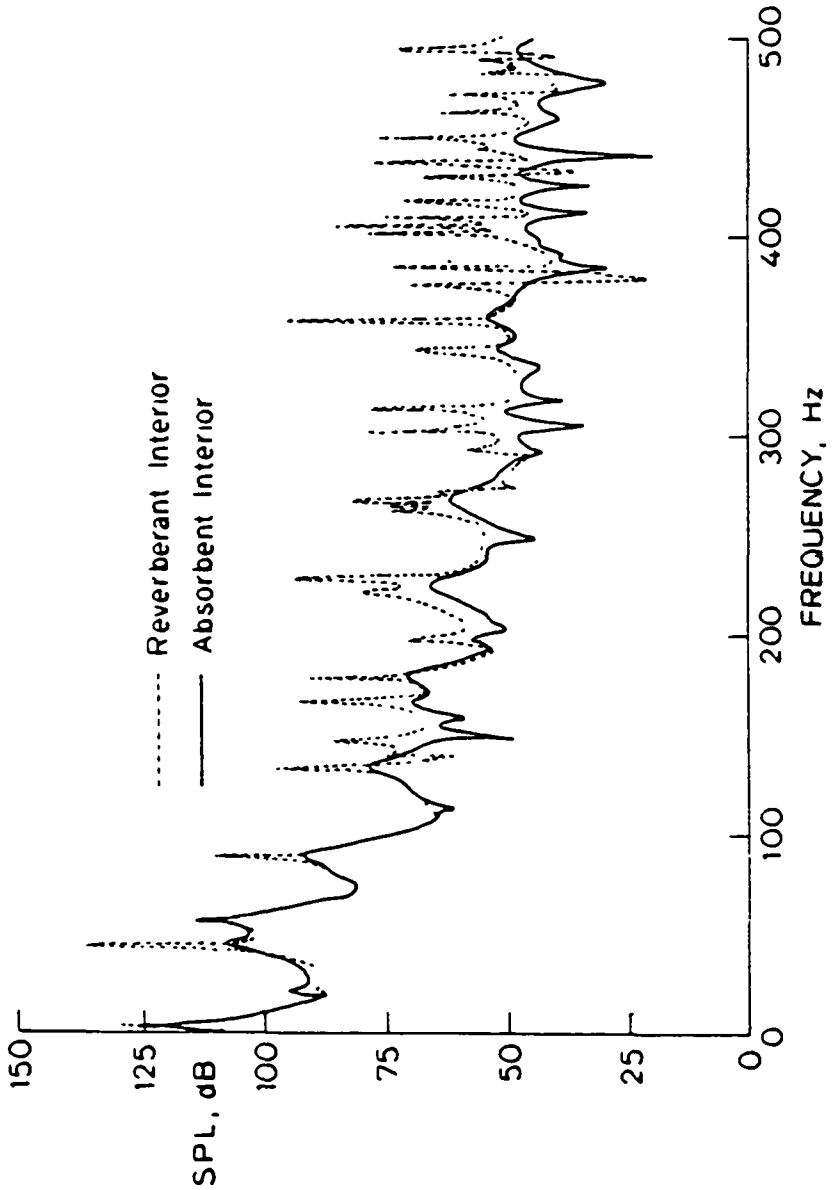

Figure 25. Sound Pressure Levels Due to End Plates(at x=L) for Different Acoustic Conditions(Exterior Uniform Pressure)

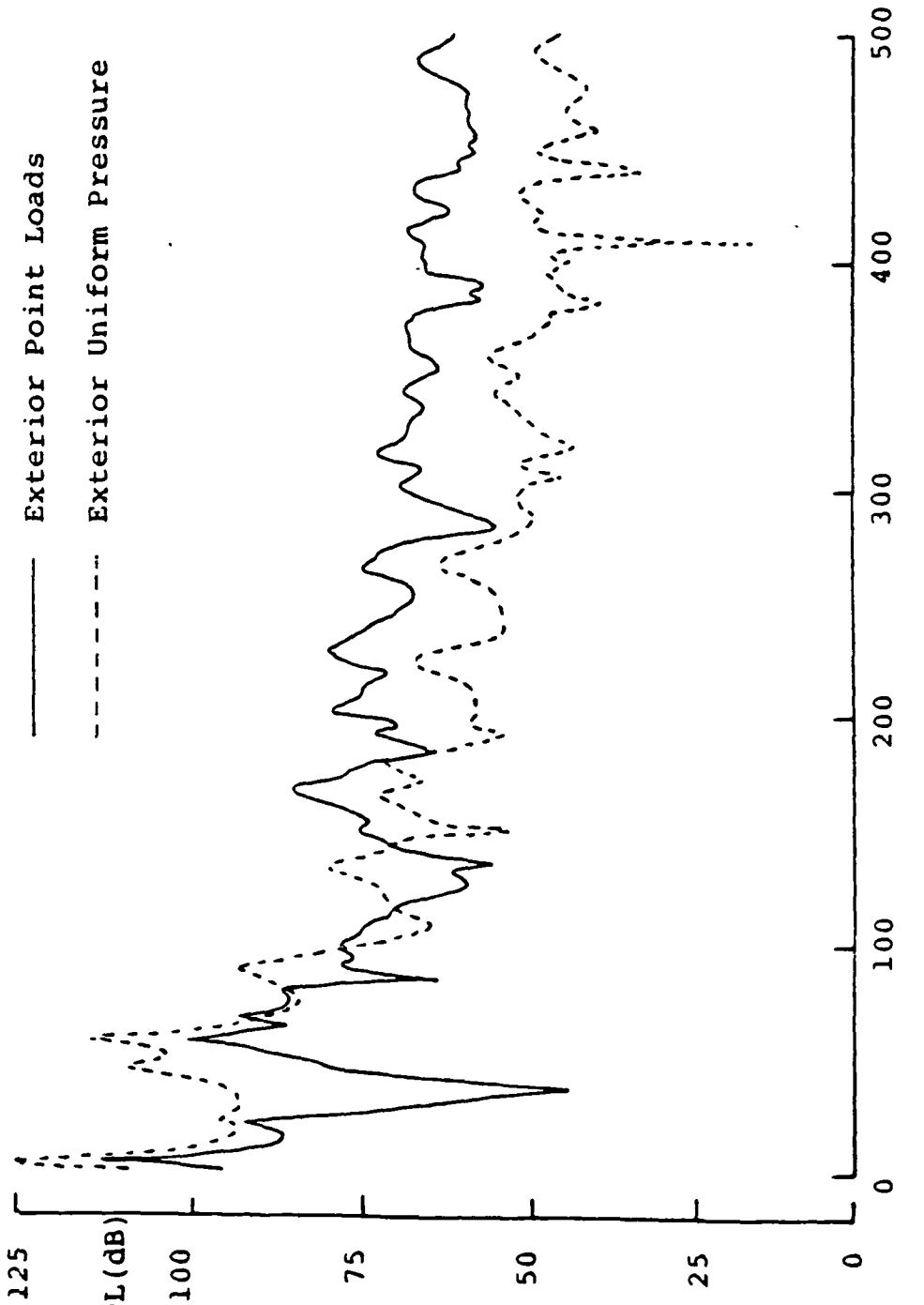

Figure 26. Sound Pressure Levels Due to End Plates (at x=L) for Different Loading Conditions

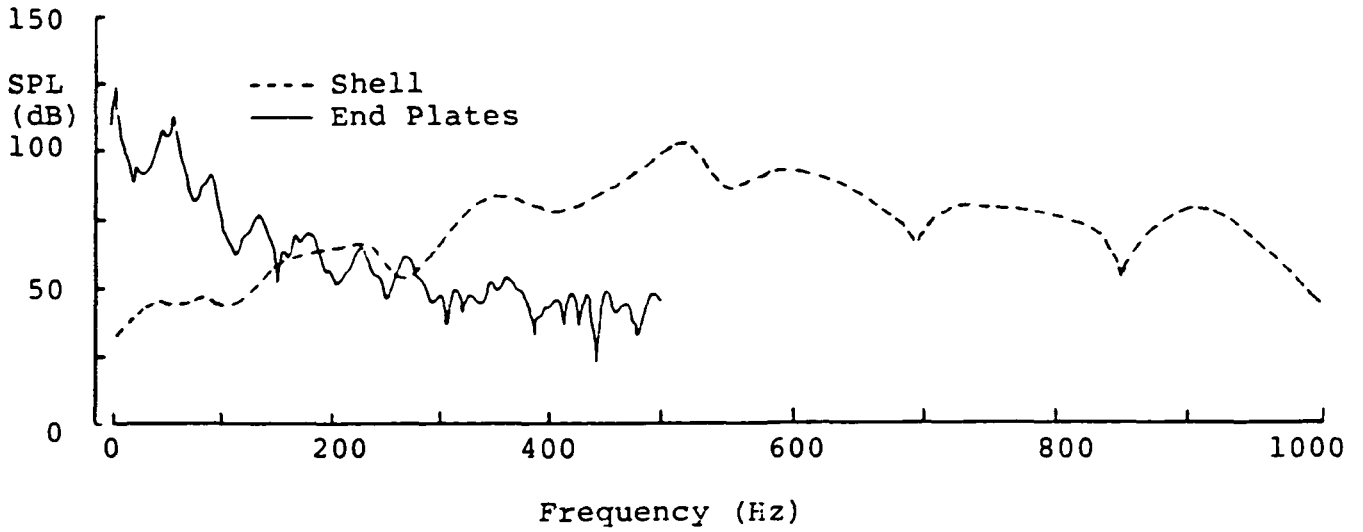

Figure 27. Sound Pressure Levels Due to Individually Vibrating Shell and End Plate Systems(Exterior Uniform Pressure)

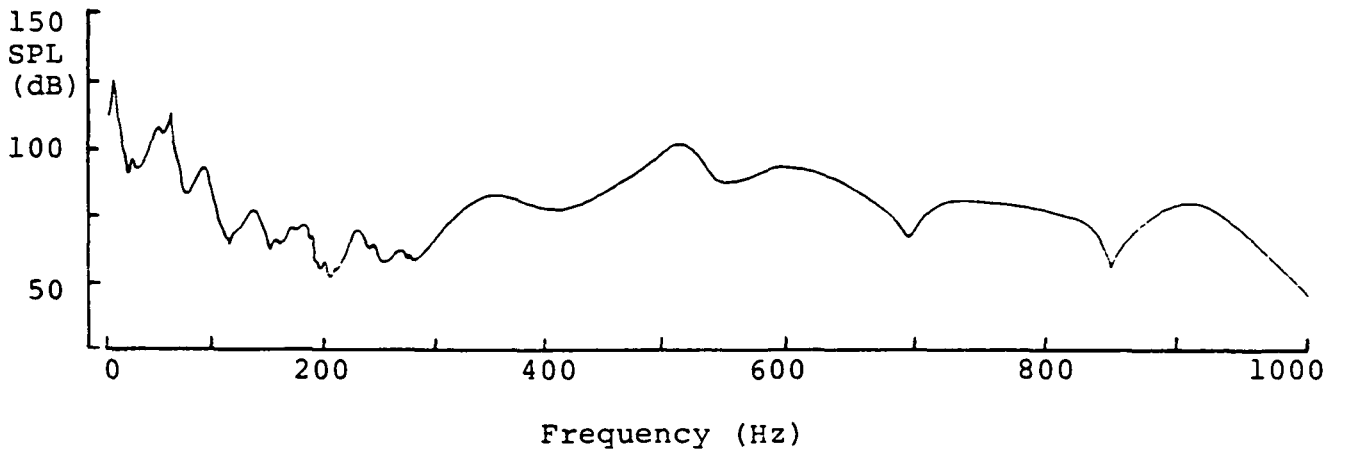

Figure 28. Total Interior Noise Due to Exterior Uniform Pressure

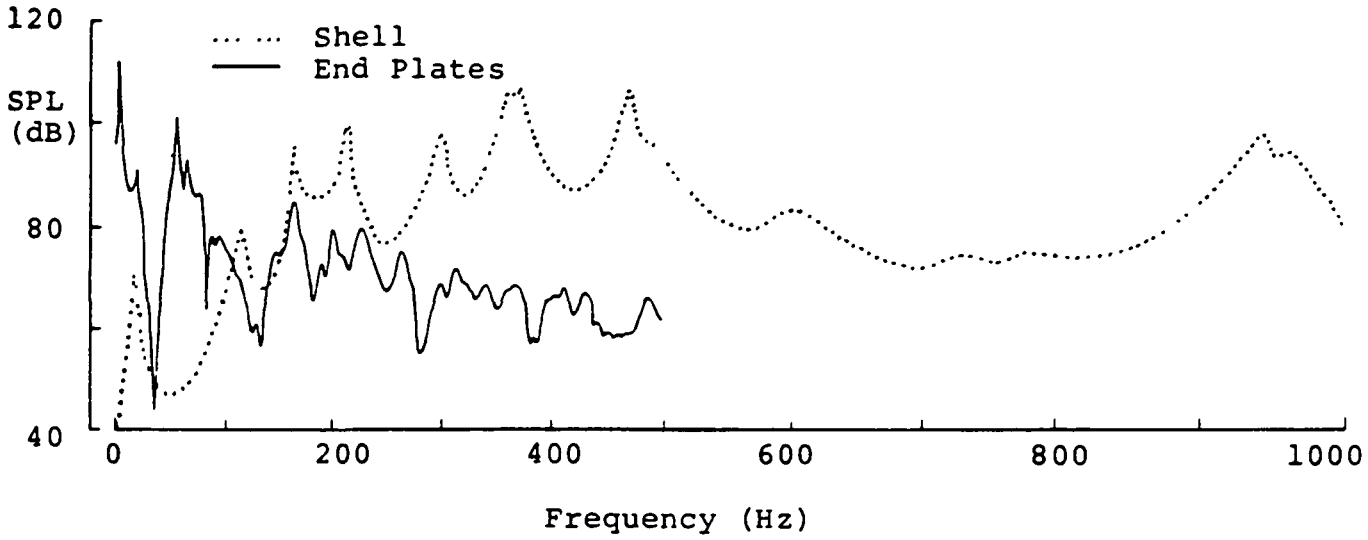

Figure 29. Sound Pressure Levels Due to Individually Vibrating Shell and End Plate Systems(Exterior Point Loads)

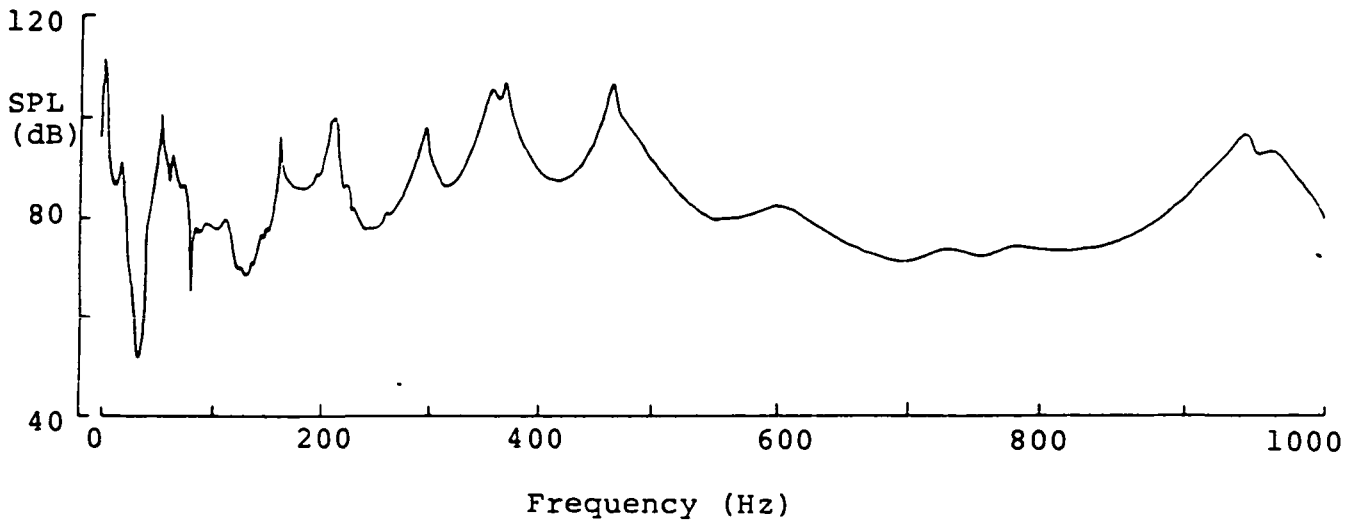

Figure 30. Total Interior Noise Due to Exterior Point Loads

Table 1.- End Plates' Coupled Modal Frequencies

s	q	D(Hz)	F(Hz)	s	q	D(Hz)	F(Hz)
0	1	57.4517	3.5678	2	1	60.2477	18.4983
0	2	61.2197	21.4450	2	2	76.4402	50.5483
0	3	78.4144	53.4869	2	3	112.5142	96.8064
0	4	115.1318	99.8367	2	4	167.5470	157.4294
0	5	169.9609	159.9363	2	5	238.6752	231.6849
0	6	241.6965	234.7966	2	6	325.9345	320.8490
0	7	328.6345	323.5924	2	7	427.6605	423.8004
0	8	430.4361	426.6012	2	8	544.0834	541.0486
0	9	547.2275	544.2151	2	9	675.0477	672.6002
0	10	678.5546	676.1352	2	10	820.9465	818.9479
1	1	58.2062	9.9993	3	1	64.1809	28.8309
1	2	67.1581	34.9606	3	2	89.0700	68.1579
1	3	93.6944	74.0991	3	3	134.2777	121.4190
1	4	139.7819	127.4795	3	4	197.6342	189.1329
1	5	203.0434	194.7783	3	5	276.9535	270.9519
1	6	282.4519	276.5709	3	6	371.2432	366.7382
1	7	377.0500	372.6645	3	7	480.5413	477.1080
1	8	486.0809	482.6870	3	8	604.2222	601.4952
1	9	610.0399	607.3391	3	9	742.9498	740.7407
1	10	748.0262	745.8323	3	10	895.3002	893.4334

Table 2. - Acoustic Modal Frequencies (Hz)

i	j	k	ω_{ijk}	i	j	k	ω_{ijk}	i	j	k	ω_{ijk}	i	j	k	ω_{ijk}
0	0	1	0.0000	1	1	2	199.4405	2	2	3	371.7686	3	3	4	544.1061
0	0	2	142.4452	1	1	3	317.8213	2	2	4	489.9615	3	4	1	209.3995
0	0	3	261.3043	1	1	4	436.4621	2	3	1	163.6457	3	4	2	349.6330
0	0	4	376.4491	1	2	1	114.9657	2	3	2	301.8392	3	4	3	474.1628
0	1	1	68.1583	1	2	2	251.1765	2	3	3	423.4321	3	4	4	595.7382
0	1	2	198.1604	1	2	3	369.7093	2	3	4	541.7625	4	0	1	90.2400
0	1	3	317.0195	1	2	4	488.4008	2	4	1	203.2323	4	0	2	168.6236
0	1	4	435.8786	1	3	1	158.9122	2	4	2	345.9747	4	0	3	276.4475
0	2	1	112.7304	1	3	2	299.2993	2	4	3	471.4717	4	0	4	387.1139
0	2	2	250.1613	1	3	3	421.6252	2	4	4	593.5985	4	1	1	113.0876
0	2	3	369.0204	1	3	4	540.3516	3	0	1	67.6800	4	1	2	217.7402
0	2	4	487.8795	1	4	1	199.4405	3	0	2	157.7061	4	1	3	329.6129
0	3	1	157.3026	1	4	2	343.7610	3	0	3	269.9269	4	1	4	445.1218
0	3	2	298.4478	1	4	3	469.8497	3	0	4	382.4847	4	2	1	144.4002
0	3	3	421.0213	1	4	4	592.3110	3	1	1	96.0528	4	2	2	265.9397
0	3	4	539.8804	2	0	1	45.1200	3	1	2	209.3995	4	2	3	379.8939
0	4	1	198.1604	2	0	2	149.4204	3	1	3	324.1635	4	2	4	496.1549
0	4	2	343.0200	2	0	3	265.1712	3	1	4	441.1017	4	3	1	181.3488
0	4	3	469.3078	2	0	4	379.1435	3	2	1	131.4866	4	3	2	311.7921
0	4	4	591.8812	2	1	1	81.7396	3	2	2	259.1549	4	3	3	430.5835
1	0	1	22.5600	2	1	2	203.2323	3	2	3	375.1755	4	3	4	547.3701
1	0	2	144.2207	2	1	3	320.2143	3	2	4	492.5515	4	4	1	217.7402
1	0	3	262.2764	2	1	4	438.2077	3	3	1	171.2446	4	4	2	354.6913
1	0	4	377.1245	2	2	1	121.4247	3	3	2	306.0256	4	4	3	477.9048
1	1	1	71.7949	2	2	2	254.1977	3	3	3	426.4264	4	4	4	598.7209